OsloMet – storbyuniversitetet
Fakultet for teknologi, kunst og design
Institutt for maskin, elektronikk og kjemi
Postboks 4 St. Olavs plass, 0130 Oslo
Telefon: 67 23 50 00

PROSJEKT NR. 1902

TILGJENGELIGHET
Open

BACHELOROPPGAVE

BACHELOROPPGAVENS TITTEL	DATO
Monitoring of dehydration by temperature measurements at the skin surface before, during and after exposure to infrared laser light.	23. mai 2019
	ANTALL SIDER / BILAG 67/20
FORFATTERE Elias Kvamme Hatlevik, Hanne Randby, Julian Arthur Tupas Estrada, Lars Sten Stenersen	INTERN VEILEDER Peyman Mirtaheri

UTFØRT I SAMMARBEID MED	EKSTERN VEILEDER

SAMMENDRAG
The purpose of this study is to find a way to monitor dehydration in human tissue using optics. Dehydration is a common condition among elderly but there are no clinical 'gold standard' to monitor the condition. Theory on the physiology of dehydration, anatomy of human skin, electromagnetic radiation, lasers, laser-tissue interaction and heat transfer in tissue is provided to support the basis of our project. In this study, human skin was exposed to infrared radiation from a laser diode and the temperature response was registered. Three different test procedures were performed, one on the ear lobe and two on the forearm, on four test subjects. Near-infrared laser diodes (780 nm and 980 nm) were used due to absorption characteristics of water molecules. The laser energy is absorbed and converted to thermal energy. The magnitude of temperature change at different hydration levels, when exposed to the same amount of energy, could potentially reveal a correlation. The hardware was controlled with a Raspberry Pi Zero, and test software was coded in Python. Temperature versus time were plotted in scatter charts and analysed. Examining the graphs, through calculating the area under curve, slope and percentage change in temperature before and after laser exposure, gave inconclusive results. In total, 13% of the tests displayed the expected outcome. Nonetheless, our study unfolded a research field of great potential, since no similar studies prior to this was found.

3 STIKKORD
Dehydration
Infrared laser diode
Infrared temperature sensor

Abstract

The purpose of this study is to find a way to monitor dehydration in human tissue using optics. Dehydration is a common condition among elderly but there are no clinical ‘gold standard’ to monitor the condition. Theory on the physiology of dehydration, anatomy of human skin, electromagnetic radiation, lasers, laser-tissue interaction and heat transfer in tissue is provided to support the basis of our project. In this study, human skin was exposed to infrared radiation from a laser diode and the temperature response was registered. Three different test procedures were performed, one on the ear lobe and two on the forearm, on four test subjects. Near-infrared laser diodes (780 nm and 980 nm) were used due to absorption characteristics of water molecules. The laser energy is absorbed and converted to thermal energy. The magnitude of temperature change at different hydration levels, when exposed to the same amount of energy, could potentially reveal a correlation. The hardware was controlled with a Raspberry Pi Zero, and test software was coded in Python. Temperature versus time were plotted in scatter charts and analysed. Examining the graphs, through calculating the area under curve, slope and percentage change in temperature before and after laser exposure, gave inconclusive results. In total, 13% of the tests displayed the expected outcome. Nonetheless, our study unfolded a research field of great potential, since no similar studies prior to this was found.

Table of contents

List of figures

List of tables

1 Introduction

Dehydration is a commonly recognized clinical health problem among older adults (Fortes et al., 2015, p. 222; Miller, 2015, p. 10). The condition is difficult to identify with today's standards and leads to negative health outcomes for the individual and burdens healthcare systems across societies. To address the problem, this bachelor project will demonstrate a monitoring device based on optical technology. Optical technology can provide rapid, non-invasive real-time measurements of physiological states. The device is a "proof of concept" with the purpose of detecting dehydration before medical interventions are necessary so that preventative measures can be made. Firstly, the report will provide background information on 1) the problem's prevalence in society, 2) current clinical standards and 3) state-of-the-art literature on related optical measuring techniques. The latter is reviewed in order to eligibly define our hypotheses and establish our methodology with appropriate instrumentation tools. Next follows a theoretical chapter explaining the scientific concepts and principles of our hypotheses. Finally, the methodology and measuring technique is presented along with results and a discussion of future work.

2 Background Information

2.1 Dehydration in society

"Dehydration is one of the ten most frequent diagnoses responsible for the hospital admission of elderly in the United States" (Sfera, Cummings & Osorio, 2016). An estimation of hospitalization costs from dehydration admissions was found to be nearly 5.5 billion dollars in 2004 in the US (Kim, 2007). The condition is prevalent in long-term care facilities for elders, in both institutionalized and homecare, as found by Hooper, Downing, Jimoh & Bunn (2015) and Lešnik, Piko, Železnik & Bevc (2017), among others. Hooper et al. (2015) assessed 188 elderly living in residential care in the UK and found that 20% were dehydrated and 28% had impending dehydration. The average age was 87. Lešnik et al. (2017) compared dehydration among 192 patients in institutional care and 218 patients in homecare in Slovenia and found dehydration in 51% from institutional care and 41.3% from homecare. The average age was 82 and 78, respectively. Both studies used *serum osmolality* as a hydration marker, a method that will be addressed later. These findings are supported by numerous articles and papers following a quick search on "Google" including the terms *dehydration* and *elders*.

Consequences of dehydration are profound for the affected individual and puts a heavy burden on society. For the individual, the quality of life can be severely diminished as the condition is associated with falls, fractures, confusion, heat stress, constipation, urinary tract infections, kidney stones, renal failure, drug toxicity, stroke, and poor wound healing (Miller, 2015). For society, the condition burdens the healthcare system by consuming time and resources when, in most cases, the condition could have been prevented. It leads to longer hospital stays and increased staff workloads and can require costly and complex interventions involving a wide range of health professionals (Campbell, 2011).

Risk factors of dehydration are many. In older people, the risks are associated with reduced bodily functions. According to Hooper (2016) the most common contributing factors are diabetes, poor kidney function and reduced cognitive skills. The feeling of thirst is often absent or reduced, making it difficult for the individual to keep track of an adequate fluid intake ("Mange eldre er dehydrerte" [Many elders are dehydrated], 2016). Aside from older adults, risk of dehydration is higher among infants and young children with illnesses, people at any age having diarrhea, vomiting or fever and people performing strenuous exercise, particularly in hot weather ("Dehydrering, inntørring" [Dehydration, desiccation], 2018).

Consequently, resolving this healthcare problem has great potential of improving public health and reducing healthcare costs.

2.2 Current clinical standards

There are several methods to assess hydration status in a clinical setting today. Water is distributed in different places in the body, called *fluid compartments*, explained further in *chapter 3.2.2*. Some methods aim to measure these fluid compartments directly or indirectly and compare the sizes of compartments, while others rely on biomarkers estimating the concentration of solutes in blood or urine, or assess physiological signs and symptoms (Bak, Tsiami & Greene, 2017). The different techniques are often combined to provide a more accurate diagnosis. These will be shortly presented in the next subsections along with arguments of their strengths and weaknesses.

2.2.1 Physical signs and symptoms

Physical signs and symptoms are observed by doctors before blood or urine tests are performed. Changes in body weight is one of these symptoms. Rapid changes in body weight throughout the day is related to hydration levels because of the body's limitations of utilising *adipose* tissue, meaning fat, as energy. One litre water equals one kilogram water and therefore daily body weight monitoring, preferably after the first urine excretion and before the first meal of the day, can provide an assessment of hydration level in short periods of time before fat-burning become a factor (Bak et al., 2017).

Other physical features are consciousness level, dry armpits, dry mouth, sunken eyes, decreased skin elasticity, and delayed finger *capillary refill time*. Capillary refill time refers to applying a pressure to the fingertip, releasing the pressure and assessing the time it takes for colour to return. A study published in 2012 by a group of researchers from the University of Tsukuba, Japan, tested these features of dehydration on 27 elderly hydrated and dehydrated patients and compared the physical signs to blood and urine samples. The research calculated the sensitivity and specificity of the tests. The best indicator was dry armpits with a moderate sensitivity (44%) and high specificity (89%) (Shimizu et al., 2012). This means that this indicator is poor at diagnosing dehydration, but with high accuracy excludes dehydration.

Doctors tend to rely on physical symptoms and often diagnose dehydration without considering biochemical changes found in blood and urine samples (Bak et al., 2017). This can lead to wrong diagnosis and inappropriate treatment because the symptoms do not distinguish different types of dehydration. Physical symptoms are often associated with other normal diseases or physiological states but can be useful to suspect water and electrolyte imbalances. According to Bak et el. (2017), "the greatest limitation associated with assessment of signs and symptoms is the fact that most signs are subjective and there are usually no 'normal' ranges associated with them".

2.2.2 Isotopic tracers

This method directly measures the amount of total body water using i*sotope tracers*. These are radioactive compounds detectable, in this case, in a biological system. They are used to mark a material to study its progress and distribution through the system. The isotopic tracer must behave as the marked material and must have a distinguishable property so it can be detected in the presence of the marked material ("Isotopic tracers", 2018). By using samples of a known concentration of isotope tracers, it is possible to calculate the percentages of body water contained in various fluid compartments that add up to the total body water (Bak et al., 2017). Bromide is widely used as an isotope tracer. Bromides diffuse easily through capillaries, do not pass cell membranes and must not escape to the interstitial fluid compartment. This method relies on the assumption that fluid equally distributes throughout different fluid compartments if enough time is given (Bak et al., 2017). This method is the closest to a "gold standard" measurement of dehydration in a controlled environment where

several internal and external factors are considered. However, this method is complicated, costly, time consuming, radioactively hazardous and require a high level of expertise. It is an impractical technique during daily activities and require multiple measurements throughout one day. It is therefore not applicable in a clinical setting (Armstrong, 2007; Bak et al, 2017).

2.2.3 Blood tests

When dehydrated, the heart rate increases to compensate for the reduced blood volume. So does blood pressure in major blood vessels because capillaries tighten due to high blood-sodium concentration. Thus, due to a lack of water, blood has a high viscosity which deteriorate the effectiveness of blood circulation throughout the body (Unger, n.d.). The human body largely relies on adequate blood flow for exchange of nutrients and waste material (Bak et al. 2017). Increased consumption of sodium affects the amount of water intake required to maintain a stable sodium level (Armstrong, 2007). *Hypernatremia,* high sodium concentration in blood, may trigger the feeling of thirst to restore water balance, but is a mechanism that often fails in elderly, as mentioned previously (Bak, 2017).

It is important to differentiate water depletion versus salt and water depletion when considering the correct treatment. Water depletion is characterized with hypernatremia, hyperosmolality and high urine osmolality. Fluid in the veins and capillaries (*intravascular volume)* is maintained by movement of water from tissue (extracellular space) to the intravascular space. The extracellular space is sustained at the expense of the intracellular space (fluid inside cells).

Stated in "Osmolality (Blood)" (n.d.), the concentration of dissolved particles in blood can be measured from a blood sample. The test is called *serum osmolality*, or *plasma osmolality*, and indicates electrolyte and fluid imbalance. Osmolality increases during dehydration and decreases during fluid retention. Blood parameters have been used to describe hydration status since it is relatively easy to obtain with a blood sample by medical staff but is an invasive method of obtaining results, and a hospital or laboratory setting is required where necessary equipment is available. Armstrong (2007) questions the validity of using plasma osmolality (and body weight changes) as hydration markers, and states:

> In the laboratory, certain hydration assessment techniques are effective. Under controlled conditions (i.e., when experimental, postural, activity, dietary, and environmental factors are controlled), the total body water (TBW), volume of body fluid compartments, and extracellular fluid concentration stabilize. When body fluids are equilibrated, TBW and plasma osmolality provide objective measurements of volume and concentration at a single point in time. During daily activities or exercise, when fluid compartments are constantly fluctuating (i.e., volume and concentration), a direct evaluation of a single body fluid will not provide valid information about TBW and the concentration of body fluids. For example, several studies are presented in which Plasma osmolality does not track the gain or loss of TBW (p. 583S)

Even though blood parameters may not always be reliable in diagnosis until severe fluid loss occurs, they are used when carefully inspected (Bak et al., 2017).

2.2.4 Urine tests

In healthy subjects, diluted or concentrated urine is expected with increased or decreased water consumption, respectively. Colour of urine may be affected by various foods and medicines but can be an effective method to assess hydration in a setting where high precision is not required. The best tool to measure the concentration of solutes in urine is by measuring *urine osmolality*, meaning the concentration of solutes in urine, with an osmometer or by calculating the value by a predefined equation (Bak et. al, 2017). According to Kovac

(2015), the most important in the osmols in the urine are cations Na^+, K^+, NH_4^+ and their corresponding anions and urea. Urine osmolality can be found by calculating the number of solutes in a kilogram water.

Bak et. al (2017) refer to urine osmolality as the best indicator to determine the kidney's ability to filter waste material. However, it is a less reliable method to assess dehydration levels in a singular measurement as the concentration solutes is determined by many variables independent of water balance. Urine osmolality is affected by diet and varies between cultures. This assessment method is also less effective post exercise in a singular measurement but has been applied when monitoring hydration status over time. *Urine specific gravity* (USG) is also a parameter utilized to asses dehydration levels. It is described as a ratio of the weight of urine to the weight of same amount of water. Methods used to find USG includes *hydrometry*, *refractometry*, and *reagent strips*. In hydrometry, a large urine sample is required to determine the density and behaviour of urine. It is impractical and inaccurate since it requires daily calibration and is temperature sensitive. Refractometry utilizes optics to pass light through a small urine sample and measuring the angle of refraction. Reagent strips kits offers a simpler and cheaper method to measure USG. The strip is exposed to urine, and it reacts according to the acidity level and changes the colours of the strip and is compared to a colour chart determining USG (Jardine, 2018). Since urine specific gravity is related to urine osmolality the accuracy remains the same (Bak et al., 2017).

2.2.5 Bioelectrical impedance analysis

Bioelectrical impedance analysis (BIA) has been suggested as a simple, rapid method to assess changes in hydration status. The following two paragraphs are based on O'Brien et. al's study from 2002 and the article "What is bioimpedance?" by UiO Department of Physics (2011).

Impedance is the opposition a circuit presents to a current when a voltage is applied. BIA measures the electrical impedance to a low amperage current that is affected by both water and electrolyte content of the body. Tissue consists of cells and membranes, and membranes are thin but have a high resistivity and do electrically behave as small capacitors that stores electrical energy. By using high measuring frequencies, the current passes right through these capacitors, and the result is dependent on tissue and liquids both inside and outside the cells. Single frequency instruments of 50 kHz and multifrequency instruments use a range of frequencies from 5 to 500 kHz. At low frequencies, however, the membranes impede current flow, and the results are dependent only on liquids outside the cells. Bioimpedance can therefore be used to measure volumes, shapes or tissue's electrical properties.

Changes in fluid and electrolyte content can independently alter bioimpedance measurements. Because hydration changes typically involve changes in fluid and electrolyte content, the interpretation of a change in bioimpedance will often be confounded. Data indicate that current BIA methodology is not sufficiently accurate and reliable to assess total body water under conditions of hydration change.

2.3 State-of-the-art

During the search for scientific papers related to our project, we limited the results to papers assessing hydration status in human tissue by optical methods *in vivo*. We found most methods to fall within two categories; 1) Near-infrared spectroscopy and 2) Raman spectroscopy. These are both molecular spectroscopy techniques, meaning that interaction of electromagnetic radiation with matter at molecular level is studied, such as absorption, emission and vibration ("Molecular Spectroscopy", 2017).

2.3.1 Near-Infrared Spectroscopy (NIRS)

Attas et al. (2002) used NIRS to measure skin hydration *in vivo* on three different locations on the forearm of eight volunteers. One location was subjected to a drying agent, one was maintained neutral and the other was subjected to a moisturizer. The study found the following:

> "The results based on water absorption bands at three different NIR wavelengths (970, 1200, and 1450 nm) showed obvious differences in clarity and in the distribution of water in the skin. Changes in the skin water content were most evident in the images made using the band at 1450 nm and least evident in the images made using the band at 970 nm. The differences in the resulting images were interpreted as being the result of the different penetration depths of the IR light used in the reflectance studies."

The aim of this study was to evaluate the effectiveness of a new instrumentation tool for long wavelengths of NIR (1050 – 2500 nm). However, the study confirms NIRS as a method for detection of changes in water content of tissue through the absorption bands of water.

2.3.2 Raman spectroscopy

In Raman spectroscopy, the sample is irradiated with monochromatic light; a single frequency or wavelength. The inelastic scattering, which has a different frequency than the incident light, is a part of the scattered spectrum (Caspers, 2003). The shift in frequency is related to the vibrational modes of the molecules present. Caspers states that:

> Molecules may have a great number of independent vibrational modes, many of which can be excited by a Raman scattering event. This means that a molecule has a unique combination of vibrational modes and that its Raman spectrum is highly molecule specific.

He further explains that the number of Raman scattered photons are linearly proportional to the number of irradiated molecules and one can therefore quantify molecular bonds and identify molecular composition of the sample. In his study, he demonstrated that the concentration profile of water content across the outermost layer of the skin, the stratum corneum, in both thick and thin areas, can be found *in vivo* by confocal Raman spectroscopy.

2.4 Objectives of study

After exploring state-of-the-art literature related to our project, a stand-alone, conclusive method for determining hydration status in human tissue was not found. Nonetheless, while learning about the different spectroscopy techniques, the group came up with the idea of measuring temperature at the skin surface before, during and after exposure to infrared laser light. Our hypothesis is that when tissue is exposed to electromagnetic radiation of a specific wavelength, the various components of the tissue, like water, fat and protein, will absorb some of the radiation based on unique characteristics of the molecules. The light absorbed will increase the temperature of the skin by initiating vibrational motion, which is related to heat through kinetic energy. We have two hypotheses: 1) water will be the biggest contributor to the temperature increase due to its abundance, and 2) water will be the varying component while others are near static. We intend to measure when dehydrated versus hydrated. We expect a strong temperature increase when dehydrated because less water is present, and smaller temperature increase when hydrated because more water requires more energy for the same amount of heating. An infrared laser diode will be the light source and an infrared thermometer will measure the temperature. This method has little, or no prior research done, and so forth, this study is a 'proof of concept'.

3 Theory

This chapter will provide the scientific concepts, insights and theories our hypothesis is built upon. Firstly, the physiology of dehydration and anatomy of human skin will be investigated in order to eligibly analyse and discuss our results. Thereafter, we investigate the physical phenomena of electromagnetism, thereunder infrared radiation and its interaction with matter. This is followed by an examination of laser-tissue interaction and related heat transfer.

3.1 Physiology of dehydration

Dehydration occurs due to water deficiency in the body. Salt deficiency often accompany dehydration. The causes are low fluid intake or excess fluid loss through urine, sweat and evaporation from respiration (Hauge, 2018). Body fluids contain electrolytes, which are minerals or salts with an electric charge. Examples are sodium, calcium, potassium, chlorine, phosphate and magnesium (U.S. National Library of Medicine, 2018). The balance between water end electrolytes, referred to as the *body's fluid balance*, is important for the body to maintain a stable internal environment. This internal environment is governed by the body's tendency to self-regulate, named *homeostasis*, meaning that it adapts, responds and adjusts to outside conditions. Homeostatic processes regulate body temperature, water and acid/base (pH) level, transport nutrients and waste products to and from cells, and make sure nerves, muscles, heart and brain works correctly ("Homeostasis", n.d.). Dehydration destabilise this internal environment of the body resulting in adverse health effects, in worst case death. According to Physiopedia (2018), there are primarily three types of dehydration: *hypotonic* (primarily loss of electrolytes), *hypertonic* (primarily loss of water), and *isotonic* (equal loss of water and electrolytes). Isotonic is the most commonly seen in humans.

3.2.1 Total body water

The total body water (TBW) is not constant and depends upon several factors including gender, age, weight and relative amount of body fat (Nair & Peate, 2015). It varies between 50% to 75% of body weight, with infants born at around 75%. Adult men and women average around 60% and 55%, respectively (Helmenstine, 2018). "Dehydration" (2017) states that the average person loses about 2.5% of total body water during a day. The feeling of thirst occurs at around 2-3% while mental performance and physical coordination start impairing at 1% (Helmenstine, 2018). From "Vurdering av dehydrering hos voksne [Assessment of Dehydration in Adults]" (2016), a weight loss less than 5% is considered *mild* dehydration, 5-10% is considered *moderate* and more than 10% is considered *severe*. According to Hauge (2018), death occurs at around 20% fluid loss. According to the study by Péronnet et al. (2012), ingested water appears in plasma and blood cells within 5 minutes and is completely absorbed within approximately 75 to 120 minutes.

3.2.2 Distribution of body fluid

Body fluid is divided into two compartments based on distribution; *intracellular* and *extracellular* fluid. The intracellular fluid exists inside cells and comprises two-thirds of the total body fluid. The extracellular fluid comprises the remaining one-third and exists outside cells. Extracellular fluid is further divided into *plasma* and *interstitial* fluid (Nair & Peate, 2015). Plasma, also called *blood plasma*, is the liquid portion of blood consisting of water with different solutes like proteins, amino acids, hormones, salts and metabolites (Evensen, 2018). Interstitial fluid is the fluid in 'gaps' between cells and the blood vessels. Figure 1 illustrates the total distribution of body fluid.

Figure removed due to Copyright regulations.

Figure 1: Distribution of body water. Reprinted from *Anatomy and Physiology for nurses* in At a Glance, by M. Nair & I. Peate, 2015. Copyright 2013 by Muralitharan Nair and Ian Peate

The intracellular and extracellular fluid is separated by the *plasma membrane*. This membrane, also called the cell membrane or cell wall, separates the inside of the cell to the outside. It is semipermeable, meaning that selected molecules can penetrate. The selective permeability assists in maintaining the unique composition of fluid compartments and transport nutrients and waste products to and from cells (Nair & Peate, 2015), illustrated by the arrows in the Figure 1. This process will be explained in the section below.

3.2.3 Maintaining the body fluid balance

Water and molecules circulate by *diffusion* across the cell membranes. Diffusion means random movement of particles from regions of high concentration to regions of low concentration. Thus, changes in concentration of the intracellular or extracellular fluid changes the transport of nutrients and waste in and out of cells. Through a semipermeable membrane, the process is called *osmosis* and continues until the equilibrium concentration is reached (Shepherd, 2011, p. 13). Figure 2 illustrates this process. The pink fluid can penetrate the membrane but not the purple particles. Starting at different concentrations, the penetrable fluid will diffuse to the side with higher concentration until equilibrium is reached. This results in a pressure on each side of the membrane, defined as the pressure required to stop osmosis from happening. The pressure is determined by the molecules present in the solution (Kierulf, 2016, 2018).

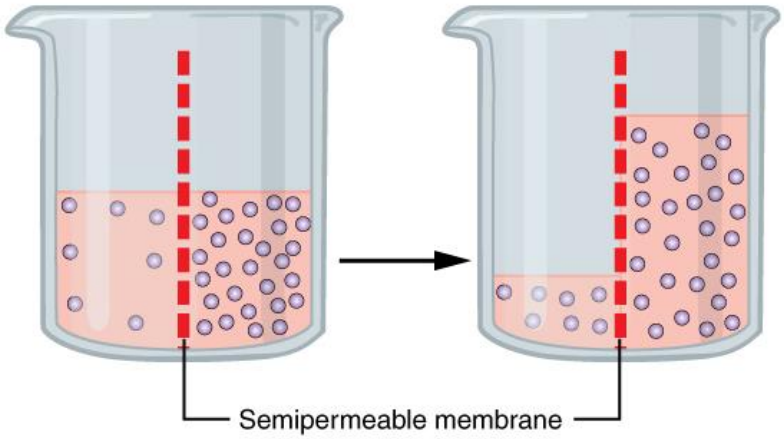

Figure 2: Osmosis. From *Wikipedia*. Retrieved from https://en.wikipedia.org/wiki/Osmosis. CC BY 4.0.

According to Kierulf, the osmotic pressure is tightly regulated by the kidneys to compensate for changes in water and salt concentration. As little as 1% change in water content of the blood is detected by nerve cells. Excessive fluid decreases the salt concentration in the blood and lowers the osmotic pressure. Fluid loss increases the salt concentration in the blood and raises the osmotic pressure. These osmotic pressure changes stimulate nerve cells telling the kidneys to contain or release fluid through urine secretion. During dehydration, this body mechanism is off-balance depriving cells of nutrients and accumulating waste.

3.2 Anatomy of human skin

To understand the response from the skin when irradiated with infrared light, we must know its shape and composition. From the "Great Medical Encyclopedia" article written by Langeland (2019), the human skin has three layers; the outermost layer: *epidermis*, the middle layer: *dermis*, and the innermost layer: *subcutis*, also called hypodermis. The different layers are illustrated in Figure 3.

Figure removed due to Copyright regulations.

Figure 3: Human skin layers. From *WebMD*. Retrieved from https://www.webmd.com/skin-problems-and-treatments/picture-of-the-skin#1. Copyright 2013 by WebMD LLC.

The epidermis ranges from 0.3 to 1.5 mm thickness. This layer is made up of cell layers lining the outer surface of the skin. 90% of these cells are keratinocytes which produce the protein *keratin*. Since this layer is not supplied by blood vessels, it receives nutrients through diffusion from the lower layer. The epidermis continually renews as the lower cells splits and pushes older cells outwards. During this process, called *cornification*, the cells 'mature', produce keratin, and are eventually filled with this protein. Finally, the cells die, and forms a keratin layer. This layer is the skin's protective barrier against the surroundings. The middle layer, dermis, ranges from 1.5 to 4 mm thickness. It provides strength and elasticity to the skin and is built from connective tissue. As a supplement to Langeland's article, University of Leeds (n.d.) and Fossum (2009) describe that connective tissue is composed of an extracellular matrix of fibers and 'ground substance' with cells in between. This 'ground substance' fills the space between the fibers and cells and is made up of large molecules that easily absorb water. Thus, the extracellular matrix is made up of 90% water. Further, Langeland (2019) describes that the dermis is richly supplied by blood vessels and nerve endings. The innermost layer, subcutis, is composed of fat and connective tissue. The thickness of this layer varies because the amount of fat varies with gender, diet and body weight. This skin layer also contains sebaceous glands and sweat glands.

3.3 Electromagnetism

Electromagnetism is a term most people are familiar with, but few really comprehend. The following text is largely based on Knight's book "Physics for Scientists and Engineers: With Modern Physics: A Strategic Approach" (2004) unless explicitly stated and aims to clarify this natural phenomenon.

3.3.1 Forces and fields

As stated in "Fundamental interaction" (2009), electromagnetism is one of the four fundamental forces that control how objects or particles interact. The other three are gravitational, strong and weak forces. Any interaction in nature can be traced back to one of these forces. Electromagnetism governs the science of charges and related forces and fields. Responsible for charges are electrons and protons, having the fundamental unit of charge, *e*, which are equal in magnitude but negative and positive, respectively. These charged particles exert forces on one another at a distance, called a *long-range force*, meaning that forces transmit through empty space. The mechanism of this force exertion is described as an *electrical* field, occurring at every point in space, said to "alter the space around the charge". A single charge is responsible for the electrical field, while in *magnetic* fields, *magnetic dipoles* are responsible. Magnetic dipoles, also called *magnets*, always have a positive and negative pole. The origin of this field is charges in *motion*. Thus, a magnetic field appears in addition to an electrical field and is why they are interrelated.

3.3.2 Radiation

Electromagnetic radiation, or waves, are *oscillations* of the electromagnetic field. All electromagnetic waves travel at the speed of light in vacuum, and transfer energy as all other waves. The average energy transfer over one oscillation, or cycle, is called the wave's intensity and the number of oscillations per second is called the frequency. Inversely proportional to frequency is wavelength. For clarification, the words *light*, *waves* and *radiation* are used interchangeably, but refers to the same physical phenomena of electromagnetic oscillations.

Light can be modelled in three ways: 1) the *wave model*, 2) the *ray model* and 3) the *photon model*. In the wave model, light is considered to have the same behaviour as mechanical waves, such as water waves. Thus, the radiation can be described with properties such as wavelength and frequency. In the ray model, light is considered to travel in a straight line. This is useful when describing direction, reflection and focus of lenses, especially in *optics*, referring to the study of light and its properties with related instrumentation. In the last model, light is considered a photon, which is a "bundle of light energy" ("Electromagnetic radiation", 2015), having both wave-like and particle-like properties. This is useful when studying energy interactions in atoms and molecules. We will make use of all models when describing laser-tissue interaction in later chapters.

Electromagnetic waves come at a range of different frequencies, or wavelengths, and are categorized accordingly on the *electromagnetic spectrum*. Starting at the largest wavelengths, comes radio waves, microwaves, infrared radiation, visible light, UV light, X-rays and gamma rays, see Figure 4.

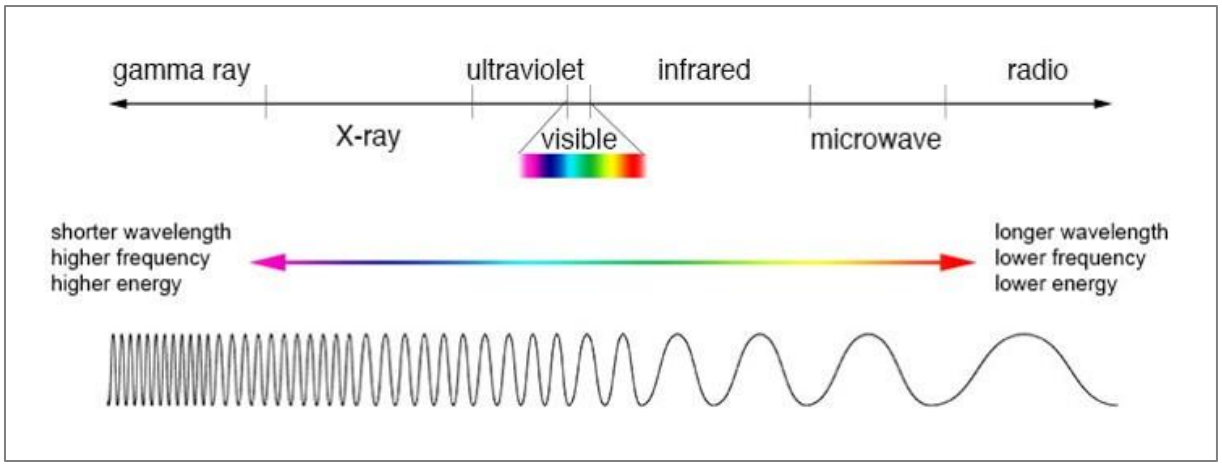

Figure 4: The electromagnetic spectrum. From *Humboldt State University*. Retrieved from http://gsp.humboldt.edu/olm_2015/Courses/GSP_216_Online/lesson1-2/spectrum.html. Copyright 2014 by Humboldt State University

3.3.2.1 Infrared Radiation

Our study revolves around infrared (IR) radiation, also called heat radiation or thermal radiation, which is present in all objects with a temperature above absolute zero. The temperature of the object determines the frequency and intensity of radiation (Grøn, 2018). Knight (2004) explains that the source of radiation is the movement of molecules and atoms, possessing what is called *thermal energy*. Thermal energy is defined as the average kinetic energy of all the moving atoms and molecules and the potential energy stored in molecular bonds. As the thermal energy changes, due to energy transfers to or from surroundings, so does electromagnetic radiation and temperature of the object (an exemption to temperature change is when phase change occurs).

Shorter wavelengths of IR, from around 700 to 2500 nm, is called the *near-infrared (NIR)* region. This is our region of interest because various molecules in the human body possess distinctive absorption characteristics in this range, which enables optical monitoring of physiological processes (Bronzino, 2006, p. 71-1). Water is the target molecule of our study.

3.4 Temperature response of IR absorption

In a single atom, the electrons transit between orbitals called *electronic* energy levels, or states. According to Ashenhurst (2016), when atoms come together to form a molecule, the molecular bonds introduce a form of energy called *vibrational energy*. He visualizes this by imagining the bond as a mechanical spring that can vibrate. This vibration includes motions of stretching, bending and twisting among others. Vibrational motions are part of the kinetic energy in matter, and thus, introducing vibrational motion in molecules increases its thermal energy.

Energy required to induce vibration is quantified, having discrete values, just as for electronic energy levels (Ashenhurst, 2016). Figure 5 visualise vibrational energy levels as sublevels within electronic states.

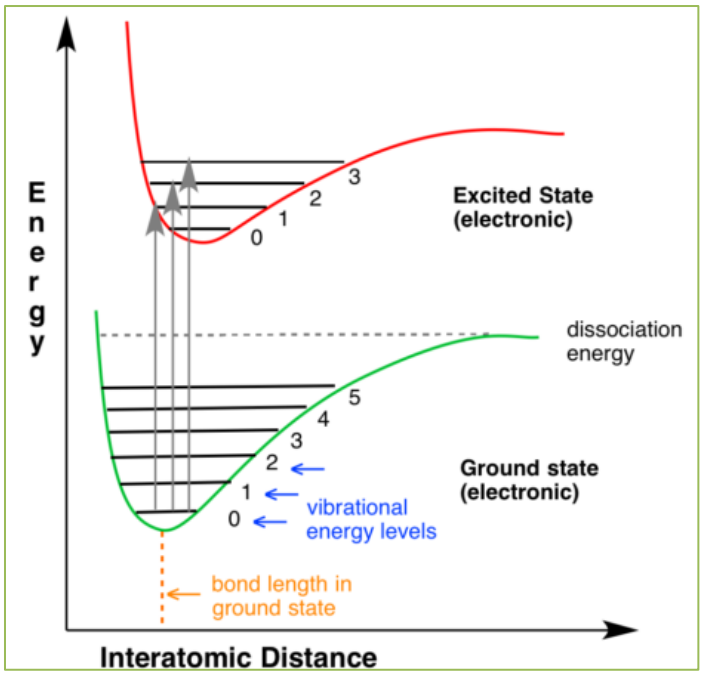

Figure 5: Electronic and vibrational energy levels. From *Master Organic Chemistry*. Retrieved from https://www.masterorganicchemistry.com/2016/11/11/bond-vibrations-*ir-spectroscopy/*

The 'dissociation' line in the Figure 5 represents the amount of energy required to break the molecular bond. Knight (2004) states that vibrational excitation can be induced by the absorbance of photons with an energy corresponding to the difference between vibrational levels. These photons are usually in the infrared region of the electromagnetic spectrum.

According to Foist (n.d.), each chemical bond in a molecule has unique vibrational modes that leads to unique fingerprints, called *absorption bands*, at these specific frequencies or wavelengths in the spectrum. Relevant to our study, is water absorption, which displays similar absorption characteristics as human skin in the near-infrared region, see Figure 6. From these characteristics, we believe that water content in human skin will strongly influence absorbance ability, which in turn influences the temperature response.

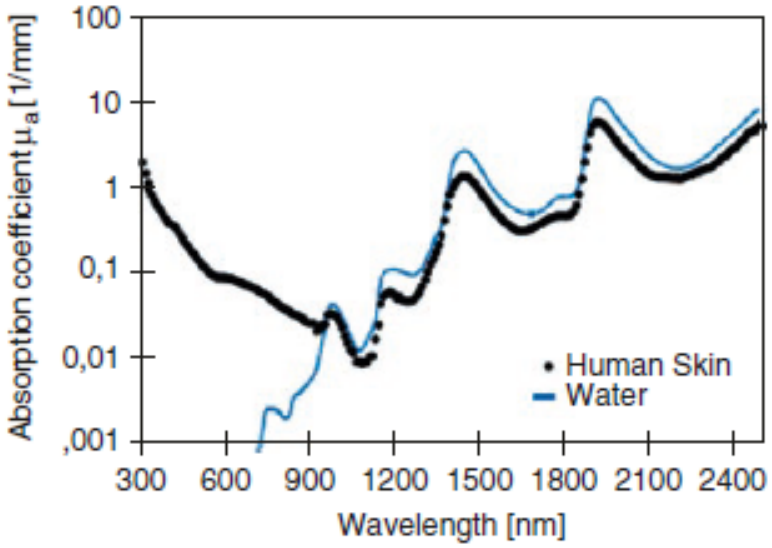

Figure 6: Absorption characteristics of human skin and water in the near-infrared region. Reprinted from *Optical Imaging* (p. 429), by Alves et. al. (2017).

3.5 Mechanisms of laser-tissue interaction

Lasers are widely used in biology and medicine. The word *laser* is an acronym, an abbreviation, of "Light Amplification by the Stimulated Emission of Radiation" (Hecht, 2018). In a laser, atoms and molecules are stimulated by a power source to emit light at specific wavelengths, thus producing *monochromatic* light. This means that it consists of a single wavelength or frequency ("Monochromatic", n.d.). The purpose is to control light to deliver a concentrated beam for different applications.

Medical lasers can be divided into *therapeutic* and *diagnostic* branches. The main difference is in the interaction between lasers and tissue. In diagnosis, the aim is to study the behaviour of tissue non-invasively, not damaging the tissue. In therapy, lasers are used to affect a specific region for treatment, such as cutting during surgery or destroying cancer tissue (Ansari & Mohajerani, 2011; NCI Dictionary of Cancer Terms, n.d.). This chapter will focus on optical properties of lasers' interaction with tissue with a diagnostic approach.

3.5.1 Propagation in tissue

When light is propagated in tissue, four optical phenomena are present: *reflection*, *scattering*, *transmission* and *absorption*, shown in Figure 7. Reflection refers to the repelling of light on the tissue surface without entering the tissue. Approximately 4% to 7% of light over the entire spectrum of 250 nm to 3000 nm are reflected off the skin, for both dark and light skin (Anderson & Parrish, 1981). The amount of light reflected increases with increasing laser angle to the surface, with the least reflection when the laser bream is directed perpendicular to the tissue. Scattering of light occurs after light has entered the tissue. Scattering is due to the heterogenous structure of tissue, with variations in particle size and refraction properties between different parts of the tissue determining the amount of scatter. Scattering diffuse the beam of light within the tissue, resulting in a larger radiation area than anticipated. Scattering also limits the depth of penetration because it can occur backward as well as forward. *Transmission* refer to the light that passes through the tissue without having any effect on the tissue or the properties of the light. The laser's behaviour in interaction with biological tissue mainly depends on the laser's wavelength due to absorption peaks of biomolecules (Carroll & Humphreys, 2006).

Figure removed due to Copyright regulations.

Figure 7: Optical phenomena of laser-tissue interaction. From *Pocket Dentistry*. Retrieved from https://pocketdentistry.com/laser-fundamentals

3.5.2 Penetration depth

In general, the amount of scattering when a laser enters a medium, is characterized by the average scattering coefficient of the tissue. This is inversely proportional to the wavelength of the laser. Thus, longer wavelengths penetrate deeper in tissue than shorter wavelengths. An exception to this rule is wavelengths beyond 1300 nm, in the mid infrared region, barely penetrating epidermis (Carroll, & Humphreys, 2006). Figure 8 shows the penetration depths of various wavelengths. The depth of radiation penetration also depends on the photon absorption process characterized by the wavelength dependent absorption coefficient of the tissue, that provides the energy conversion of the photon to the cell (Ash et.al., 2017). Figure 9 show the relation between absorption and wavelength of the laser in different tissue components.

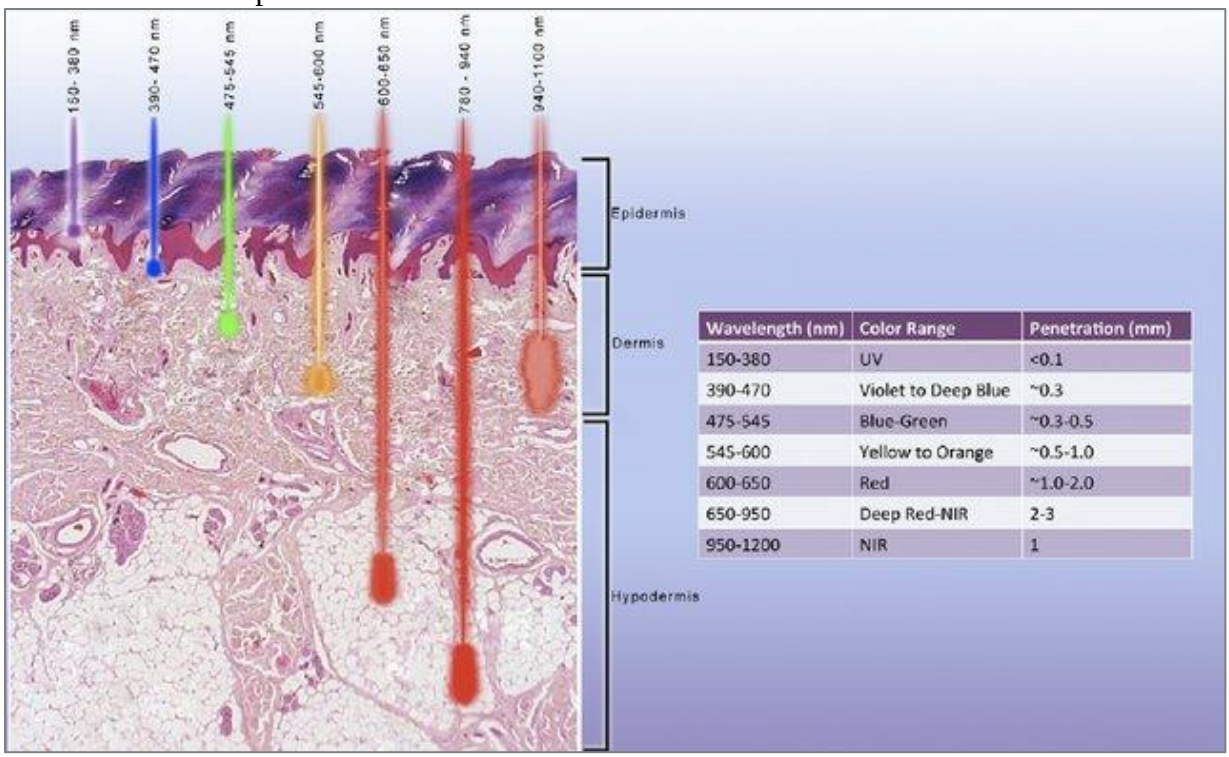

Figure 8: Tissue penetration depths of various wavelengths. Reprinted from "Low-Level Laser (Light) Therapy (LLLT) in Skin: Stimulating, Healing, Restoring", by P. Avci et al., 2017, *Seminars in Cutaneous Medicine and Surgery, 32(1),* 44.

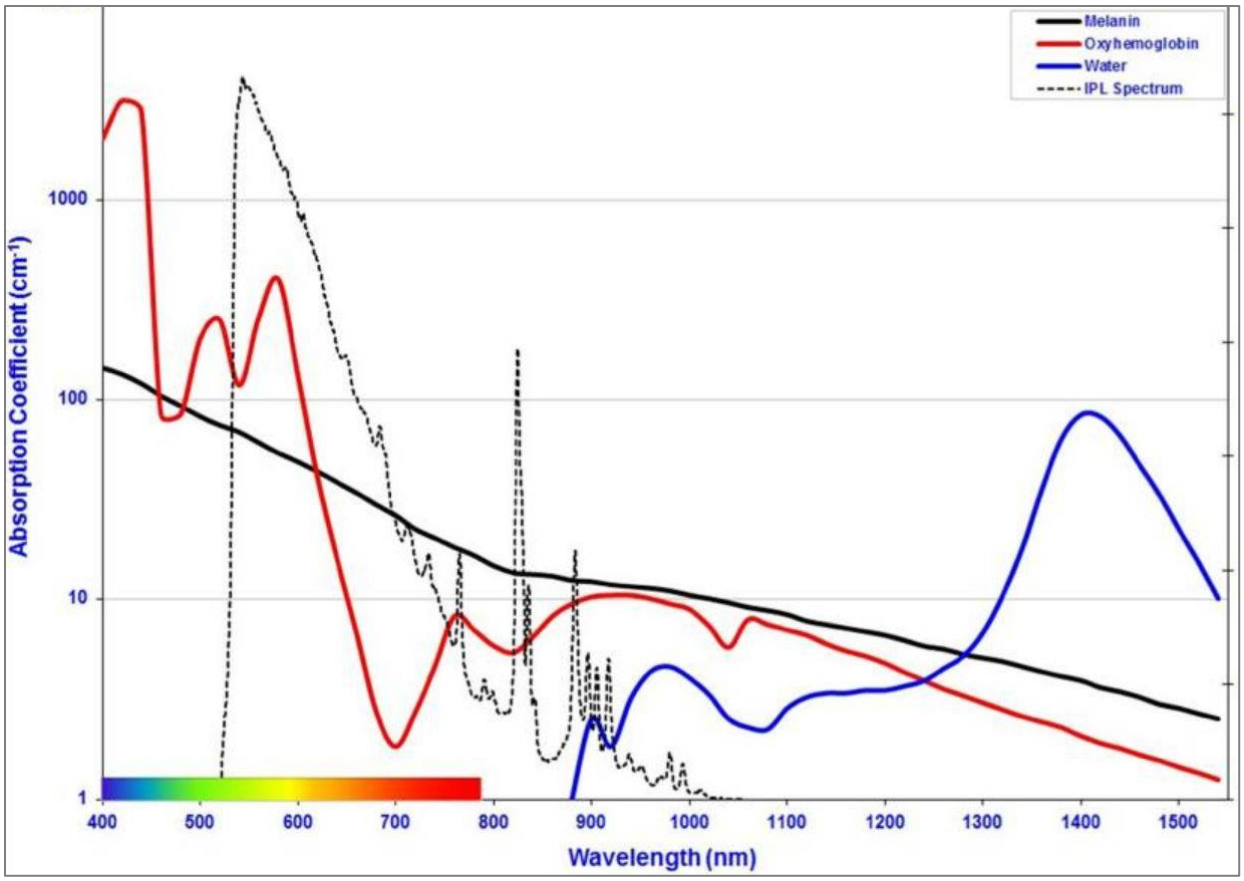

Figure 9: Absorption coefficients of melanin, oxyhemoglobin and water. Reprinted from "Effect of wavelength and beam width on penetration in light-tissue interaction using computational methods", by C. Ash, M. Dubec, K. Donne & T. Bashford, 2017, *Lasers in medical science, 32(8),* 1912. Copyright 2017 by the Authors

3.5.3 Beam form

Most skin affecting lasers produce a beam with a Gaussian profile where the intensity is at its strongest at the centre and dissipate at the periphery. Clinically, this beam form deliver energy to the tissue in a more uniform way. Another beam form is a doughnut-shaped or target-shaped laser beam with the intensity of the laser at the edge of the beam being greater than the centre. These beam forms, shown in Figure 10, tend to have a more constant intensity profile than the gaussian beam form (Carroll, & Humphreys, 2006).

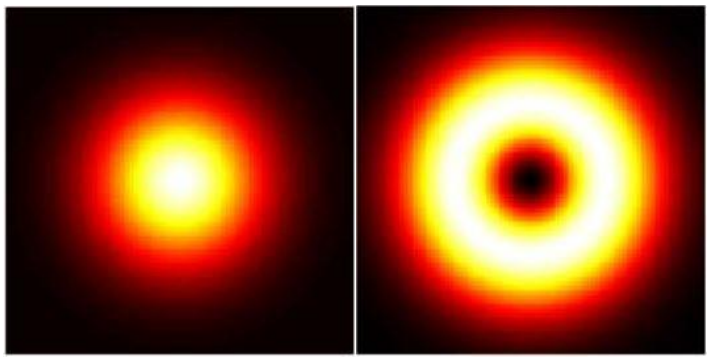

Figure 10: Beam form. From *BiteSizeBio.* Retrieved from https://bitesizebio.com/21988/the-power-of-sted-microscopy-part-1-how-does-it-work/

The cross-section of the laser, also called the spot size, is important because of laser scattering. The spot size directly affects the laser's *fluence* and *irradiance*. Fluence is defined as optical energy [J] per unit area, while irradiance is defined as radiant flux, which is the power [W] (energy per unit time) received by a surface per unit area (Paschotta, n.d).

In Figure 11, the fluence rate of photons with wavelength of 780 nm launched at the angle of 60 degrees to the tissue surface shows the scattering trajectory of the high intensity photons, in red colour, on a simulated two-layered tissue.

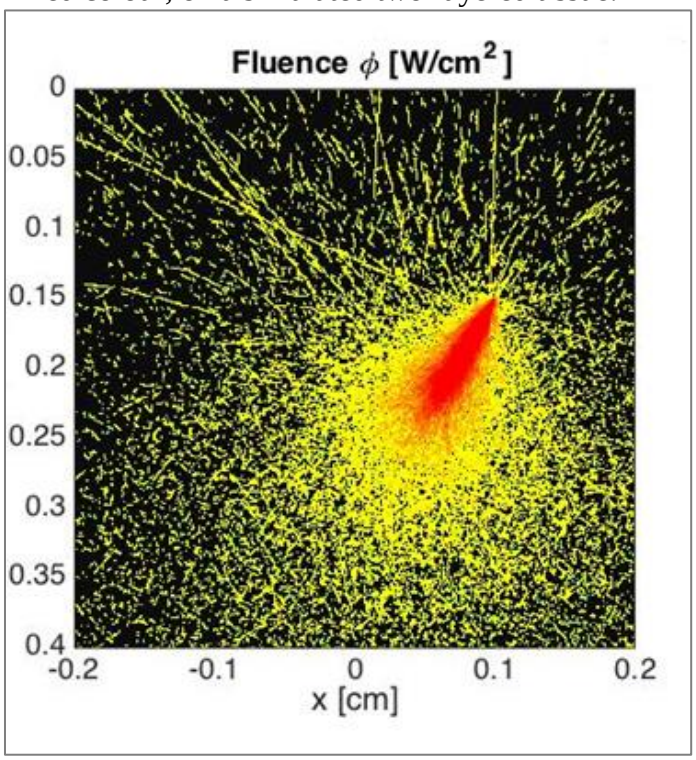

Figure 11: Fluence rate and trajectory of photons with the wavelength of 780 nm at a 60-degree angle (Mirtaheri P., personal communication, April 30, 2019)

By shrinking the spot size, the energy density or power density increases by a factor of 4, since the units are inversely proportional to the square of the radius of the spot size. A small spot size allows for more scattering in all directions than a larger spot size. This result in a faster energy reduction in tissue. (Carroll & Humphreys, 2006). According to Ash (2017), a beam width of 4 to 6 mm is usually used to penetrate to the mid-dermal and deeper layers of skin where blood vessels resides. Although penetration depth increases with a larger spot size, at 5 to 12 mm, there is a limit where increasing the spot size has no effect on penetration depth. For a smaller spot size, increased laser intensity at the target is recommended to maintain penetration depth.

3.5.4 Photothermolysis

According to the first law in photochemistry, Grotthus-Drapers law: for light to produce an effect on material, it must be absorbed. The second law, Stark-Einstein law states: one resultant primary physical or chemical act occurs per photon absorbed (Burton et al., 2014). The absorption of photons inevitably produces an effect in tissue. The light-absorbing tissue components are known as *chromophores* and absorb light differently depending on type of chromophore and wavelength of the laser. Absorption occurs when the laser frequency matches with the frequency associated with the molecule's energy transition. Often targeted chromophores in skin are melanin, haemoglobin, water and tattoo ink. The energy absorbed by a chromophore results in conversion from vibrational movement to thermal energy when electrons interact with neighbouring atoms ("Tissue optical properties", n.d.).

Even though photothermolysis is a therapeutic treatment used for tissue destruction, its concept of targeting specific chromophores, such as water, and relaxation time relevant to this study. The theory of photothermolysis states that the laser energy is absorbed by a target chromophore without causing significant damage to surrounding tissue and is used in a range

of therapeutic treatments. This can be achieved by regulating fluence, pulse width and wavelength of the laser. If the pulse duration is shorter than the relaxation time of the chromophore, one can prevent spread of thermal energy beyond the target chromophore. Thermal relaxation time is defined as the time needed for the target chromophore to cool to half its peak temperature after laser irradiation. To achieve heat diffusion in tissue by a laser, the pulse duration must be longer than the relaxation time of the tissue, but thermal damage can occur due to heat diffusion. (Carroll & Humphreys, 2006). Thermal relaxation time of water is shown in Figure 12.

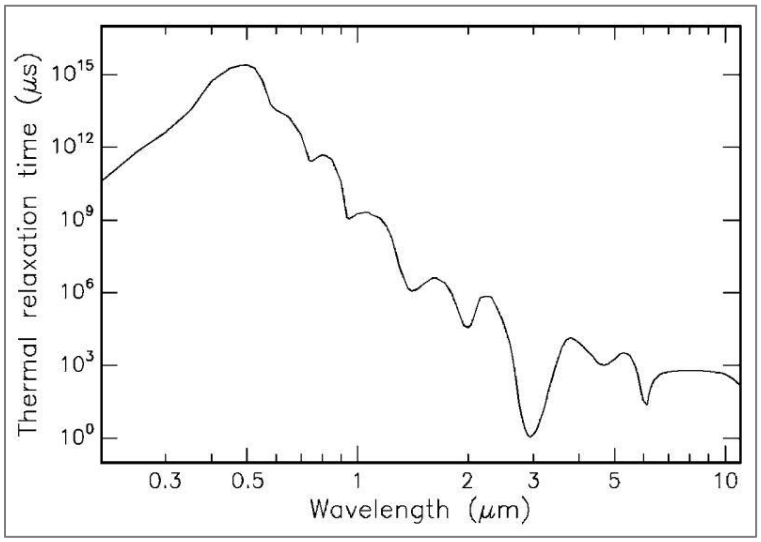

Figure 12: Thermal relaxation time of water is dependent on laser wavelength. Reprinted from *Laser-tissue interactions: Fundamentals and applications*, by M. H. Niemz, 1996, p. 73, Berlin: Springer.

3.6 Heat transfer in tissue

Understanding exact geometry of vessel network and its effect on temperature distribution in living tissues is one of the most complicated problems of the bioheat field, due to the many factors that are in play (Kashcooli et. al., 2017). In 1948, Harry Penne developed Penne's bioheat transfer equation, that has been the standard model for heat distribution in tissue for more than half a century. The equation describes the heat exchange between blood flow and solid tissues. Penne conducted a series of experiments that measured the temperature on human forearms and derived an equation including local tissue temperature, arterial temperature, blood specific heat, tissue specific heat, local tissue-blood perfusion rate, and the tissue's thermal conductivity. Even though the equation is an approximation, and does not have a physically consistent theoretical basis, it did predict temperature fields well in many applications (Huang & Horng, 2015). Penne's model is still used in research papers today where the equation has been investigated and expanded on to support theories on bioheat transfer, as well as new heat transfer models are emerging for different scientific purposes.

In theory, by using laser as a heat energy source, when applied to the surface of the skin the temperature should rise. Heat generation on tissue from a laser is determined by laser parameters and optical tissue properties such as irradiance, exposure time and the absorption coefficient. Heat transport is characterized by thermal tissue properties, such as heat conductivity and heat capacity. In real-life laser-tissue interaction there are heat loss to be considered. They are based on heat conduction, heat convection, or heat radiation, though the latter two can be neglected in most laser applications. One example of heat convection in tissue is heat transfer due to blood flow, as seen in Table 1, but due to low perfusivity of most tissue, heat convection is often negligible (Niemz, 1996).

Tissue	Perfusion rate (ml $min^{-1} g^{-1}$)
Fat	0.012 – 0.015
Muscle	0.02 – 0.07
Skin	0.15 – 0.5
Brain	0.46 – 1.0
Kidney	$\simeq$ 3.4
Thyroid gland	$\simeq$ 4.0

Table 1: Blood perfusion rates on selected human organs. Reprinted from *Laser-tissue interactions: Fundamentals and applications*, by M. H. Niemz, 1996, p. 69, Berlin: Springer.

Heat conduction, on the other hand, is the primary mechanisms for heat transfer to unexposed tissue structures. Heat capacity and thermal conductivity are important parameters used to describe the dynamics of temperature behaviour in tissue and materials (Niemz, 1996).

Specific heat capacity is the relationship between heat energy [kJ] exchanged per weight unit [kg] of a substance and the corresponding temperature change [^{o}C]. The specific heat capacity of water is 4.18 and of the human body (blood and tissues) 3.49, respectively, which means that 1 kg water need 4.18 kJ of energy to increase the temperature by 1^{o}C, and blood and tissue need 3.49 kJ of energy for the same temperature increase (Zubieta-Calleja & Paulev, 1998). Table 2 shows the heat capacity average of various tissues.

Tissue type	**Average heat capacity (J kg^{-1} $^{o}C^{-1}$)**
Blood	3617
Blood vessel wall	3930
Fat	2348
Muscle	3421
Nerve	3613
Skin	3391
Water	4178

Table 2: Average heat capacity in tissue. From *IT'IS Foundation*. Retrieved from https://itis.swiss/virtual-population/tissue-properties/database/heat-capacity/. (Hasgall et. al, n.d.). Copyright 2010-2019 by IT'IS Foundation

Heat conductivity (k) of a material is defined by how fast a material can diffuse heat. It is described as a thermal energy transferred in a certain amount of time, through the thickness and surface area of a material due to the temperature difference between two interacting objects (Burger et al., 2018). Heat conductivity can be derived from the equation for thermal conduction (Equation 1):

$$\frac{Q}{t} = \frac{kA\Delta T}{d} \qquad (1)$$

Q [J] is the amount of energy transferred in a time t [s], k is the thermal conductivity constant for a material, A [m²] is the surface area transferring heat, ΔT [^{o}C] is the initial temperature difference in materials, and d [m] is the thickness ("What is thermal conductivity", n.d.). As shown table 3 below, the thermal conductivity constant k is larger for materials that transfers heat well.

Tissue type	Average thermal conductivity k (W m^{-1} $°C^{-1}$)
Blood	0.52
Blood vessel wall	0.46
Fat	0.21
Muscle	0.49
Nerve	0.49
Skin	0.37
Water	0.60

Table 3: Average thermal conductivity in tissue. From *IT'IS Foundation*. Retrieved from https://itis.swiss/virtual-population/tissue-properties/database/thermal-conductivity/. (Hasgall et. al, n.d.). Copyright 2010-2019 by IT'IS Foundation

The thermal properties are approximately same for water and most tissues since human tissue consist of such high amounts of water. Thus, a decrease in heat conductivity due to a low water content is compensated with a parallel decrease in heat capacity of tissue (Niemz, 1996).

Based on these principles of heat transfer in tissue, we hope to find a correlation between water content and temperature changes.

3.7 Laser safety

Exposure to laser light can be hazardous and can cause severe eye injuries and damage the skin. The biological effects of laser light may depend, as stated in the University of Washington's laser manual (University of Washington, 2007), on a number of factors including the wavelength of the light, its power, whether it possesses a continuous wave nature (CW) or pulsed, or whether it is the result of a direct exposure of laser light rather than a diffuse reflection. Therefore, all lasers are classified in certain safety classes. There are three main standards that are used when classifying laser lights. These are The American National Standards Institute (ANSI) standard, The Center for Devices and Radiological Health (CDRH) standard and The International Electrotechnical Commission (IEC) standard. (Rockwell Laser Industries, n.d.). More information on these standards are found in Appendix B.

The lasers used in this experiment are a 780 nm 10 mW laser diode and a 980 nm 30 mW laser diode. These are both within the classification of IEC standard class 3B. The 3B class is defined as:

> Moderate power lasers (CW: up to 500mW, Pulsed up to 30mJ) in wavelength range of 300 nm to far infrared. Direct eye exposure to Class 3B lasers is hazardous; however, diffusely scattered radiation is generally safe. Direct exposure to skin is a potential hazard." (National Laser Company, n.d.).

3.8 Ethical considerations

Exposing the human skin to laser radiation introduce ethical questions and considerations. The ethical research guidelines of OsloMet, "Etiske retningslinjer for forskning ved OsloMet - storbyuniversitetet (OsloMet)" [Ethical guidelines for research at OsloMet – Oslo Metropolitan University] (2014), regards scientific misconduct, research ethics and respect for intellectual property, crediting authors, co-authors and publishers of original work.

Class 3B lasers are described as potentially hazardous with direct exposure to the skin. The applied laser diodes are in the lower end of the power range of class 3B, and thus, we considered the health risks of skin exposure negligible. All tests were performed on the authors voluntarily with their consent.

4 Materials and Methods

This chapter will provide the details on materials and device setup, software, test procedures and methods used to analyse the test results.

4.1 Equipment and tool list

Equipment			
Qty	**Part number**	**Description**	**Vendor**
1	N/A	Laser 780 nm 10 mW with driver	eBay
1	N/A	Laser 980 nm 30 mW with driver	eBay
2	MLX90614	Infrared thermometer	eBay
2	N/A	Raspberry Pi Zero W	eBay
2	1RFZ44N	N-channel MOSFET	eBay
2	N/A	Resistor 270 Ω	eBay
1	N/A	Wire Jumper Pin Header Connectors 2.54 mm Housing Female Kit	eBay
1	N/A	Ethernet cable (stripped)	N/A
1	N/A	Heat shrink tube	N/A
1	N/A	Solder	N/A
1	N/A	Hot glue sticks	N/A
1	N/A	2 mm generic plastic sheet	N/A
1	N/A	Self-Adhesive Velvet Flock paper (anti-reflective)	eBay
1	N/A	USB cable A to micro B	N/A
1	N/A	Steel wire 1 mm	N/A
1	N/A	Elastic strap for armband	N/A

Table 4: Equipment list

Tools			
Qty	**Part number**	**Description**	**Manufacturer**
1	WECR-20	Soldering station	Weller
1	N/A	Hot air gun	Generic
1	C12DD	Cordless drill	Milwaukee
1	N/A	Drill bits in various sizes	Generic
1	N/A	Sheet metal shearer	Generic
1	N/A	Hot glue gun	Generic
1	N/A	Vernier calliper	Generic

Table 5: Tool list

Software		
	Description	**Manufacturer**
	Excel	Microsoft Office
	PyCharm (Python IDE)	JetBrains

Table 6: Software List

To craft our test devices, equipment and tools from Table 4 and 5 were used. A 2 mm plastic sheet was cut, drilled and heated to form the mounts for the lasers and thermometer, which was glued on. Wires and electronic components were soldered and wired according to the descriptions in the hardware schematics and setup (See chapter 4.4 and 4.5).

4.2 Main components

4.2.1 Infrared thermometer

The MLX90614 by Melexis is an infrared temperature sensor used for a wide variety of applications. It is low-cost and has a small footprint with an accuracy of 0.5 °C in the range of 0 to 50°C. The measurement resolution is 0.02°C. The thermometer consists of a *thermopile* detector and a signal processor. Thermopile refers to serial connected *thermo-couples* giving an average temperature measurement from each thermo-couple. This yields higher sensitivity and greater output.

Figure 13: MLX90614 on a pcb. From *eBay*. Retrieved from https://www.ebay.com/itm/MLX90614ESF-BAA-GY906-MLX90614-Contactless-Temperature-Sensor-Module-for-Arduino/183649183999?epid=2293138168&hash=item2ac25828ff:g:yjIAAOSwAopbaWQy

The signal processor converts the low voltage of the thermopile into a digital value with a 17-bit analogue-to-digital converter and outputs through the System Management Bus (SMBus). The Infrared thermometer uses a 3.3V supply voltage and a 2-wire SMBus for connection. For further information, see datasheet at Melexis' official website.

4.2.1.1 Calibration of IR thermometer

In order to verify the accuracy, linearity and sensitivity of the thermometer, we performed a calibration at "Kiwa Teknologisk Institutt" [Kiwa Institute of Technology] facility in Oslo. We received help from one of their calibration engineers and used the "Fluke Calibration 4180 Precision Infrared Calibrator". We followed their internal procedure, called "Kalibrering av IR termometer, Dok ID 2379" [Calibration of IR Thermometer, Doc. ID 2379], which is similar to Fluke's application note: "Infrared Thermometer Calibration – A Complete Guide", which can be accessed through their official webpage.

In our armband device, the thermometer is placed approximately 1 cm from the skin. With that in mind, we placed the thermometer 1 cm from the calibrator's surface and adjusted the emissivity to 0.98 instead of the most used standard 0.95. This adjustment was made in consultation with the engineer on sight. Because the thermometer is being used to read the temperature of the human skin, we calibrated the sensor in the range of 30°C to 40°C.

After setting the temperature on the calibrator's surface, we gathered 10 readings of the surface temperature with our thermometer. This was repeated for increments of 0.5°C in the range of 30 to 40°C.

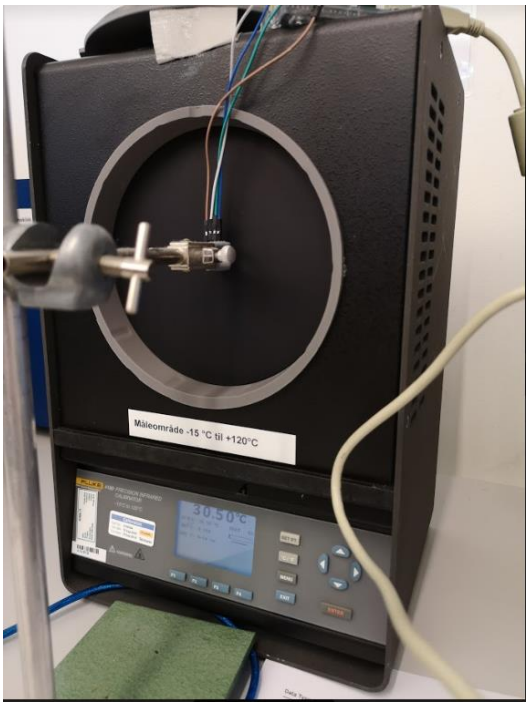

Figure 14: The setup of the calibration, with the thermometer set approximately 1 cm from the calibrators surface. March 8, 2019.

We tested three different temperature sensors of the MLX90614 type and used the most consistent one in our device. Figure 15 shows a plot of the temperature deviations from true temperature of *Temperature sensor 1*, which is the one we used in our experiment:

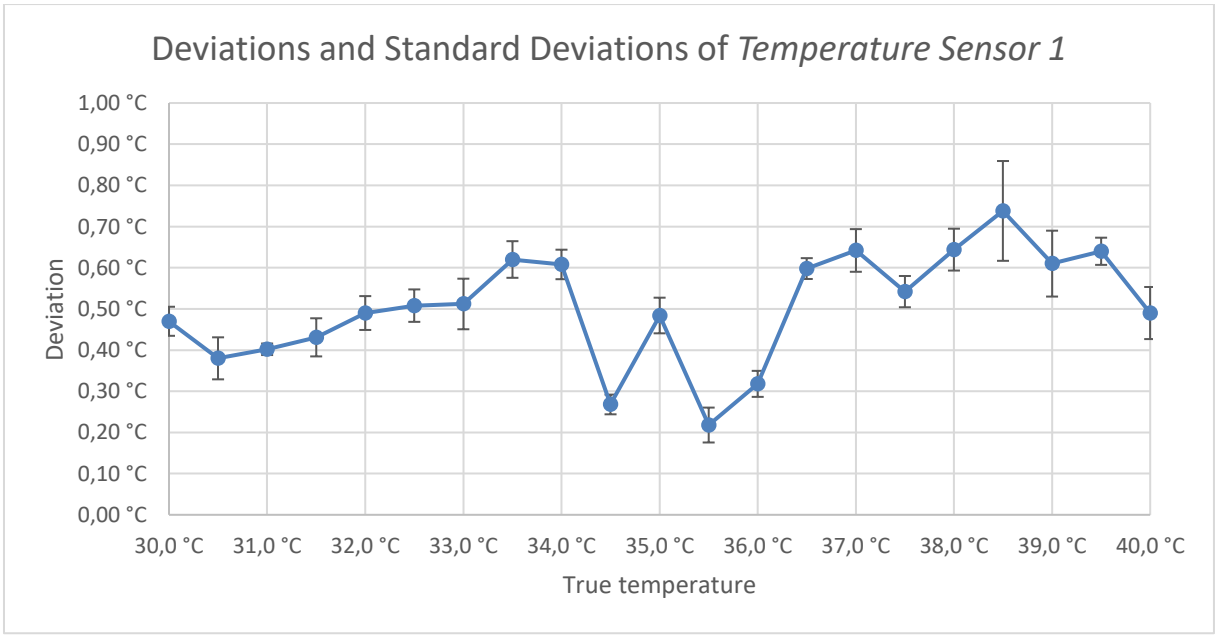

Figure 15: All temperatures are in accordance with ITS-90. The data points in the plot are the average of 10 measurements. Uncertainty in IR reference is 0.30 °C (Coverage probability of approx. 95%). The graph shows the measured temperatures' deviation from true temperature with standard deviations shown in the error bars.

As displayed in Figure 15, the largest deviation from true temperature occurs at 38.5°C. It deviates with 0.74°C $\pm$ 0.12°C. We expect to measure temperatures below this value at the skin surface because extremities display lower temperatures than the average body temperature of 37°C. The deviations are smaller at lower temperatures, and we do not

expect these deviations to impact the measurements significantly. See appendix C for complete certificate of Calibration.

4.2.2 Laser diode

To irradiate the skin, we use *laser diodes* of two different wavelengths; 780 nm and 980 nm. They are used in separate setups consisting of one laser diode and a laser *driver*. A laser diode is a semiconductor device made of two different materials. One a *P-material*, the other an *N-material*, sandwiched together. The P-material carries positive 'holes' from missing electrons. The N-material carries extra negatively charged electrons. Establishing a voltage across the P-N junction, connecting the P-material to a positive terminal and the N-material to a negative terminal, called *forward electrical bias*, causes the respective holes and electrons from opposite sides to combine giving off a photon in the process. A laser driver is used to provide constant current to the laser diodes. This is necessary because laser diodes are current sensitive semiconductors where any instability in the drive current will affect the laser diode's performance characteristics. Specifically, it will affect the output power and wavelength (Laser Lab Source, n.d.).

Figure removed due to Copyright regulations.

Figure 16: Laser diode construction. From *Elprocus.* Retrieved from https://www.elprocus.com/laser-diode-construction-working-applications/

Figure 17: 780 nm and 980 nm lasers used in the dehydration monitoring device. From *eBay*. Retrieved from https://www.ebay.com/itm/5pcs-Laserland-8-13mm-10mW-780nm-IR-Infrared-Dot-Laser-Diode-Module-LD-3vdc-5vdc/131802751657?hash=item1eb00e62a9:g:iH4AAOSw-kdXz5YT and https://www.ebay.com/itm/980nm-30mW-Infrared-IR-Laser-Diode-dot-Module-TTL-0-15KHZ-12x40mm/122227588631?epid=1167872982&hash=item1c7554fe17:g:nXwAAOSwxIRZ5v0O

4.2.3 Raspberry Pi Zero

The *Raspberry Pi Zero* is one of the newest members in the Raspberry Pi family of small and affordable computers. The Zero has 1 GHz single-core CPU (*central processing unit*) with 512 MB of RAM (*random-access memory*). It has various peripheral bus communication systems to connect with a wide range of sensors, cameras and other types of hardware. In this project, the SMBus (*System Management Bus*) is being used to communicate with the MLX90614 infrared thermometer. The SMBus is a derivative of the more known I2C bus, which is a communication system designed for easy communication between components on the same circuit board ("I2C – What's That?", n.d.), and use the same pins (3V3, Ground, SDA and SCL). It can also be used in connection with components through cables.

Various operating systems can be installed specific to the intended usage of the Zero. In this project, the *Raspbian* operating system is installed, much because it has the most user-friendly graphical interface for our application (for installation and setup of Raspbian, please refer to Appendix D). Figure 18 shows a photo of the minicomputer and a map of the connection pins and their application. There are 40 pins, and the ones used to control hardware are called GPIO-pins (*General Purpose Input/Output*). All the pins are numbered from 1 through to 40, but each also has a name. They can be referenced by either.

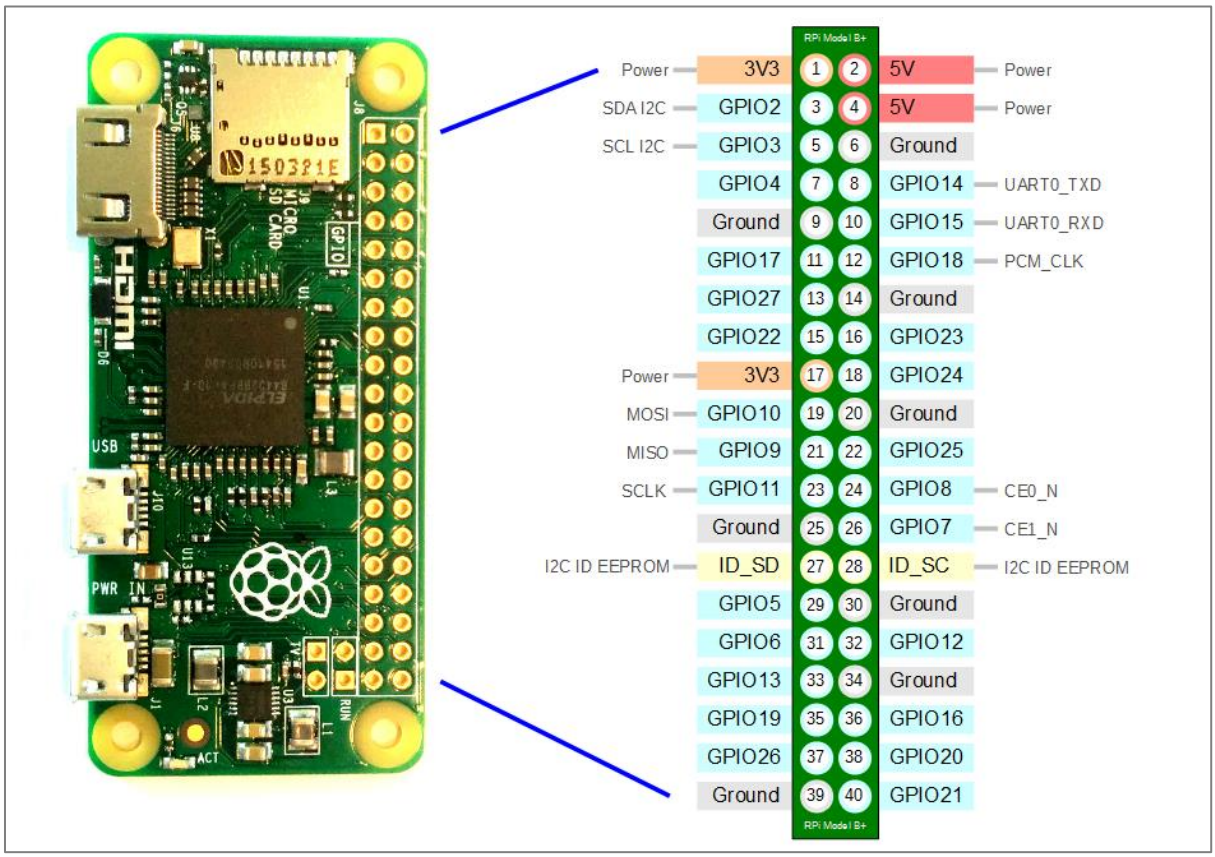

Figure 18: Raspberry Pi Zero and GPIO pinout orientation. From *Raspberry Pi Stack Exchange.* Retrieved from https://raspberrypi.stackexchange.com/questions/83610/gpio-pinout-orientation-raspberypi-zero-w

4.3 Target area

The reason for choosing the earlobe as a measuring point is that measuring at the earlobe is less prone to artefacts caused by movements because there are no muscles that can move like in other places. As Penne's heat transfer equation derived from experimenting on a resting forearm, we decided to use the forearm as a second testing site.

4.4 Schematics

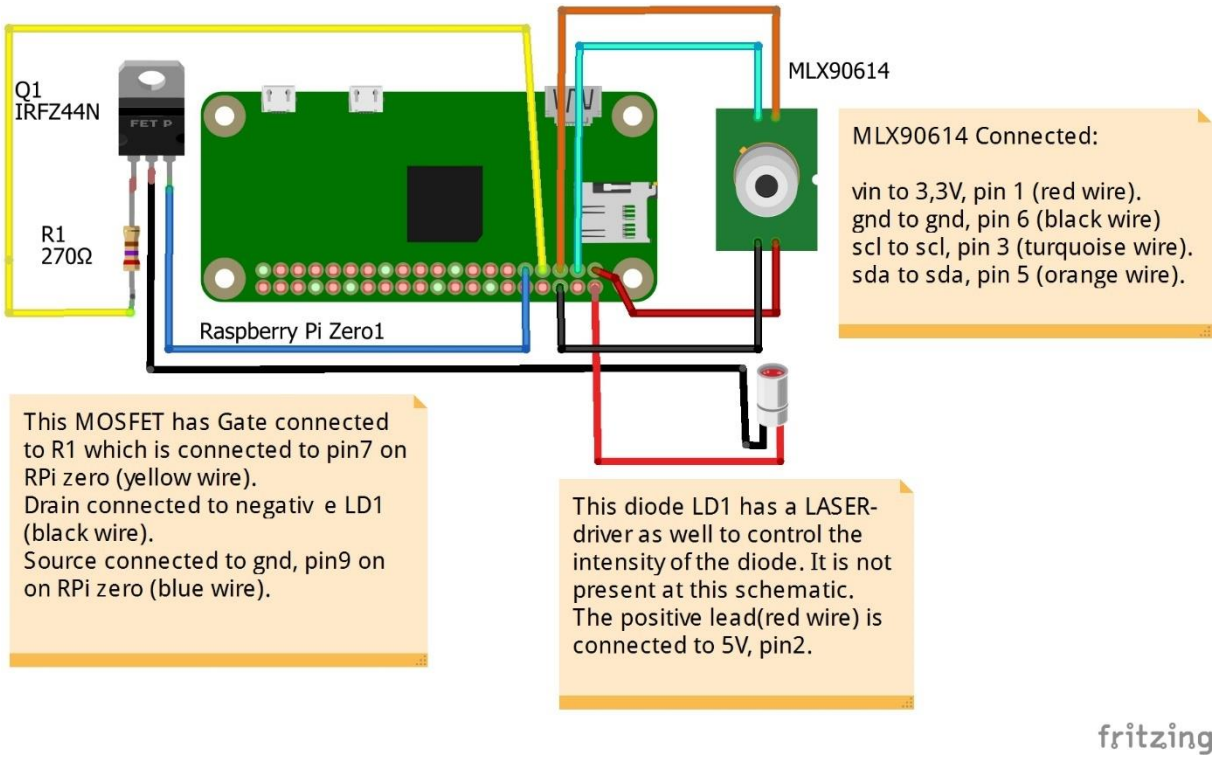

Figure 19: Hardware Schematics

4.5 Setup

The main components of the device setup are the lasers with drivers, infrared thermometer and the Raspberry Pi Zero. Raspberry Pi controls the laser and reads the temperature values from the infrared thermometer through a custom designed Python program, which will be described in *chapter 4.6*. The infrared thermometer is connected to the Raspberry Pi through pin numbers 1, 3, 5 and 6, and communicates through SMBus. This enables the Raspberry Pi to communicate with the thermometer for temperature readings.

The laser is connected to pin number 2 (5V) and controlled through pin number 7 via the gate of the MOSFET. The MOSFET is used because the GPIO pins have a maximum current output of 16 mA (Fustini, 2012) and the laser diode consumes in the range of 60 to 100 mA, so the laser cannot be directly powered from the GPIO pin. The MOSFET delivers more current to the laser diode than the Raspberry Pi can. To be certain that the limit of 16 mA is not exceeded, a resistor of 270 Ω is placed before the gate of the MOSFET. The voltage from the digital pin is 3.3V at high and 0V at low, so the maximum current to the gate, according to Equation 2, will be:

$$\text{Current} = \frac{\text{Voltage}}{\text{Resistance}} = \frac{3{,}3\text{V}}{270\Omega} = 12\ \text{mA} \qquad (2)$$

The gate of the MOSFET controls the current between the *drain* and *source*, thus controlling if the laser diode is connected to ground or not. This will in turn determine whether the laser is on or off.

4.5.1 Ear-clip

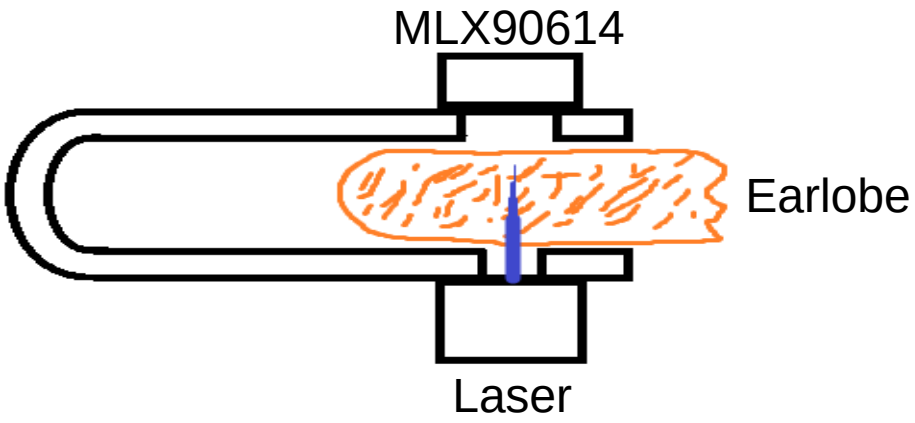

Figure 20: Ear-clip setup

In the ear-clip setup, a transmittance setup is used where the laser is placed on one side of the earlobe and the thermometer on the other side, as shown in Figure 20. The direct contact between the device and skin surface prevents light from the surroundings to affect the measurements.

4.5.2 Armband

In the armband setup, a reflectance-based setup is used where the laser is at an angle to the skin's surface. The thermometer is placed approximately 1 cm above laser beam's target area to avoid direct exposure to the laser beam. The setup is housed inside a small box to prevent light from surroundings to affect the measurements. The wall inside the box is covered with anti-reflective paper to minimize reflections reaching the thermometer. In Figure 21 is a conceptual drawing of the setup.

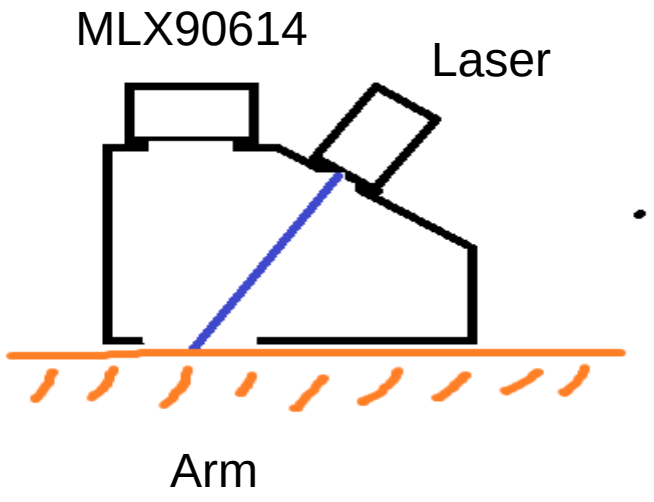

Figure 21: Armband setup

4.6 Software

To perform the measurements with the hardware, a software to control the laser and temperature readings is needed.

The temperature values, along with the time passed, are stored in .csv-files on the Raspberry Pi. This is done through a Python-program called *Hydration.py* along with two modules, *tempir.py* and *Tests.py*. For details on the code, please refer to the programs Hydration.py, tempir.py and Tests.py which can be found in “attachment.zip”.

Hydration.py is opened in the terminal window and has a user interface in the form of a menu with various options. The following options will be explained. To start the software, you need to navigate to the directory folder where the program is stored. In our case, it is called "sensor_rev5" using the *cd* and *ls* commands in the terminal window. In the correct directory, write "python Hydration.py" to start the software. Once the program has started it will look like the display in Figure 22:

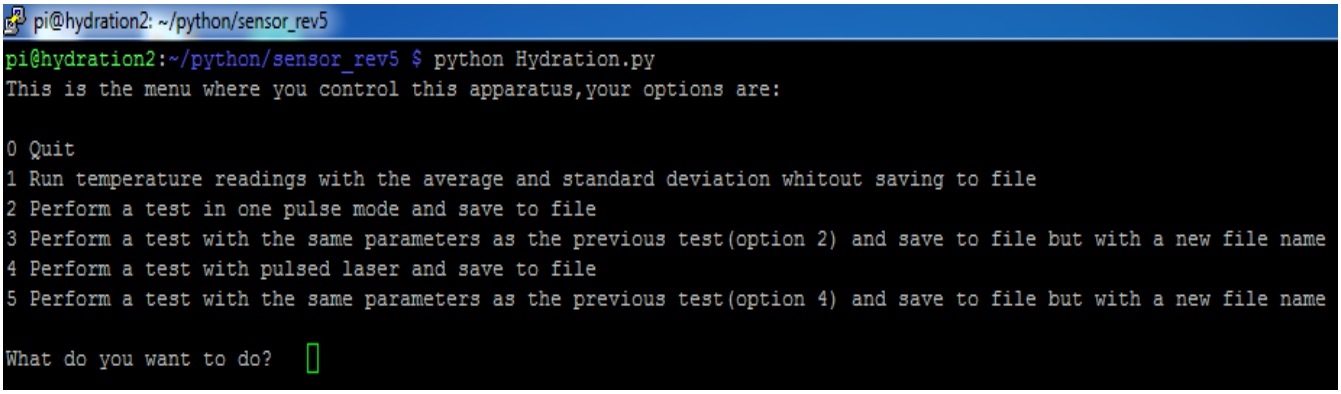

Figure 22: Program menu

Figure 23 visualise the process flow of the software:

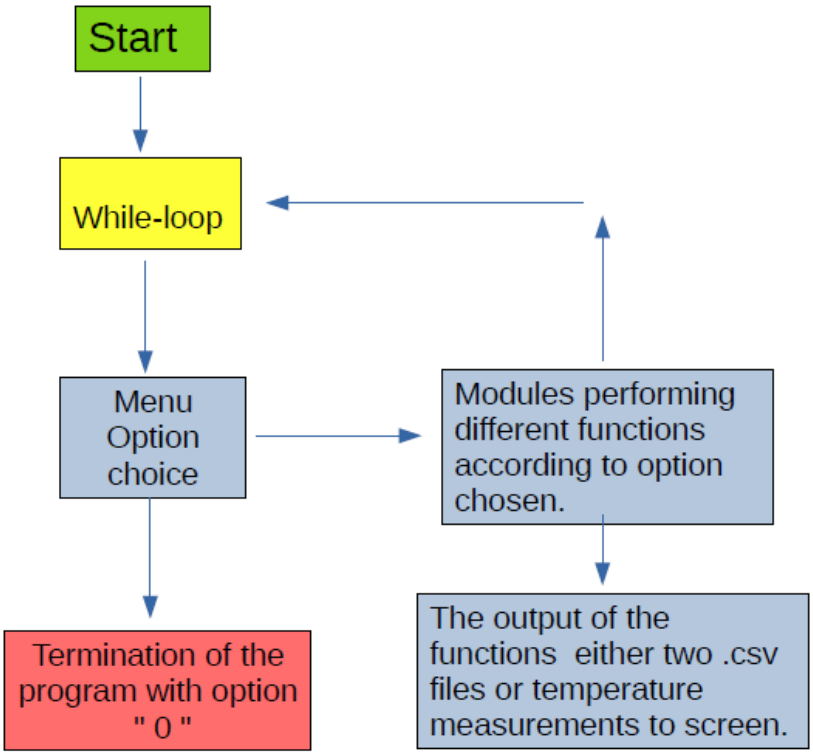

Figure 23: Process diagram

The program menu has six options with different functionality:

"0" Quit
This option will terminate the program.

"1" Run temperature readings with average and standard deviation without saving to file
This option will perform 10 measurements of the temperature with a delay of 1 sec between each measurement. The measurements will be printed to screen along with the average value of the 10 measurements along the standard deviation of the 10 measurements. This function will not save values to file but is rather intended as way of checking if the temperature readings are stable before commencing the intended test.

"2" Perform a test in one pulse mode and save to file *(referenced as "single-pulse")*
This option will perform a test with a single pulse from the laser, as illustrated in Figure 24.

- First you will be asked what you would like to name the files that will be produced from this test. Make sure you start the file name with " and end with ".
- Next you will be asked how many iterations you would like the "start" section of the pulse.
- Next you will be asked how many iterations you would like the "mid" section of the pulse.
- Next you will be asked how many iterations you would like the "end" section of the pulse.
- Finally, you will be asked how long, in milliseconds, you would like the delay for each iteration (for start, mid and end sections). To get the time passed for each section you simply multiply the number of iterations with the delay.

There will be two .csv files produced in the folder "sensor_rev5" after the test is performed. One with the raw data and one with smoothed data from a Savitzky-Golay filter, further explained in c*hapter 4.6.1*.

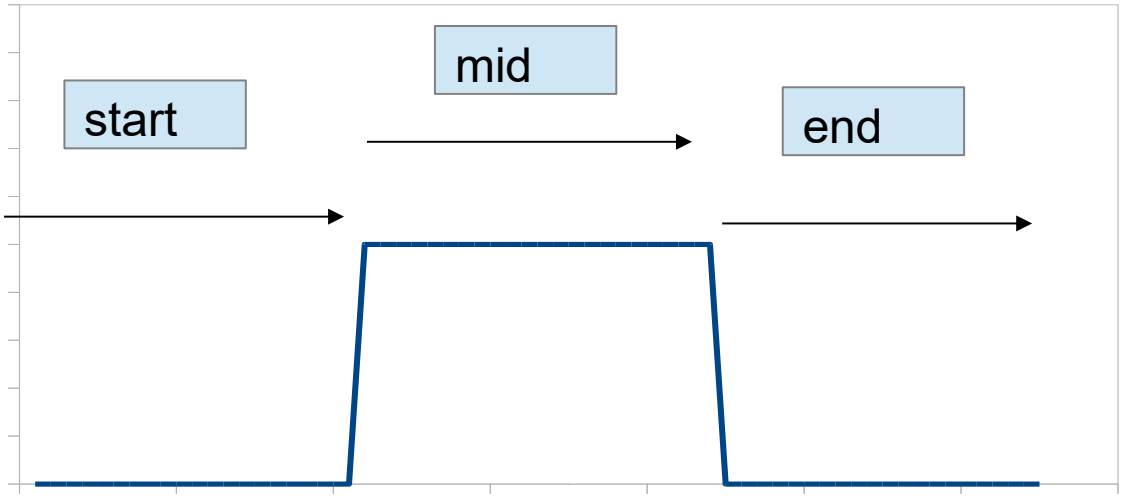

Figure 24: A single, continuous pulse with three programmable sections.

"3" Perform a test with the same parameters as the previous test (option 2) and save to file with a new file name
This option performs a test with the same parameters as the previous test or with default parameters, but with a new file name. The purpose of this option is to make multiple testing

with the same parameters less laborious as you only need to fill in a new file name to perform a new test.

- You will be asked what you would like to name the files that will be produced from this test. Make sure you start the file name with " and end with ".

There will be two .csv files produced in the folder "sensor_rev5" after the test is performed. One with the raw data and one with values smoothed with a *Savitzky-Golay-filter*.

"4" Perform a test with pulsed laser and save to file

This option performs multiple cycles of pulses after one another.

- First you will be asked what you would like to name the files that will be produced from this test. Make sure you start the file name with " and end with ".
- Next you will be asked how many iterations (1 iteration is 5 milliseconds) you would like the "pause" section of the pulse cycle (Figure 25) should be.
- Next you will be asked how many iterations (1 iteration is 5 milliseconds) you would like the "duty" section of the pulse cycle (Figure 25) should be.
- Finally, you will be asked how many "cycles" you would like the test to have (Figure 25).

There will be two .csv files produced in the folder "sensor_rev5" after the test is performed. One with the raw data and one with values being smoothed with a Savitzky-Golay filter.

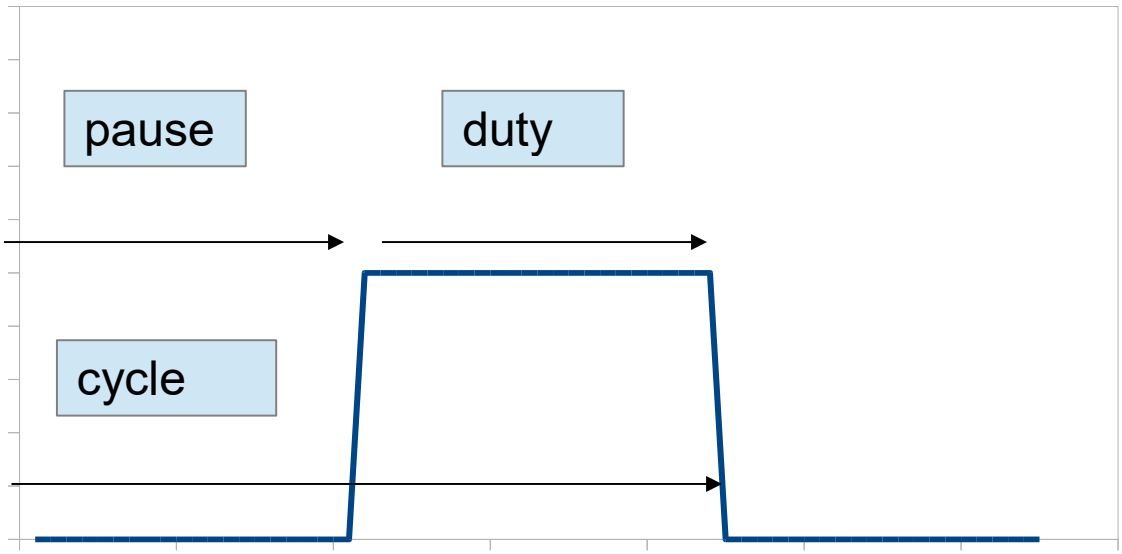

Figure 25: One cycle of the multi-pulsed wave with three programmable sections: pause, duty and number of cycles.

"5" Perform a test with the same parameters as the previous test (option 4) and save to file with a new file name

This option performs a test with the same parameters as the previous test or with default parameters, but with a new file name. The purpose of this option is to make multiple testing with the same parameters less laborious as you only need to fill in a new file name to perform a new test.

- You will be asked what you would like to name the files that will be produced from this test. Make sure you start the file name with " and end with ".

There will be two .csv files produced in the folder "sensor_rev5" after the test is performed. One with the raw data and one with values smoothed with a Savitzky-Golay filter.

4.7 Test procedure

For our experiment to be replicable, a test procedure was designed and followed. The testing is categorized into three separate methods:

Test method 1: Single-pulse wave on earlobe
Test method 2: Pulsed wave on forearm
Test method 3: Single-pulse wave on forearm

Each method was performed in one day, repeated for three days. Thus, there are in total nine days of testing. The tests are referenced accordingly in the results section. The reason we performed three separate methods, was that we beforehand did not know the optimal method to obtain the desired results.

The purpose of the "test subject prerequisite" is to induce a mild dehydration prior to the test.

4.7.1 Test method 1: Single-pulse wave on earlobe (Day 1-3)

The first method is performed with the "ear-clip" setup at the left earlobe of the test subject. Make sure the placement of the "ear clip" is attached at the same spot for each measurement. To aid in this, use a marker to draw reference points. Furthermore, the following parameters are to be used:

Test subject prerequisite:

- The test subject must not drink any fluids after the subject has gone to bed prior to the day of the test.
- The test subject is only allowed to eat one piece of bread (with moderate topping) in the morning on the day of the test.

Number of test subjects: 4
Laser wavelength: 780 nm
Laser power: approx. 10 mW
Test sequence:

- The test shall be performed with 3 *sets* of 3 *sub-tests*. There shall be a 2-minute gap between each sub-test and a gap of 1 hour between each set. After the first and second set, the test subject shall drink approximately ½ litre of water. The sets will be performed continuously with 15 minutes between each set, rotating the 4 test subjects to achieve a 1-hour gap between sets for all test subjects. The test shall produce 72 .csv-files, 36 files of raw data and 36 files of smooth valued files.

Software option:

- Prior to each sub-test, use option 1 in the software to make sure the temperature readings are stable. The standard deviation must be under 0.05°C before the subtest can be started. The sub-test is started with either option 2 or 3, depending on whether it is the first time or not. The first time the sub-test is performed option 2 must be used to set the correct default parameters. After the first time running the sub-test, option 3 can be chosen to save time. This option enables the user to run the sub-test with the default parameters already set, only setting a new name of the file to be produced.

Sub-test parameters:

- "name" the name of the test subject followed by the sequential number of the subtest.
- "start" the number of iterations before the laser is turned on. Set at: 300
- "mid" the number of iterations the laser is turned on. Set at: 300
- "end" the number of iterations after the laser is turned off. Set at: 1250
- "delay size" the size of each iteration in «start», «mid» and «end». Set at: 20

4.7.2 Test method 2: Pulsed wave on forearm (Day 4-6)

The second method is to be performed with the "Armband" setup at the left lower arm of the test subject. Make sure the placement of the "Armband" is at the same spot for each measurement. To aid in this, use a marker to draw reference points. Furthermore, the following parameters are to be used:

Test subject prerequisite:

- The test subject must not drink any fluids after the subject has gone to bed prior to the day of the test.
- The test subject is only allowed to eat one piece of bread (with moderate topping) in the morning on the day of the test.

Number of test subjects: 4
Laser wavelength: 780 nm
Laser power: approx. 10 mW
Test sequence:

- The test shall be performed with 4 *sets* of 3 *sub-tests*. There shall be a 2-minute gap between each sub-test and a gap of 1 hour between each set. After the first and second set, the test subject shall drink approximately ½ litre of water. The sets will be performed continuously with 15 minutes between each set, rotating the 4 test subjects to achieve a 1-hour gap between sets for all test subjects. The test shall produce 96 .csv-files, 48 files of raw data and 48 files of smooth valued files.

Software option:

- Prior to each sub-test, use option 1 in the software to make sure the temperature readings are stable. The standard deviation must be under 0.05°C before the subtest can be started. The sub-test is started with either option 4 or 5, depending on whether it is the first time or not. The first time the sub-test is performed option 4 must be used to set the correct default parameters. After the first time running the sub-test, option 5 can be sued to save time. This option enables the user to run the sub-test with the default parameters already set, only setting a new name of the file to be produced.

Sub-test parameters:

- "name" the name of the test subject followed by the sequential number of the sub-test.
- "pausecycle" the number of iterations before the laser is turned on. Set at: 50
- "dutycycle" the number of iterations the laser is turned on. Set at: 100
- "cycles" the number of cycles to run. Set at: 50

4.7.3 Test method 3: Single-pulse wave on forearm (Day 7-9)

The third method is to be performed with the "Armband" setup at the left lower arm of the test subject. Make sure the placement of the "Armband" is at the same spot for each measurement. To aid in this, use a marker to draw reference points. Furthermore, the following parameters are to be used:

Test subject prerequisite:

- The test subject must not drink any fluids after the subject has gone to bed prior to the day of the test.
- The test subject is only allowed to eat one piece of bread (with moderate topping) in the morning on the day of the test.

Number of test subjects: 4
Laser wavelength: 980 nm
Laser power: approx. 30 mW
Test sequence:

- The test shall be performed with 4 *sets* of 3 *sub-tests*. There shall be a 2-minute gap between each sub-test and a gap of 1 hour between each set. After the first and second set, the test subject shall drink approximately ½ litre of water. The sets will be performed continuously with 15 minutes between each set, rotating the 4 test subjects to achieve a 1-hour gap between sets for all test subjects. The test shall produce 96 .csv-files, 48 files of raw data and 48 files of smooth valued files.

Software option:

- Prior to each sub-test, use option 1 in the software to make sure the temperature readings are stable. The standard deviation must be under 0.05°C before the subtest can be started. The sub-test is started with either option 2 or 3, depending on whether it is the first time or not. The first time the sub-test is performed option 2 must be used to set the correct default parameters. After the first time running the sub-test, option 3 can be chosen to save time. This option enables the user to run the sub-test with the default parameters already set, only setting a new name of the file to be produced.

Sub-test parameters:

- "name" the name of the test subject followed by the sequential number of the sub-test.
- "start" the number of iterations before the laser is turned on. Set at: 400
- "mid" the number of iterations the laser is turned on. Set at: 1000
- "end" the number of iterations after the laser is turned off. Set at: 400
- "delay size" the size of each iteration in "start", "mid" and "end". Set at: 20

4.8 Analysis methods

Excel is the software tool used to plot diagrams and perform calculations.

To obtain a more reliable dataset for analysis, the mean temperature of each iteration of the three samples (sub-tests) at each hydration level (set) was calculated. Figure 26 visualise the test setup for one test subject performed during a test day.

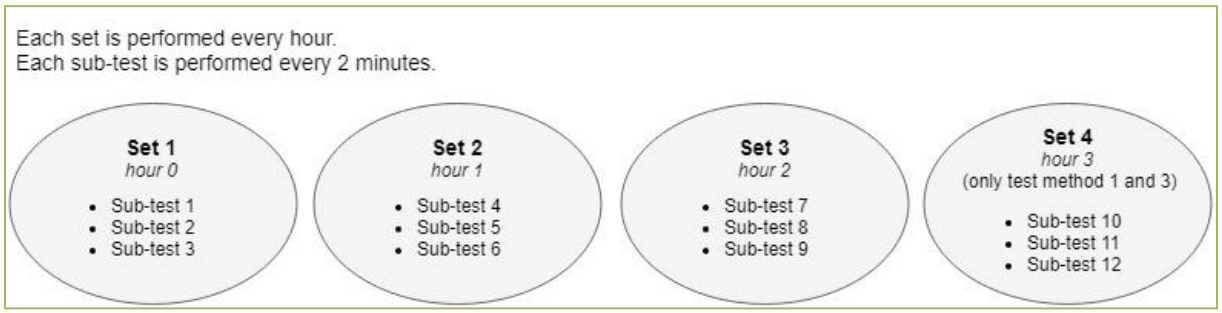

Figure 26 Test day format of one test subject.

Thus, the three sub-tests give rise to one averaged test result per hour, which is plotted graphically, time [s] versus temperature [°C] in scatter charts with connecting lines. This makes one averaged curve or graph. The averaged graph at different hydration levels, are normalized (shifted) to the starting temperature of the first averaged graph for comparison purposes.

To increase the probability of discovering a trend following hydration level, as trends are not always seen with the naked eye, three analysis techniques were performed: 1) area under the curve, 2) the slope between two specific regions of the curve, and 3) percentage change in temperature before and after laser exposure. Below is a description of the analysis calculations and the smoothing filter, the latter which was applied to the raw data in the "Hydration.py" program.

4.8.1 Smoothing filter

The smoothed data .csv-files generated from the software (Hydration.py), in addition to the raw data .csv-files, was applied to reduce noise captured from the IR thermometer in the data sets. The filter is named "Savitzky-Golay". In 2000, Savitzky and Golay's paper from 1964 was described by the editors of the journal "Analytical Chemistry" as "the dawn of computer controlled analytical chemistry" (Schafer, 2011). The filter is a type of low-pass filter that removes high frequent noise. Initially, this filter was, and still is, often used to render visible the relative widths and height of spectral lines in noisy spectrometric data (Press & Teukolsky, 1990). We use this filter as a graphical technique to smoothen our plots.

4.8.2 Area

The purpose of calculating the area under the curve is to compare the areas and determine if there is a trend in area size following hydration level.

The area under the graph where the laser is *turned on* is calculated, but with two slightly different methods. The reason for this, is that the graphs of *test method 1: single-pulse wave on earlobe* and *test method 3: single-pulse wave on forearm*, are quite different graphically than *test method 2: pulsed wave on forearm*.

When the tests are executed, the test subjects will have different starting temperatures resulting in varying offsets when calculating the area. To compensate for the differing offsets, a unique baseline for each individual graph is set by taking the average of the first measurements performed before the laser is turned on. The first test has 300 temperature measurements before the laser is turned on, the second test has 50 and the third test has 400, so the average is calculated over a span of 100, 50 and 100 measurements, respectively.

Now that the baseline has been established, the area between the baseline and the temperature graph where the laser is turned on is calculated. To do this in a simple yet representative way, the graphical width of each temperature measurement is set to 1. If we then use the logic of an integral and sum up all the temperature points making up the graph, we will get a modelled area under the graph. The next step is to subtract the baseline value from the sum of all the temperature points making up this region of the graph. We will then be left with the modelled area between the baseline and the selected region of the graph. Although this area does not represent an actual area in square cm or any other denomination, it will represent a value we can compare the other tests to.

The formulas for calculating the area under the graphs:

Test method 1:

$$\text{Area} = \Sigma(\text{measuring points with laser on}) - \left(\left(\Sigma\left(\frac{\text{100 points before laser turned on}}{100}\right)\right) * 300 \text{ measurments}\right) \quad (3)$$

Test method 2:

$$\text{Area} = \Sigma(\text{all measuring points}) - \left(\left(\Sigma\left(\frac{\text{50 points before laser turned on}}{50}\right)\right) * 7500 \text{ measurments}\right) \quad (4)$$

Test method 3:

$$\text{Area} = \Sigma(\text{measuring points with laser on}) - \left(\left(\Sigma\left(\frac{\text{100 points before laser turned on}}{100}\right)\right) * 1000 \text{ measurments}\right) \quad (5)$$

4.8.3 Slope

The purpose of calculating the slope of temperature change in the tissue right before the laser is turned on and off, is to see if there is a trend in the rate of temperature change following hydration level. To find the slope of the graphs from *test method 1* and *3*, the mean temperature and mean time of the last 10 iterations before the laser is turned on and off is calculated. This generates two data points on the graph where the slope can be found by Equation 6:

$$\text{Slope} = \frac{y_2 - y_1}{x_2 - x_1} = \frac{\text{Avg. temperature}_2 - \text{Avg. temperature}_1}{\text{Avg. time}_2 - \text{Avg. time}} \quad (6)$$

For *test method 2*, the data points are acquired differently. One cycle, or period, consists of 50 iterations with the laser off and 100 iterations with the laser on. The average of the temperature and time of the first cycle and the last cycle are used to retrieve the two data points used in Equation 6.

4.8.4 Percentage

The purpose of calculating the percentage change in tissue temperature before and after exposure to infrared light, is to determine if there is a trend following hydration level. To find the temperature change in percentage for *test method 1* and *3*, the mean temperature of all iterations before the laser was turned on and the mean temperature after the laser is turned off are calculated. Percentage change is found by using Equation 7:

$$\text{Temperature change in \%} = \frac{\text{after pulse}_{\text{avg}} - \text{before pulse}_{\text{avg}}}{\text{before pulse}_{\text{avg}}} * 100 \quad (7)$$

For *test method 2*, the average of the 100 first iterations, and the 100 last iterations are found to calculate the percentage change from the start of the induced laser to the end of the test.

5 Results and Discussion

This chapter will present the resulting monitoring devices and the results of analysis methods. At the end, comes a discussion of possible sources of error.

5.1 Measuring device

The ear-clip used during *test method 1* is shown in Figure 28. The clip was bent to the degree that it snuggly fits any test subjects' earlobe, having a slight degree of elasticity. Because of the weight of the components, the clip must be supported by holding it with your hand or else it will fall off. Markers drawn on the test subject's ear ensured the same placement of the clip for each sub-test. When the clip is placed on the ear, the laser and temperature sensor align facing each other while the test procedure is executed.

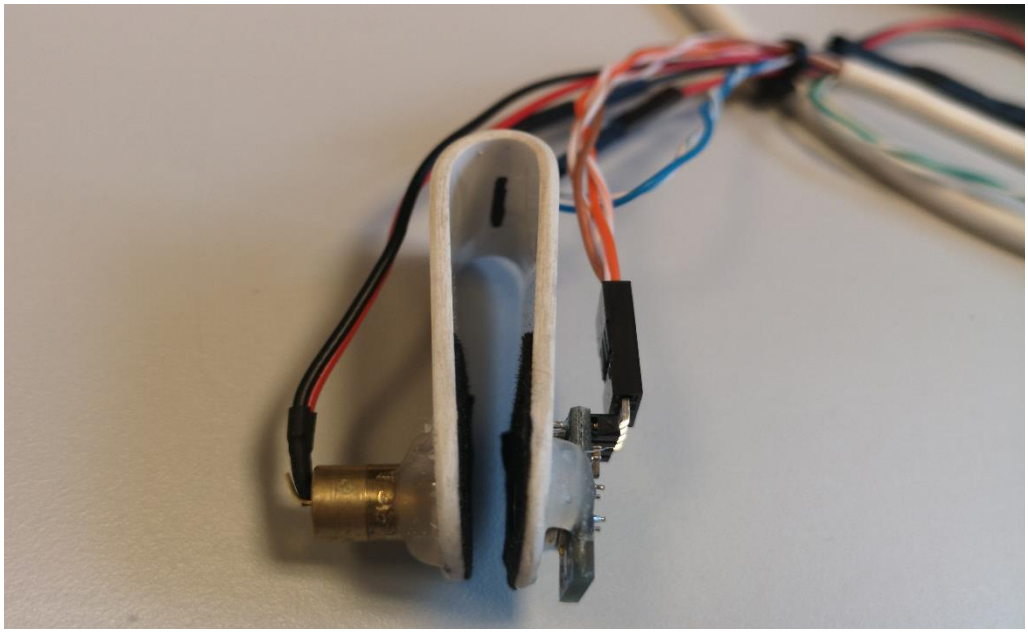

Figure 27: Photo of the actual ear-clip used

The armband shown in Figure 29a and 29b was used for *test method 2* and *3*. With an elastic adjustable strap, it fitted all test subjects. The laser was placed at an angle to the surface of the skin, with the temperature sensor placed perpendicular to the irradiated area. The flexible armband setup aided in the necessity for a fixed placement during the test. The intention of the anti-reflective paper on the inside of the housing was to prevent incoming light from surroundings and multi-scattering inside from the laser. The effect of the black coloured paper was not documented.

Figure 28a: Photo of actual armband used

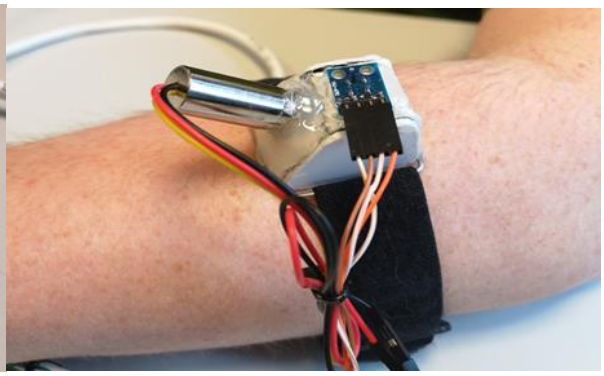

Figure 28b: Photo of the actual armband in use

5.2 Analysis results

Each test method has its own sub-chapter, containing 1) a selected representation of averaged graphs, and the results of 2) *area*, 3) *slope* and 4) *percentage* analysis methods plotted in bar diagrams sorted by day.

In the selected representation of averaged graphs, the smoothed data values are used. The reason for using the smoothed data instead of the raw data, is that it makes a better graphical representation. Figures 30a and 30b illustrates the difference in appearance between raw data and smoothed data graphs. They are named *Test 1*, *Test 2 normalized*, *Test 3 normalized* and *Test 4 normalized*, and refers to the test data from start: hour 0, hour 1, hour 2 and hour 3, according to hydration level. Test 2, 3 and 4 are normalized in reference to Test 1.

Calculations, on the other hand, are done using raw data to achieve an unbiased result. At the end of each analysis result is a statistical trend diagram, where the bars of each subject are categorized into ascending, descending or random order. The random order category includes all trends not falling into purely ascending or descending order.

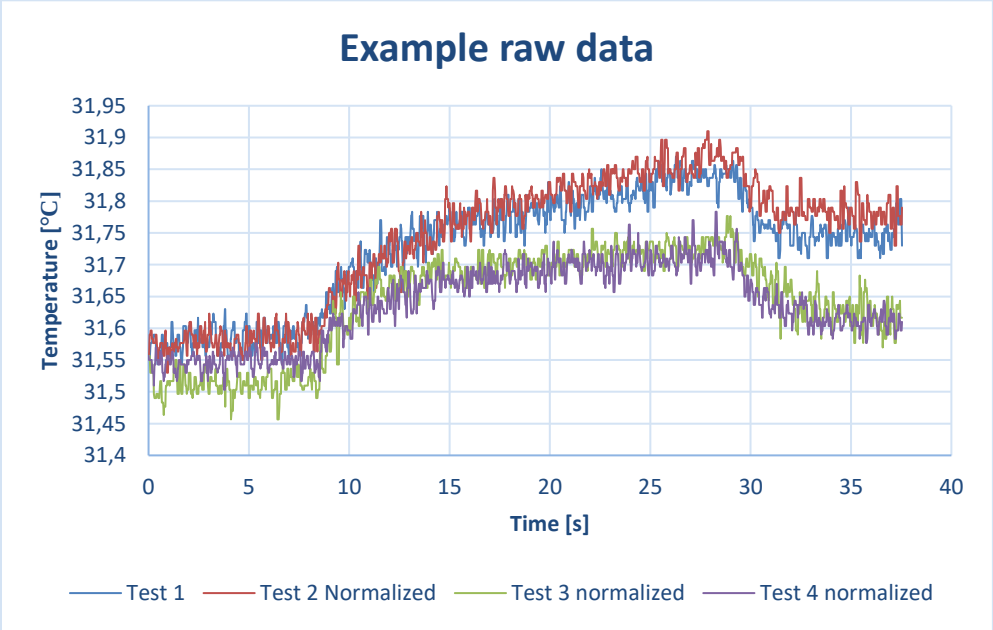

Figure 29a: Example of raw unfiltered data from IR sensor from Test day 9: Test subject 2

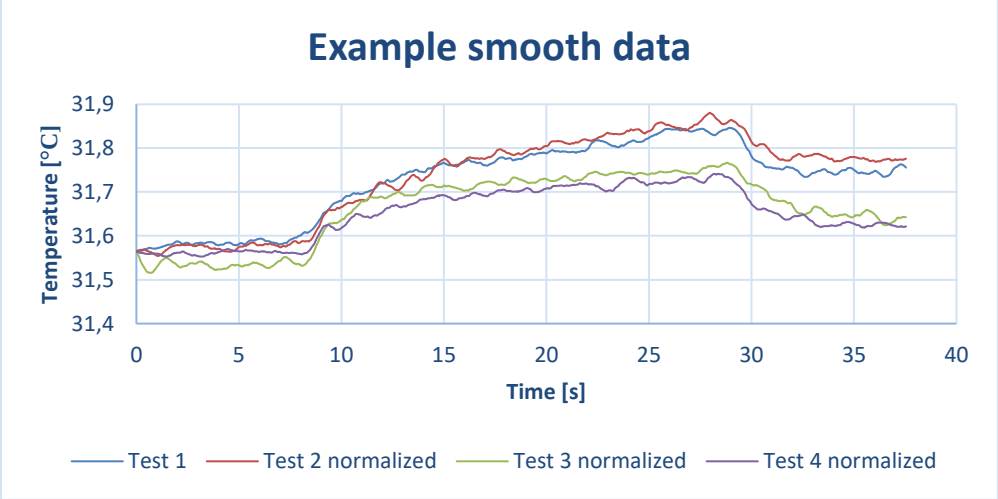

Figure 29b: Example of smooth data from Test day 9: Test subject 2 using Savitzky-Golay filter

5.2.1 Test method 1: Single-pulse wave on earlobe (Day 1-3)

5.2.1.1 Graphs

The graphs below (Figures 30a – 30d) show filtered data received from the IR temperature sensor from all test subjects from test day 3. Results from all tests can be found in Appendix A.

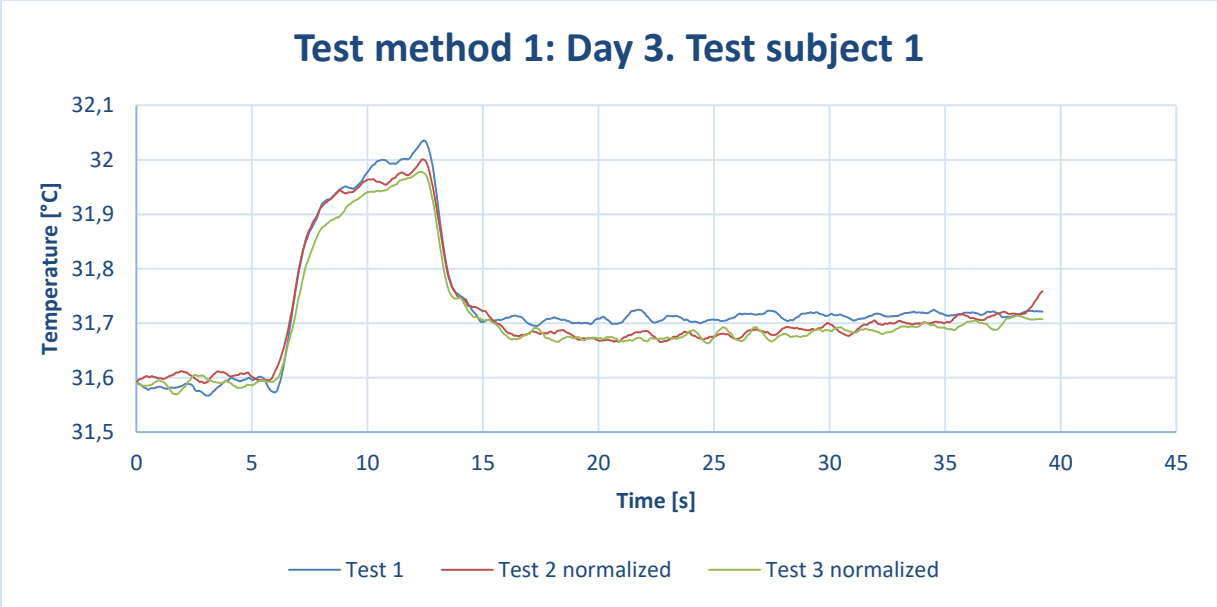

Figure 30a: Test method 1: Day 3. Test subject 1. IR temperature sensor readings during a single pulse of 780 nm laser transmission on ear lobe at different hydration levels.

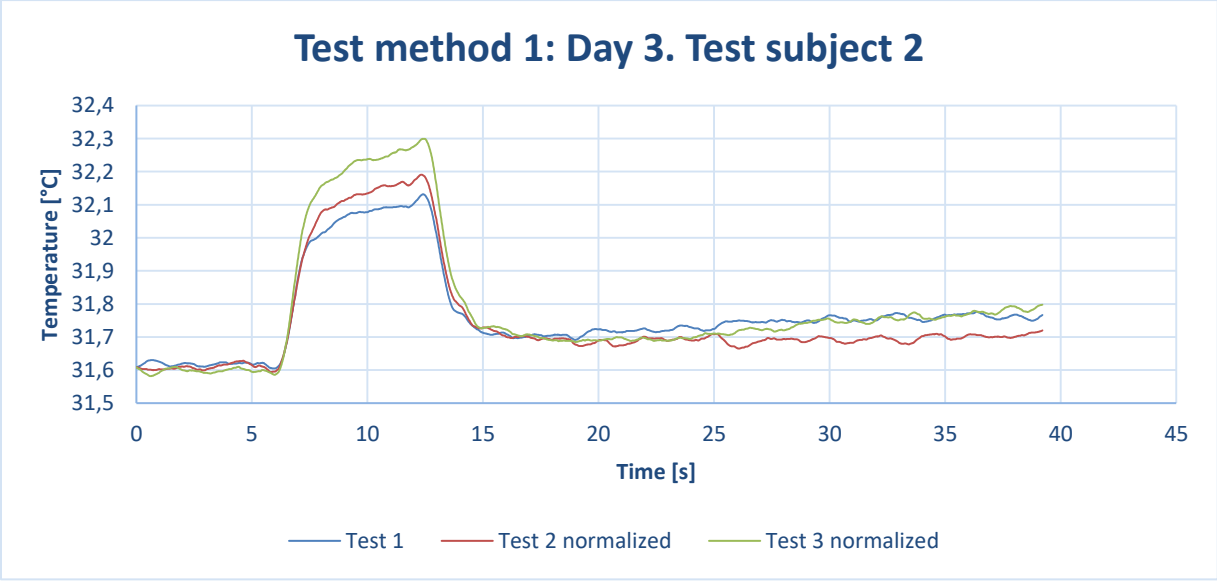

Figure 30b: Test method 1: Day 3. Test subject 2. IR temperature sensor readings during a single pulse of 780 nm laser transmission on ear lobe at different hydration levels.

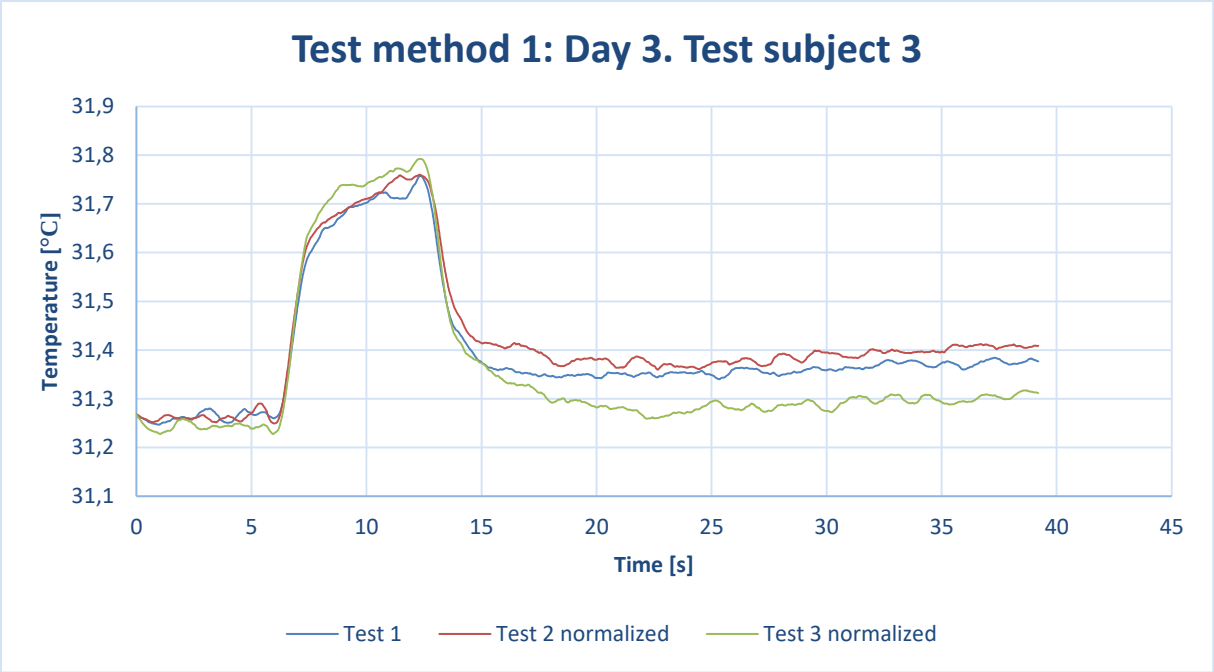

Figure 30c: Test method 1: Day 3. Test subject 3. IR temperature sensor readings during a single pulse of 780 nm laser transmission on ear lobe at different hydration levels.

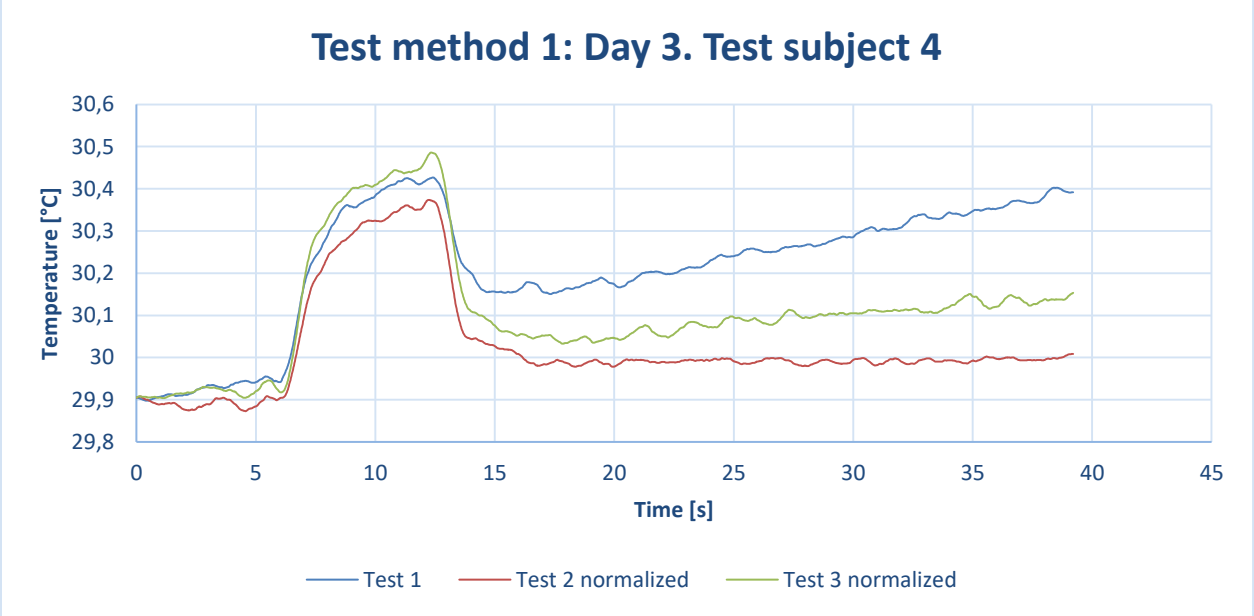

Figure 30d: Test method 1: Day 3. Test subject 4. IR temperature sensor readings during a single pulse of 780 nm laser transmission on ear lobe at different hydration levels.

From the selected graphs, it appears that the temperature curves do not follow a consistent trend regarding hydration level. We expected to see a smaller temperature increase from the laser pulse as hydration level increased. The only test subject following the desired trend, was test subject 1. Similar inconclusive results were found from test day 1 and 2, displayed in Appendix A.

5.2.1.2 Area

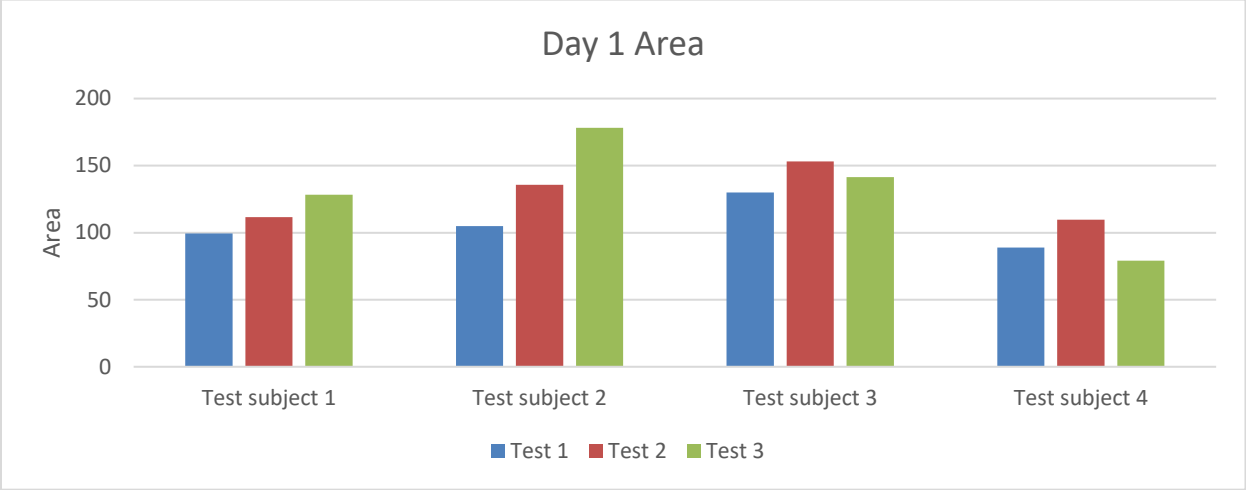

Figure 31a: Day 1. Area under curve of 780 nm single-pulse wave on ear lobe at different hydration levels.

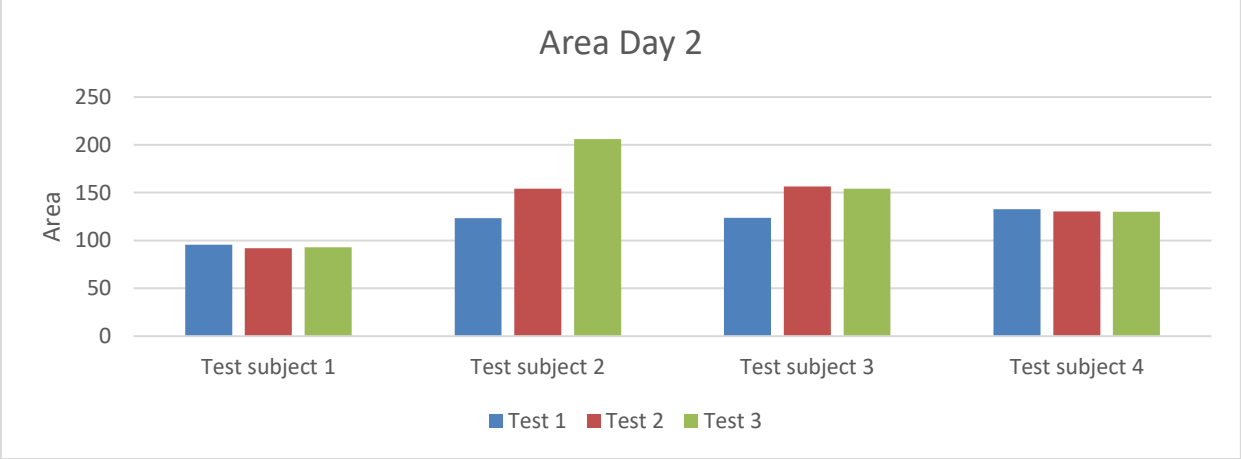

Figure 31b: Day 2. Area under curve of 780 nm single-pulse wave on ear lobe at different hydration levels.

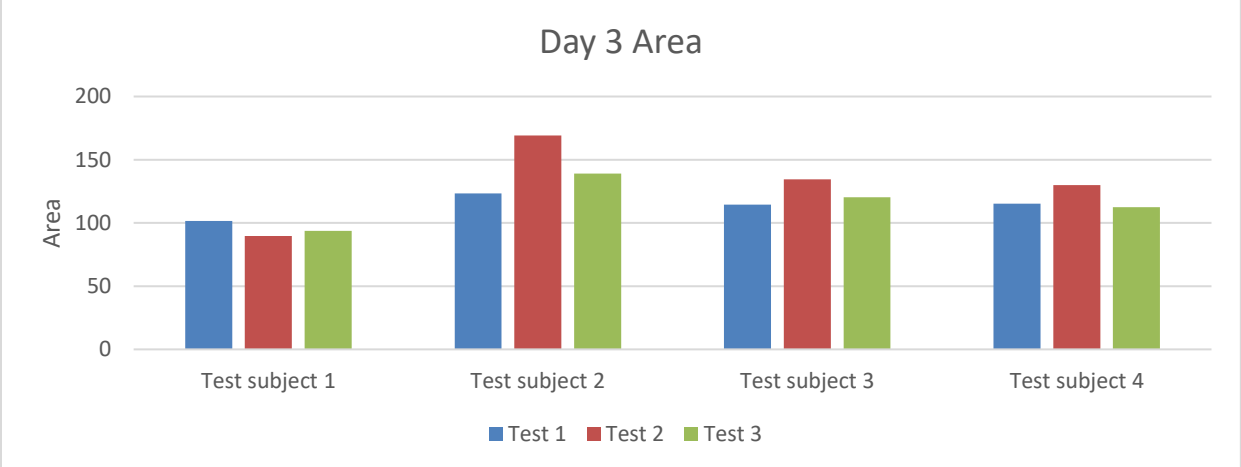

Figure 31c: Day 3. Area under curve of 780 nm single-pulse wave on ear lobe at different hydration levels.

Area Test Trends Method 1	Count
Ascending order	3
Descending order	1
Random order	8
Total Tests	12

Table 7: Trends in area from test method 1

Looking at the area statistics of *Test method 1* in Table 7, it is apparent that the random order is the biggest contributor. We expected to see a descending order of area as hydration level increased.

5.2.1.3 Slope

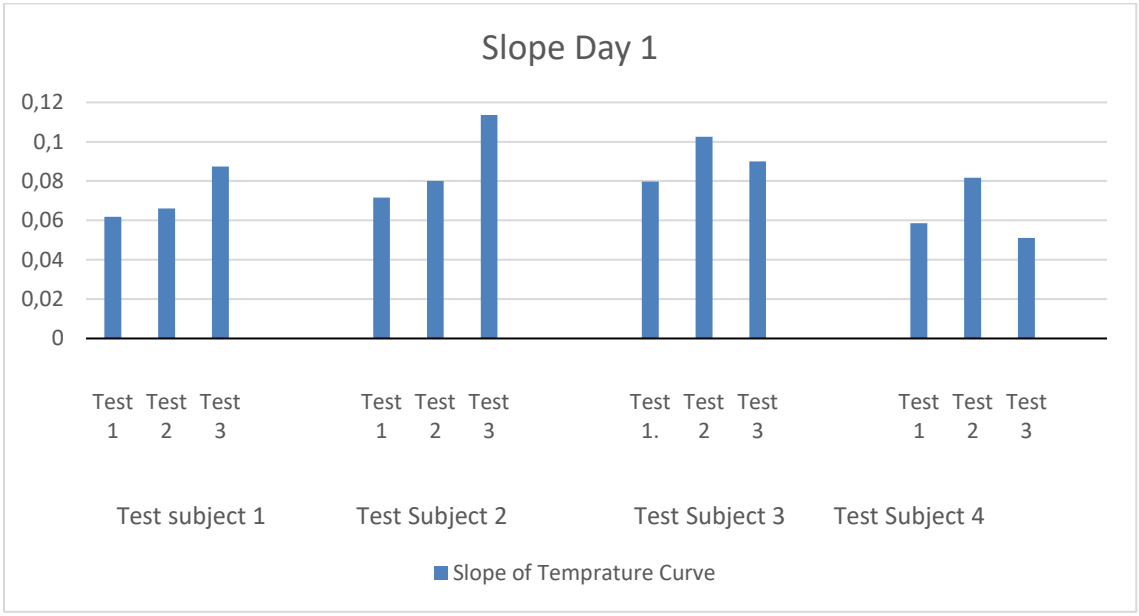

Figure 32a: Day 1. Slope with 780 nm single-pulse wave on ear lobe at different hydration levels.

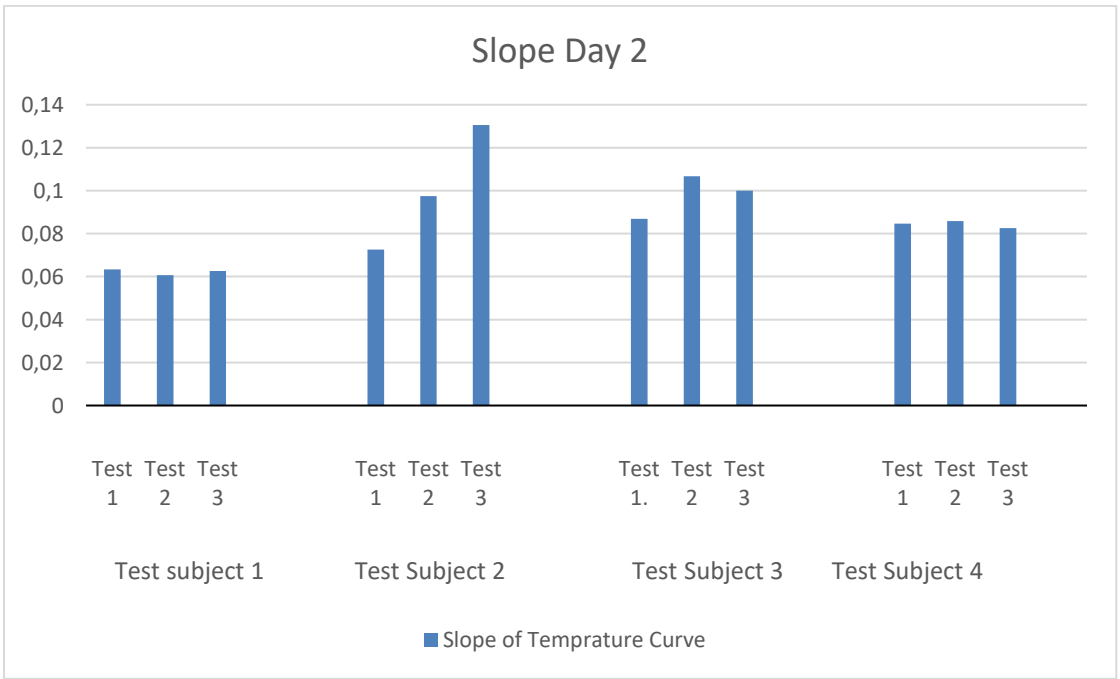

Figure 32b: Day 2. Slope with a 780 nm single-pulse wave on ear lobe at different hydration levels.

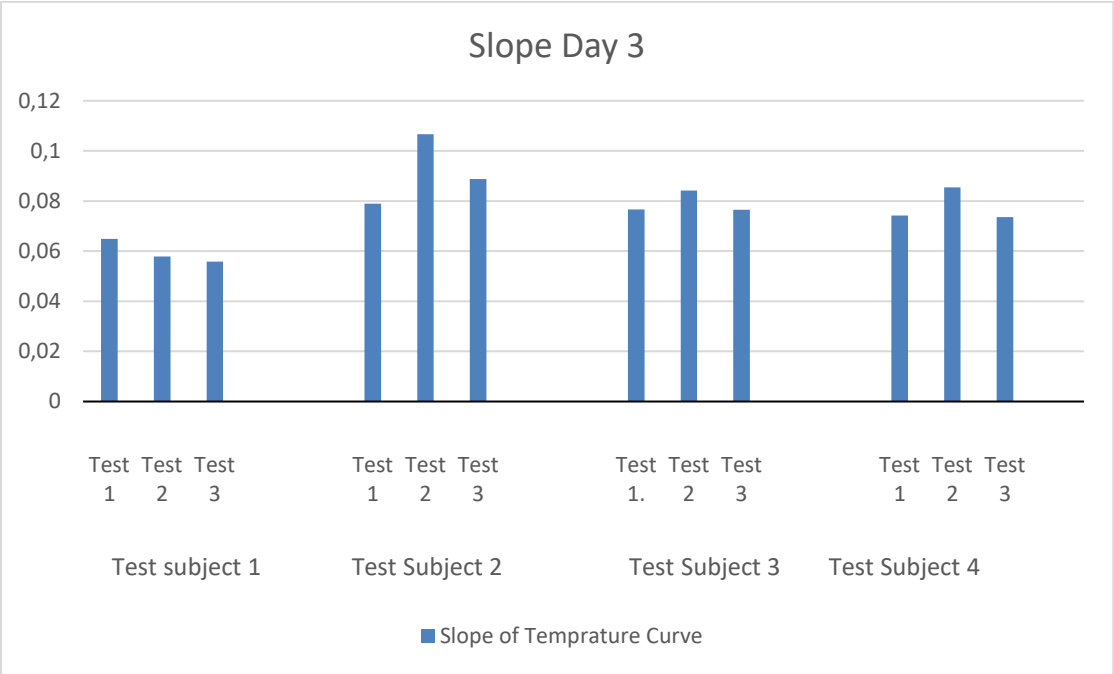

Figure 32c: Day 3. Slope with a 780 nm single-pulse wave on ear lobe at different hydration levels.

Slope Test trends Method 1	**Count**
Ascending order	3
Descending order	1
Random order	8
Total Tests	12

Table 8: Trends in slope from test method 1.

Looking at the slope statistics of *Test method 1* in Table 8, there are 3 tests with minimal slope differences as hydration level increases. 4 tests had a negative slope progression and 5 tests had a positive slope progression. We expected to see a negative slope progression as hydration level increased. This statistic is more evenly distributed than the area statistics but does not show a consistent hydration level trend.

5.2.1.4 Percentage

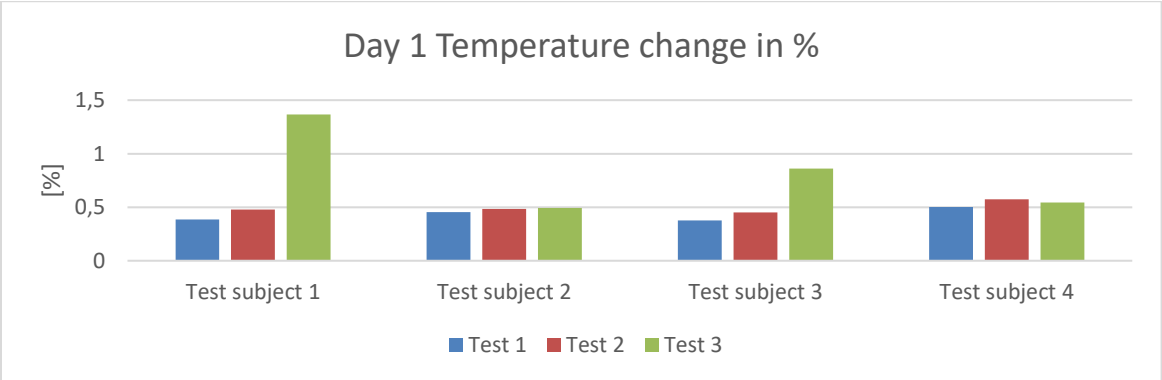

Figure 33a: Day 1. Temperature changes in % before and after a 780 nm single-pulse wave on ear lobe at different hydration levels.

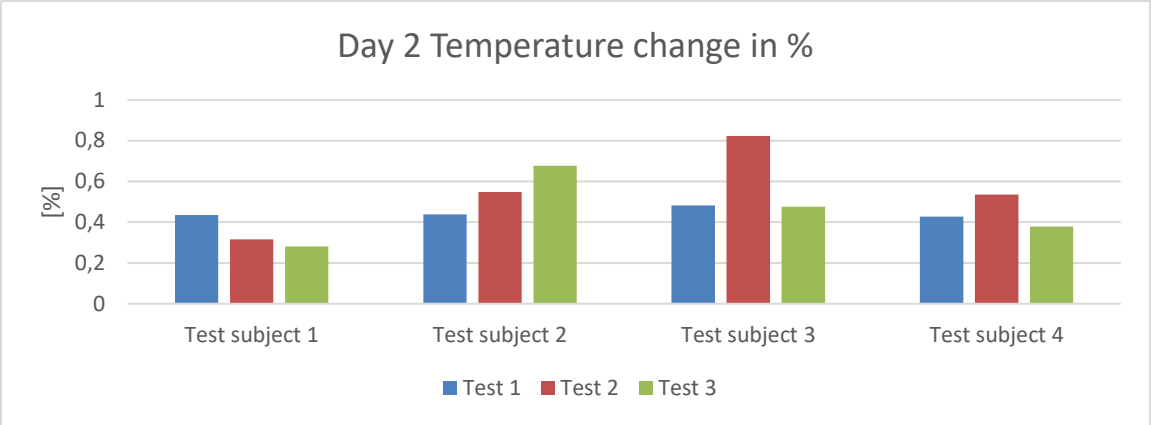

Figure 33b: Day 2. Temperature changes in % before and after a 780 nm single-pulse wave on ear lobe at different hydration levels.

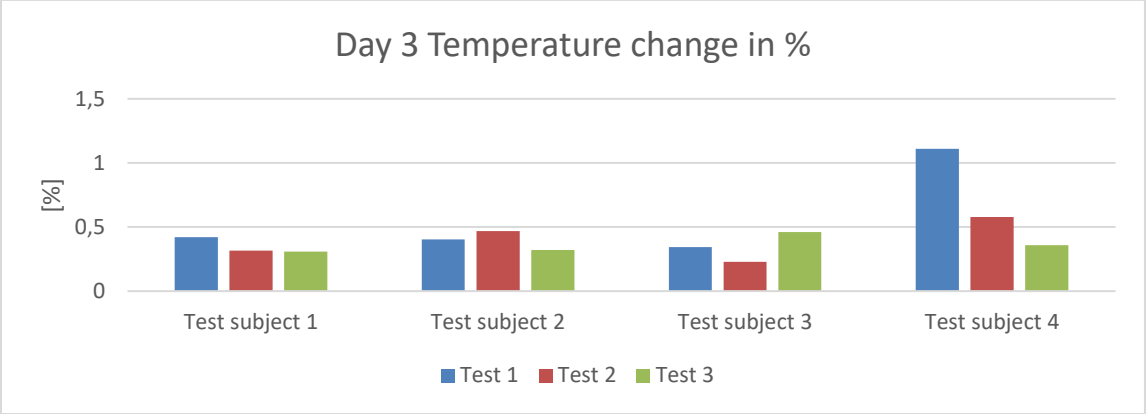

Figure 33c: Day 3. Temperature changes in % before and after a 780 nm single-pulse wave on ear lobe at different hydration levels.

Percentage Test Trends Method 1	**Count**
Ascending order	4
Descending order	3
Random order	5
Total Tests	12

Table 9: Trends in percentage change from test method 1

It is expected to see a descending trend in the development of temperature change in percentage. But from table 9, we see only 3 of the total 12 tests show a descending pattern, and 4 of them have an ascending order, while the rest are random. No consistent trend seems to be forming.

5.2.2 Test method 2: Pulsed wave on forearm (Day 4-6)

5.2.2.1 Graphs

The graphs below (Figures 34a – 34d) show filtered data received from the IR temperature sensor from all test subjects from test day 6. Results from all tests can be found in Appendix A.

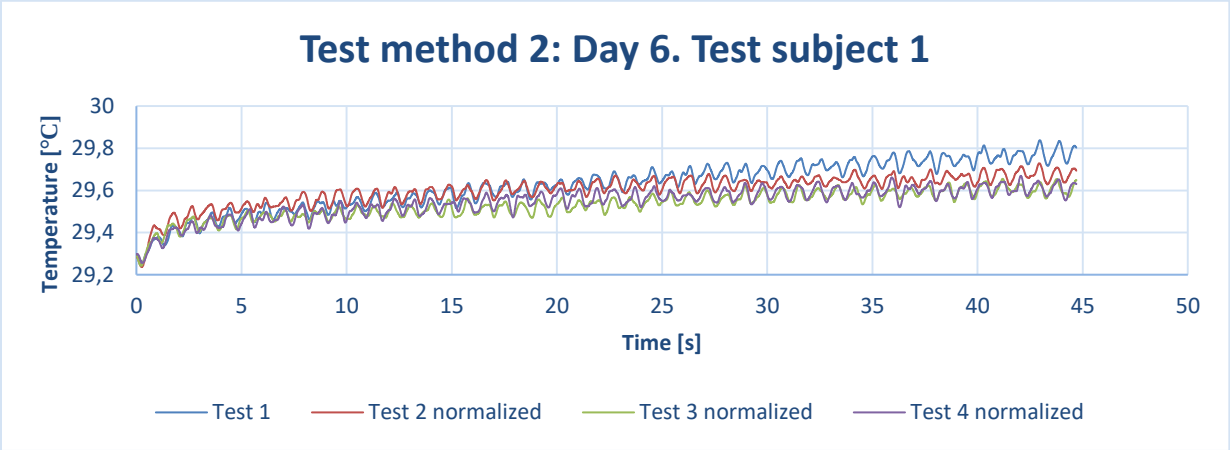

Figure 34a: Test method 2: Day 6. Test subject 1. IR temperature sensor readings during a short-pulsed laser of 780 nm reflection on forearm at different hydration levels.

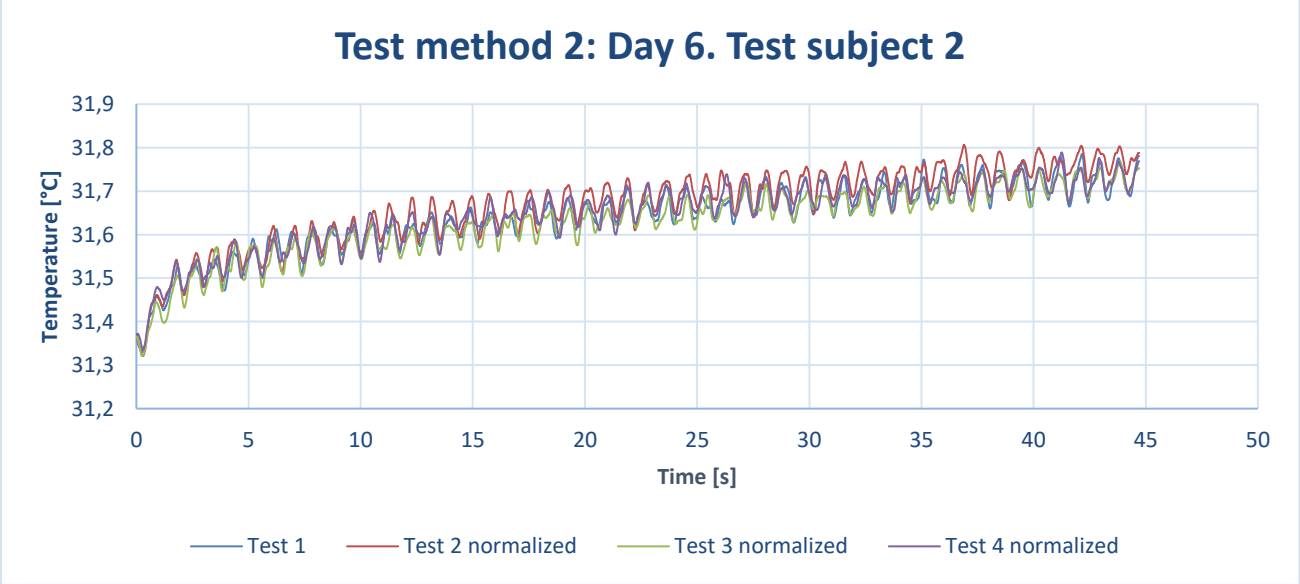

Figure 34b: Day 6. Test subject 2. IR temperature sensor readings during a short-pulsed laser of 780nm reflection on forearm at different hydration levels.

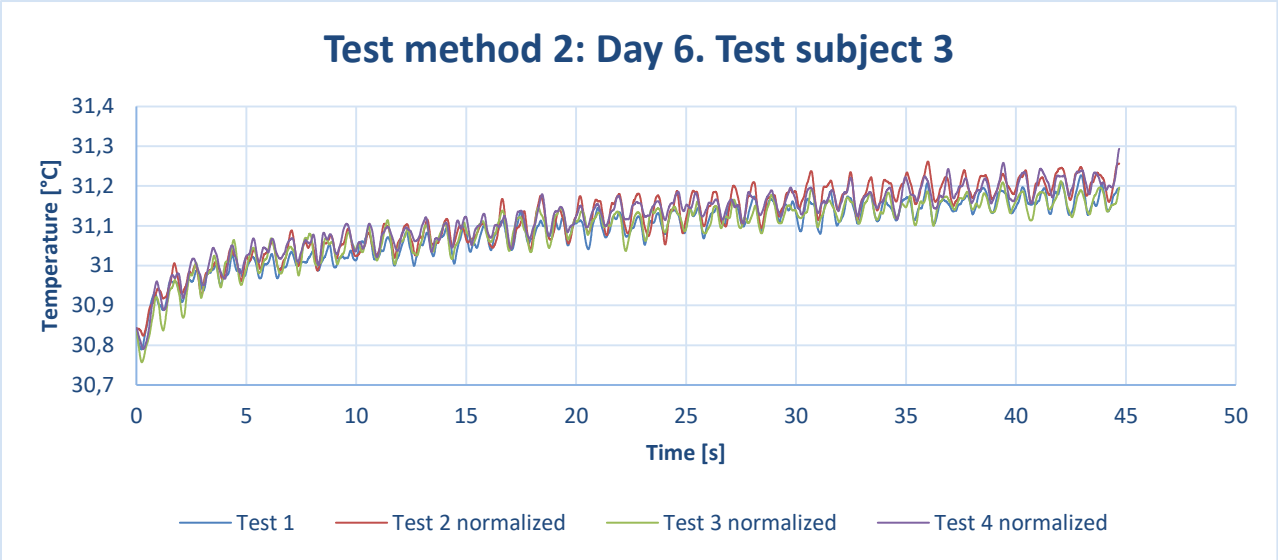

Figure 34c: Test method 2: Day 6. Test subject 3. IR temperature sensor readings during a short-pulsed laser of 780 nm reflection on forearm at different hydration levels.

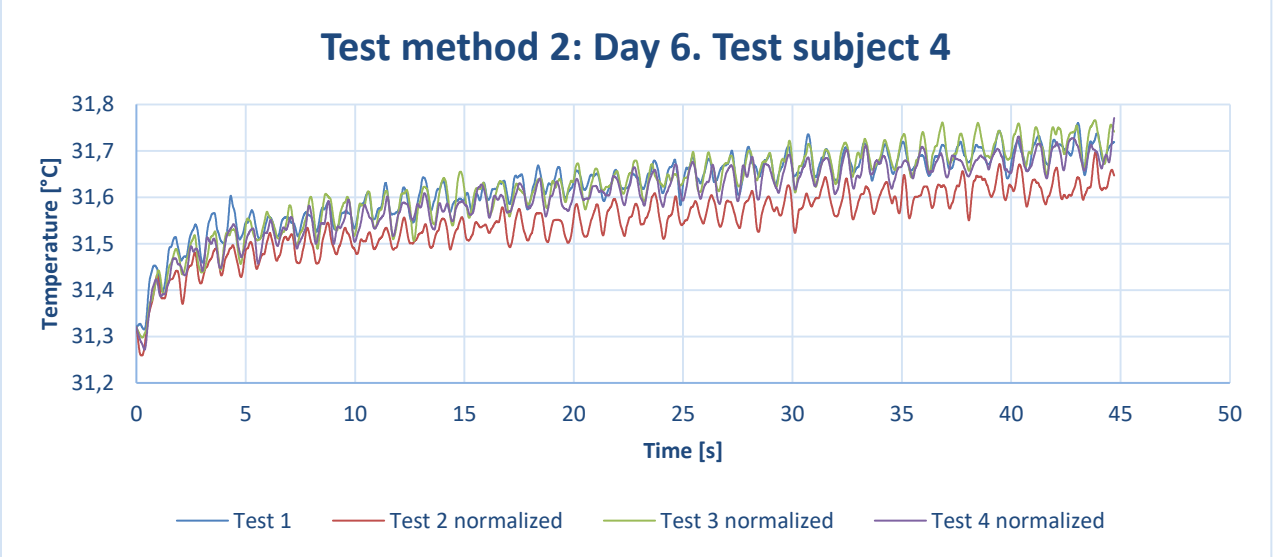

Figure 34d: Test method 2: Day 6. Test subject 4. IR temperature sensor readings during a short-pulsed laser of 780 nm reflection on forearm at different hydration levels.

Looking at the selected graphs, it appears that the temperature curves does not follow a consistent trend regarding hydration level. We expected to see a smaller temperature increase from the laser pulses as hydration level increased. The only test subject following the desired trend, was test subject 1. Similar inconclusive results were found from test day 4 and 5, displayed in Appendix A.

5.2.2.2 Area

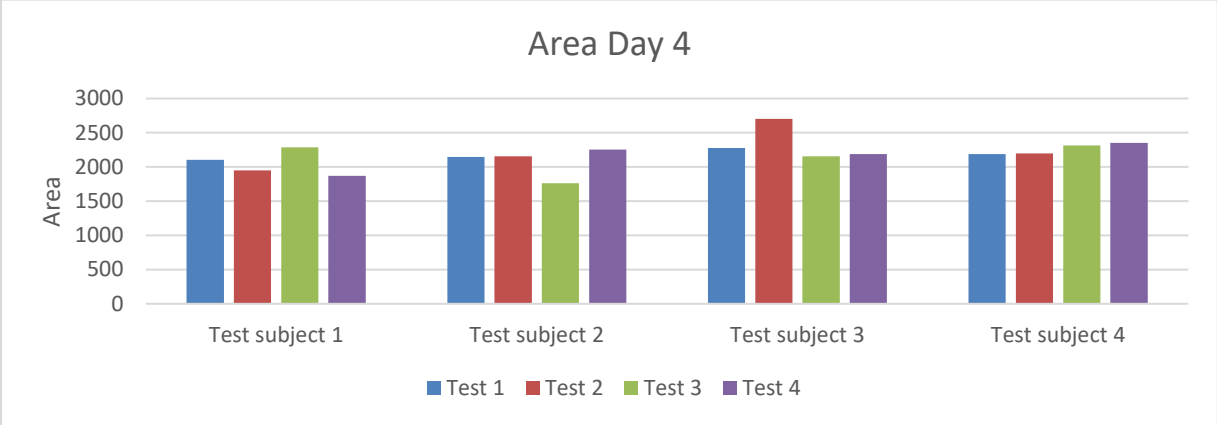

Figure 35a: Day 4. Area under 780nm laser pulse on forearm at different hydration levels.

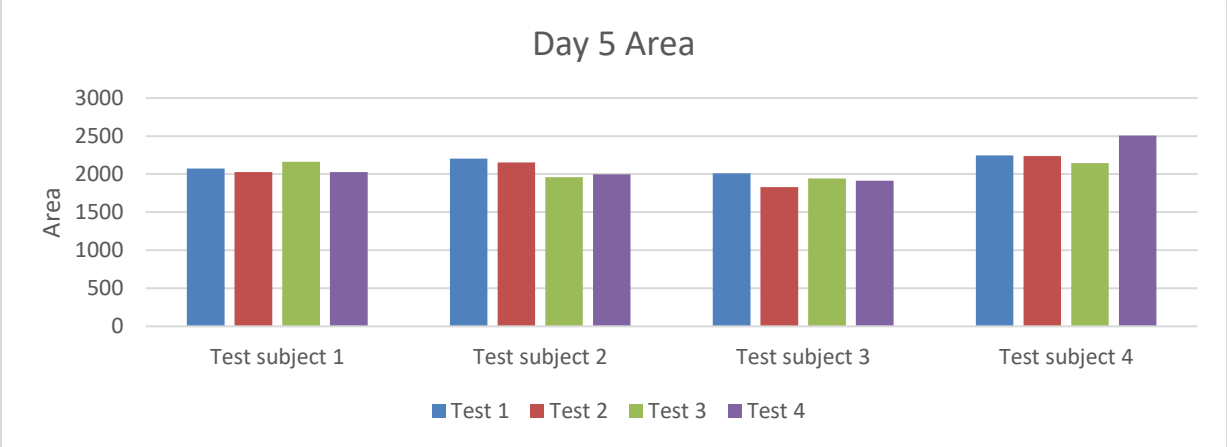

Figure 35b: Day 5. Area under 780nm laser pulse on forearm at different hydration levels.

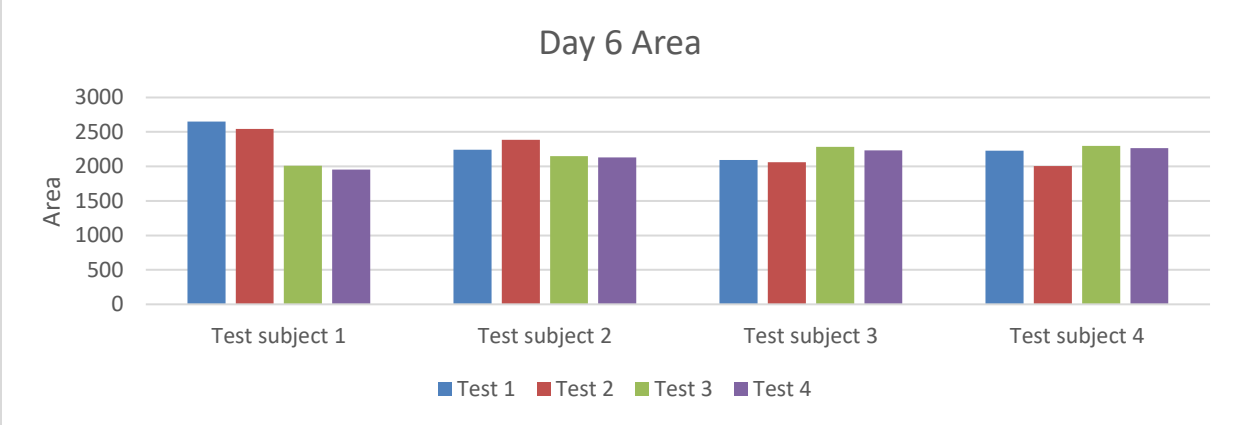

Figure 35c: Day 6. Area under 780nm laser pulse on forearm at different hydration levels.

Area Test Trends Method 2	**Count**
Ascending order	1
Descending order	1
Random order	10
Total Tests	12

Table 10: Trends in area from test method 2

Looking at the area statistics of *Test method 2*, it is apparent that the random order is the biggest contributor. We expected to see a descending order of area as hydration level increased.

5.2.2.3 Slope

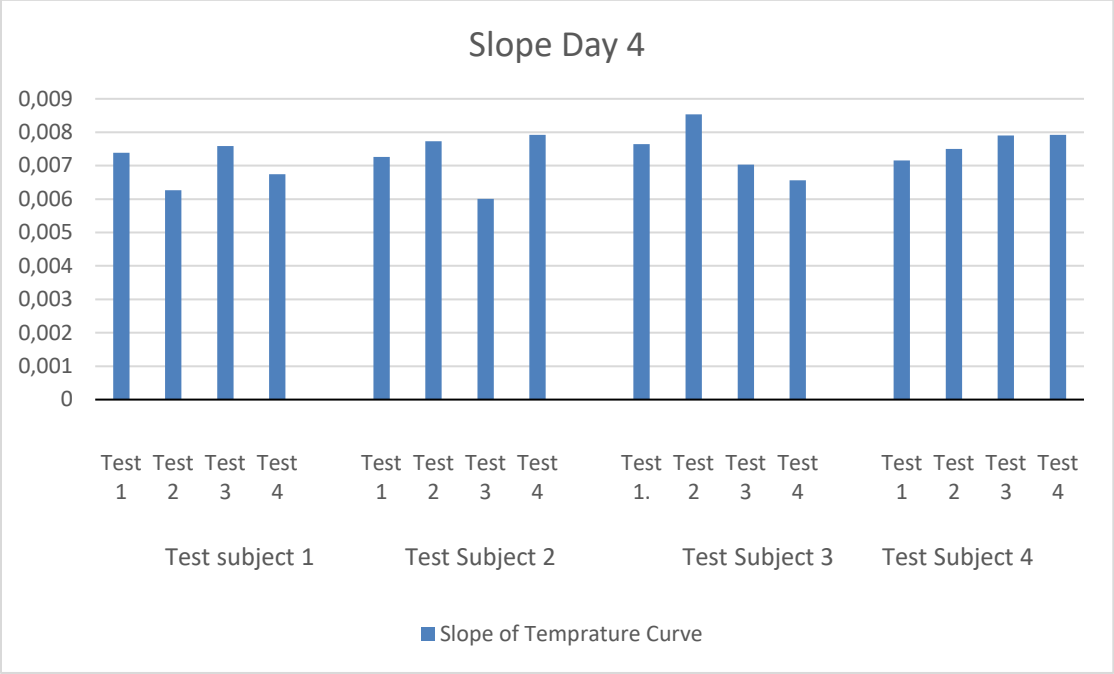

Figure 36a: Day 4. Slope with 780nm laser pulse on forearm at different hydration levels.

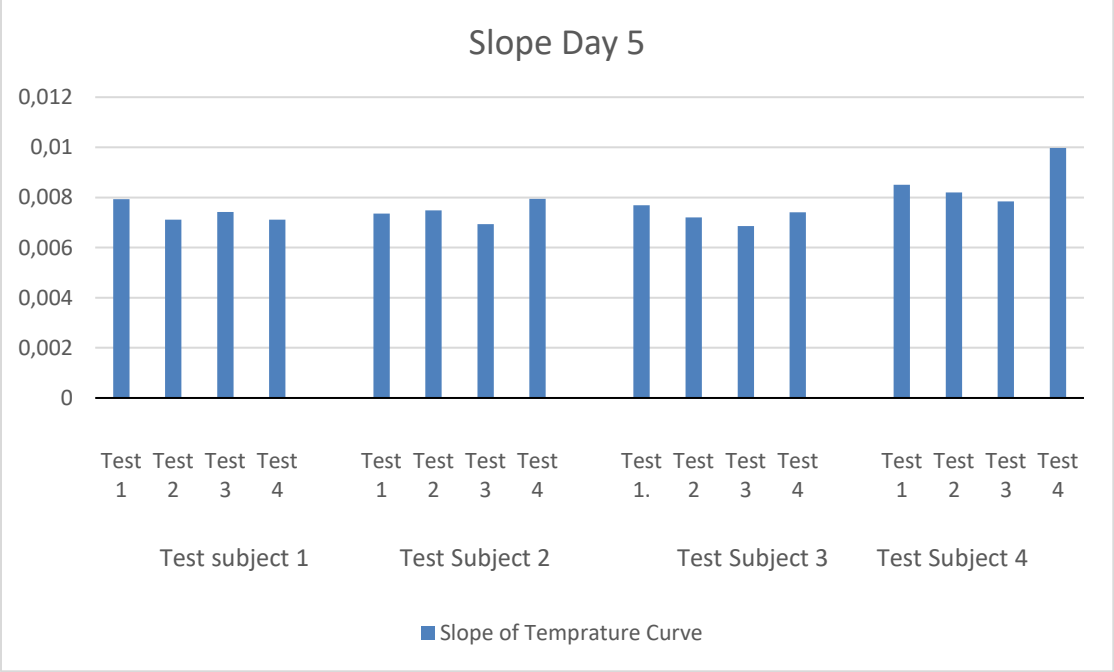

Figure 36b: Day 5. Slope with 780nm laser pulse on forearm at different hydration levels.

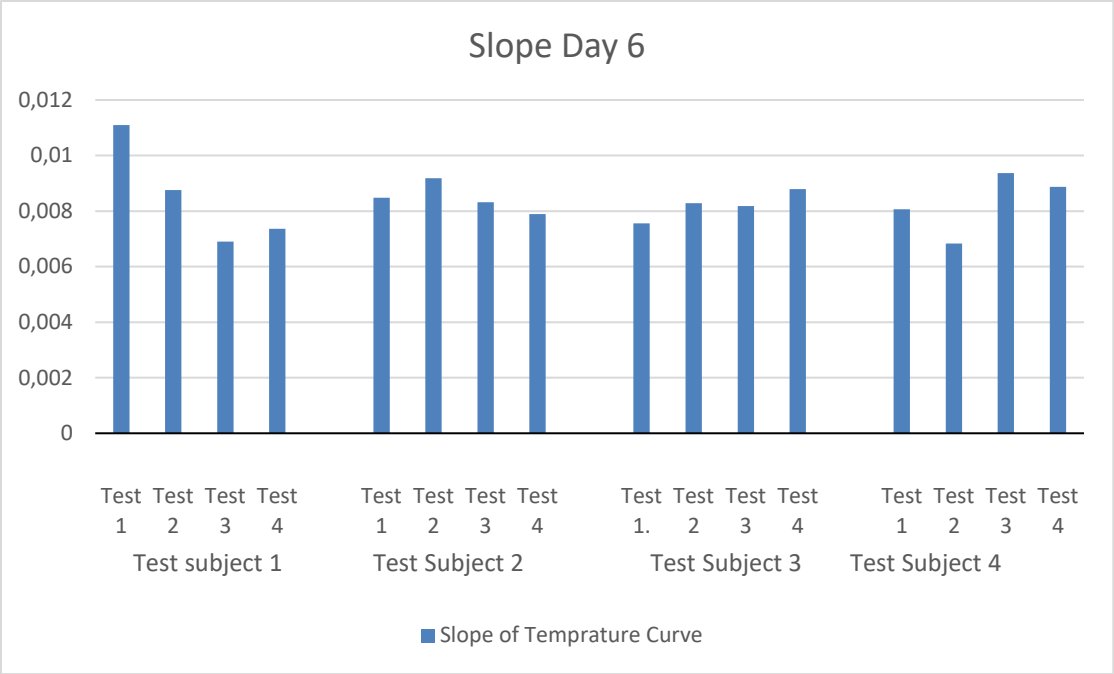

Figure 36c: Day 6. Slope with 780nm laser pulse on forearm at different hydration levels.

Slope Test trends Method 2	**Count**
Ascending order	2
Descending order	0
Random order	10
Total Tests	12

Table 11: Trends in slope progression from test method 2

Looking at the slope statistics of *Test method 2*, there are 6 tests with minimal slope differences as hydration level increases. 2 tests had a negative slope progression and 2 tests had a positive slope progression. We expected to see a negative slope progression as hydration level increased.

5.2.2.4 Percentage

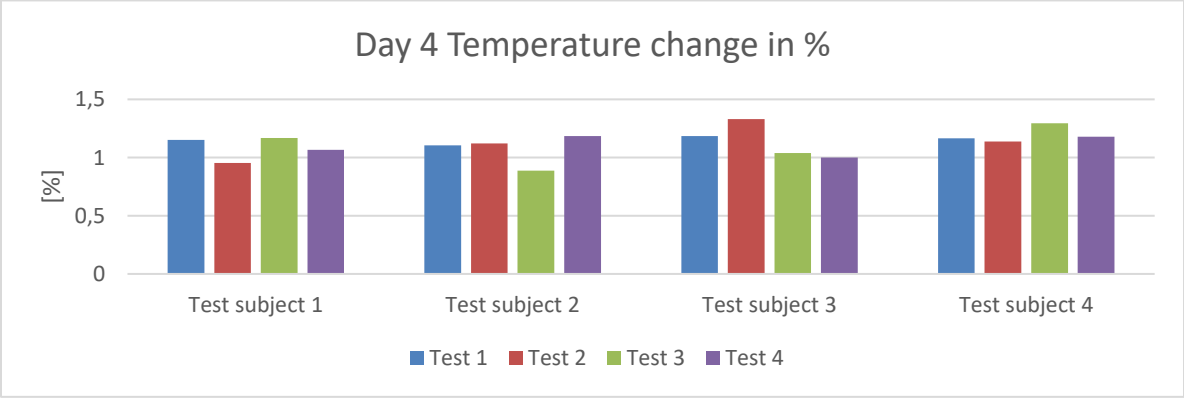

Figure 37a: Day 4. Temperature changes in % before and after a 780 nm laser pulse on forearm at different hydration levels.

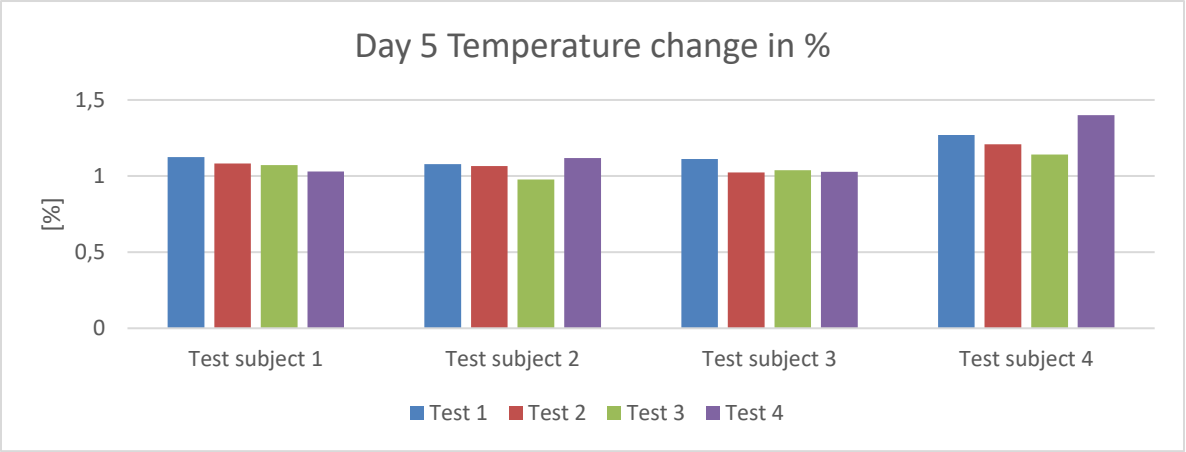

Figure 37b: Day 5. Temperature changes in % before and after a 780 nm laser pulse on forearm at different hydration levels.

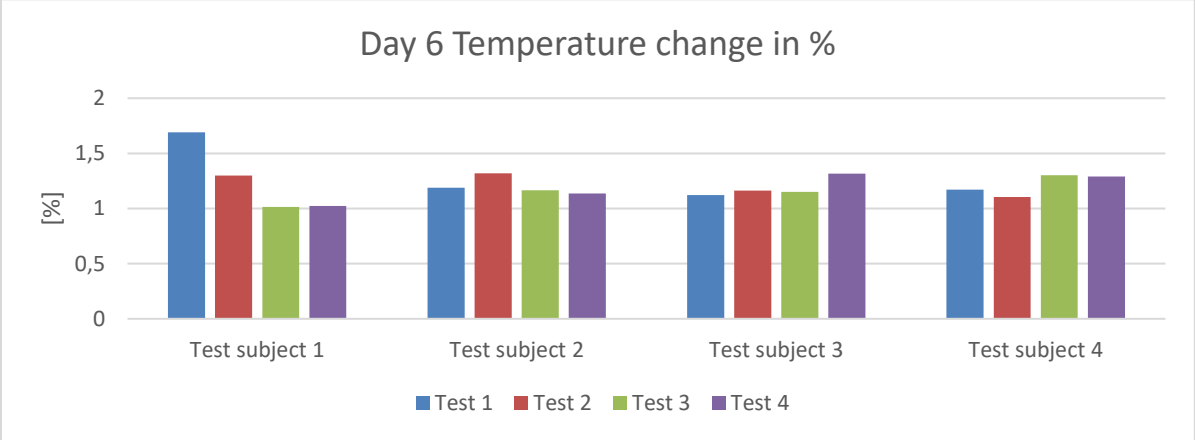

Figure 37c: Day 6. Temperature changes in % before and after a 780 nm laser pulse on forearm at different hydration levels.

Test trends	**Count**
Ascending order	0
Descending order	1
Random order	11
Total Tests	12

Table 12: Trends in percentage change from test method 2

In total, 11 of 12 tests did not show the expected result of a decrease of temperature change. But an interesting observation is that on 4 of the total 12 tests, we do see the expected descending percentage change in the three first tests. All test subjects were considered fully hydrated between test 3 and 4.

5.2.3 Test method 3: Single-pulse wave on forearm (Day 7-9)

5.2.3.1 Graphs

The graphs in Figures 38a – 38d show filtered data received from the IR temperature sensor from all test subjects from test day 9. Results from all tests can be found in Appendix A.

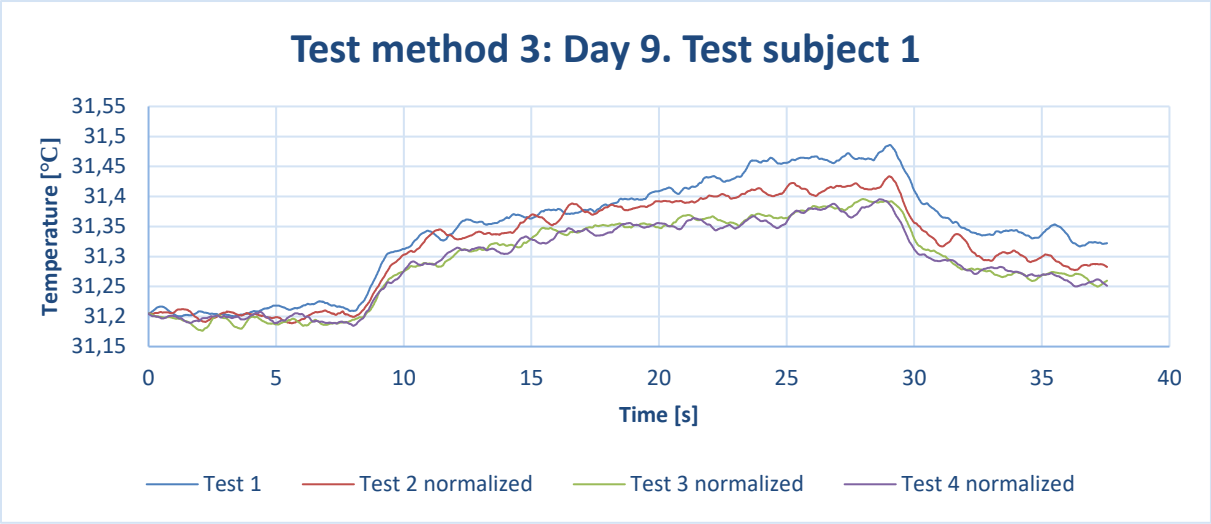

Figure 38a: Test method 3: Day 9. Test subject 1. IR temperature sensor readings during a single pulse of 980 nm laser transmission on ear lobe at different hydration levels.

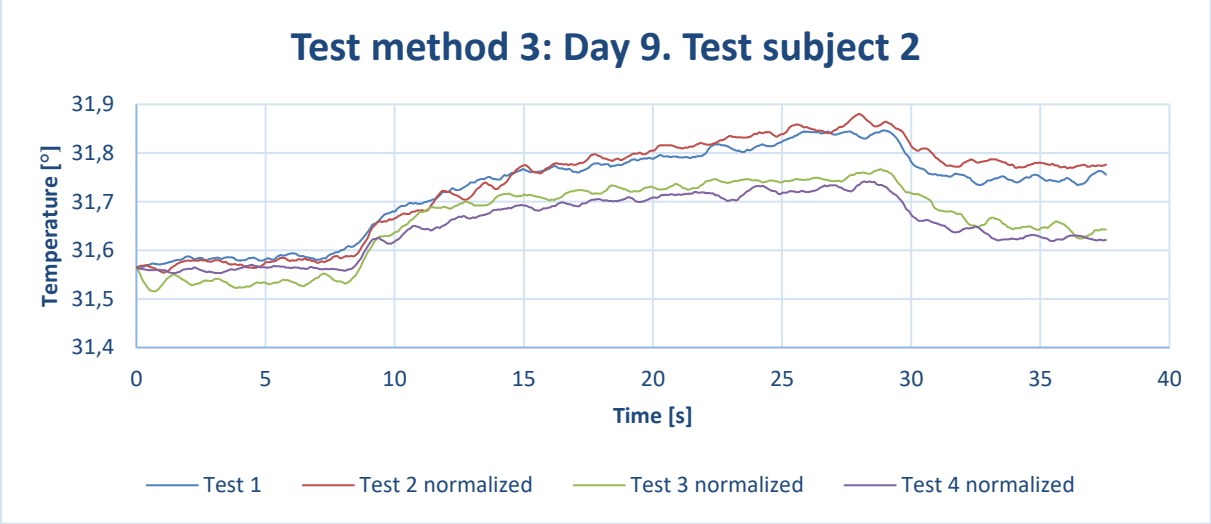

Figure 38b: Test method 3: Day 9. Test subject 2. IR temperature sensor readings during a single pulse of 980 nm laser transmission on ear lobe at different hydration levels.

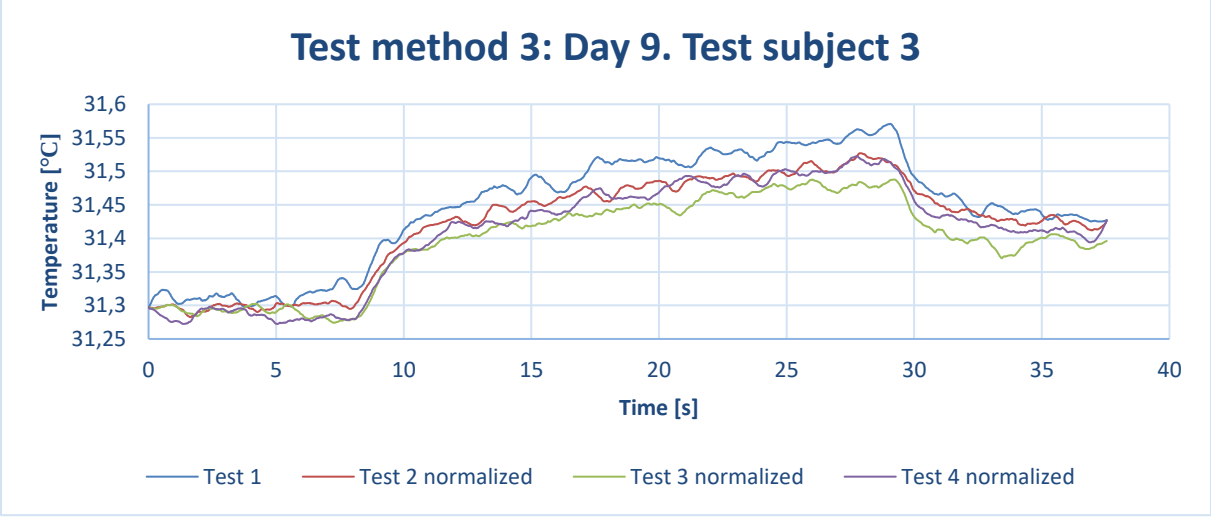

Figure 38c: Test method 3: Day 9. Test subject 3. IR temperature sensor readings during a single pulse of 980 nm laser transmission on ear lobe at different hydration levels.

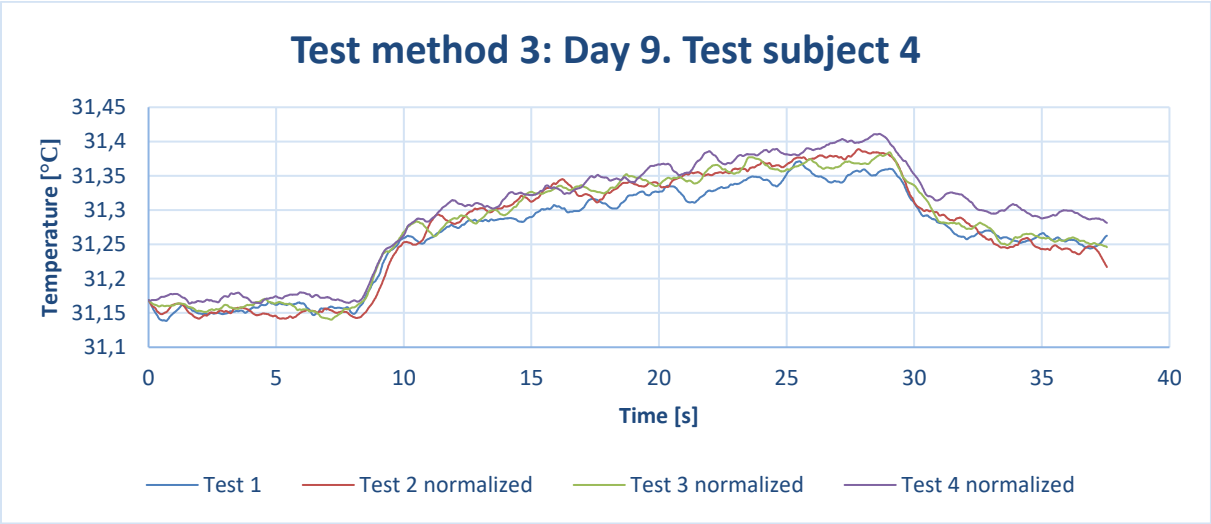

Figure 38d: Test method 3: Day 9. Test subject 4. IR temperature sensor readings during a single pulse of 980 nm laser transmission on ear lobe at different hydration levels.

Looking at the selected graphs, it appears that the temperature curves follows a more consistent trend regarding hydration level than earlier. We expected to see a smaller temperature increase from the laser pulses as hydration level increased. The only test subject not following the desired trend, was test subject 4.

5.2.3.2 Area

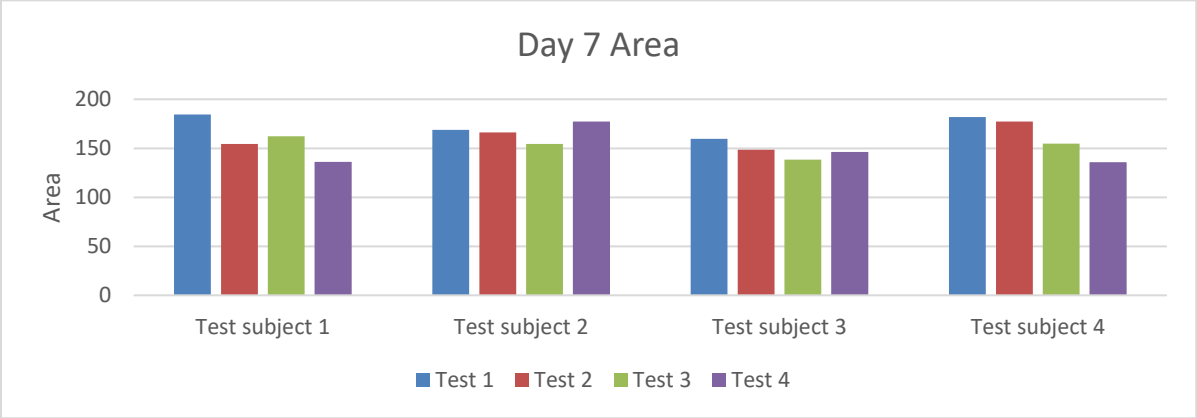

Figure 39a: Day 7. Area under curve of 980 nm single-pulse wave on forearm at different hydration levels.

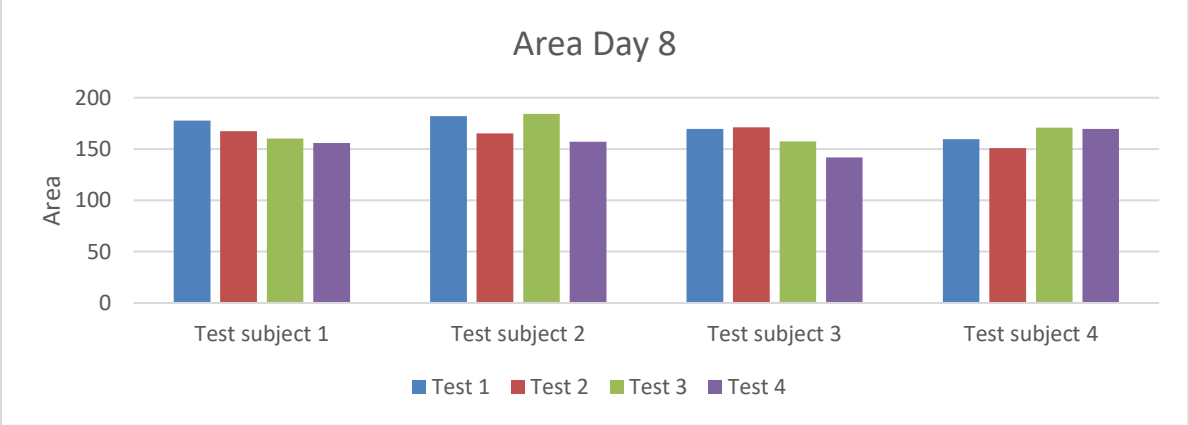

Figure 39b: Day 8. Area under curve of 980 nm single-pulse wave on forearm at different hydration levels.

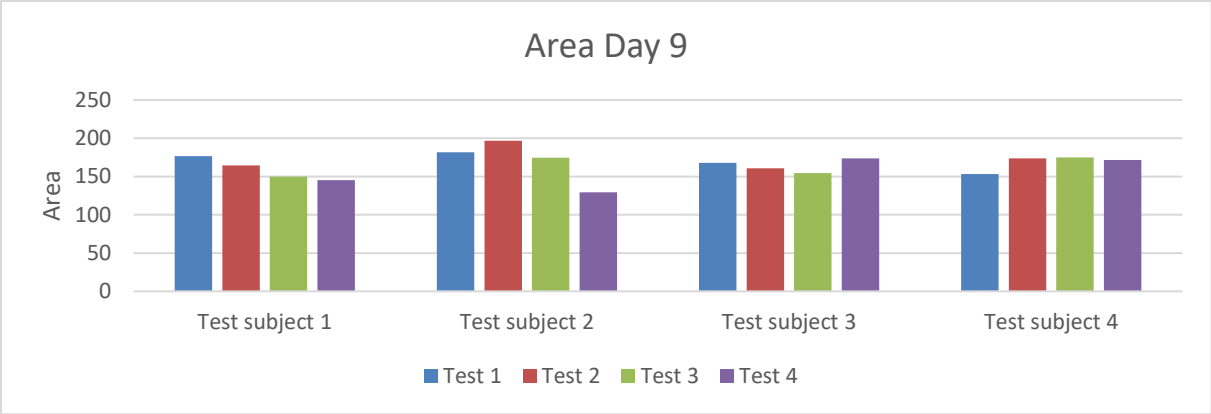

Figure 39c: Day 9. Area under curve of 980 nm single-pulse wave on forearm at different hydration levels.

Area Test Trends Method 3	**Count**
Ascending order	0
Descending order	3
Random order	9
Total Tests	12

Table 13: Trends in area from test method 3

Looking at the area statistics of *Test method 3*, it is apparent that the random order is the biggest contributor. We expected to see a descending order of area as hydration level increased.

5.2.3.3 Slope

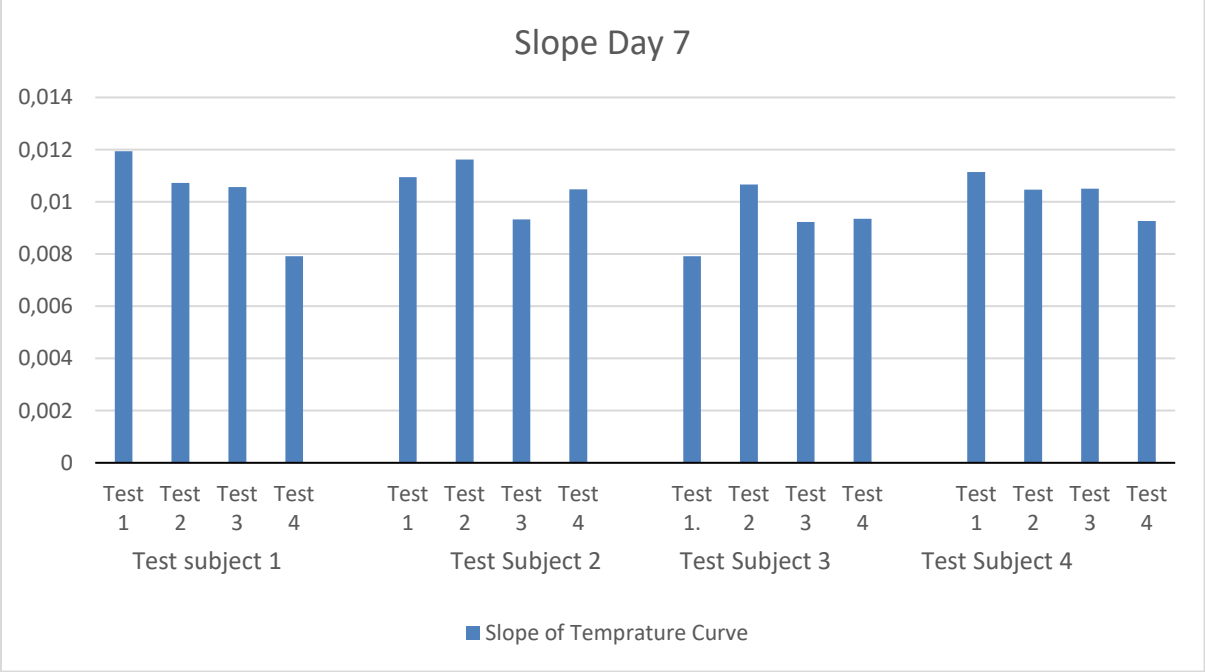

Figure 40a: Day 7. Slope with a 980 nm laser irradiation on forearm at different hydration levels.

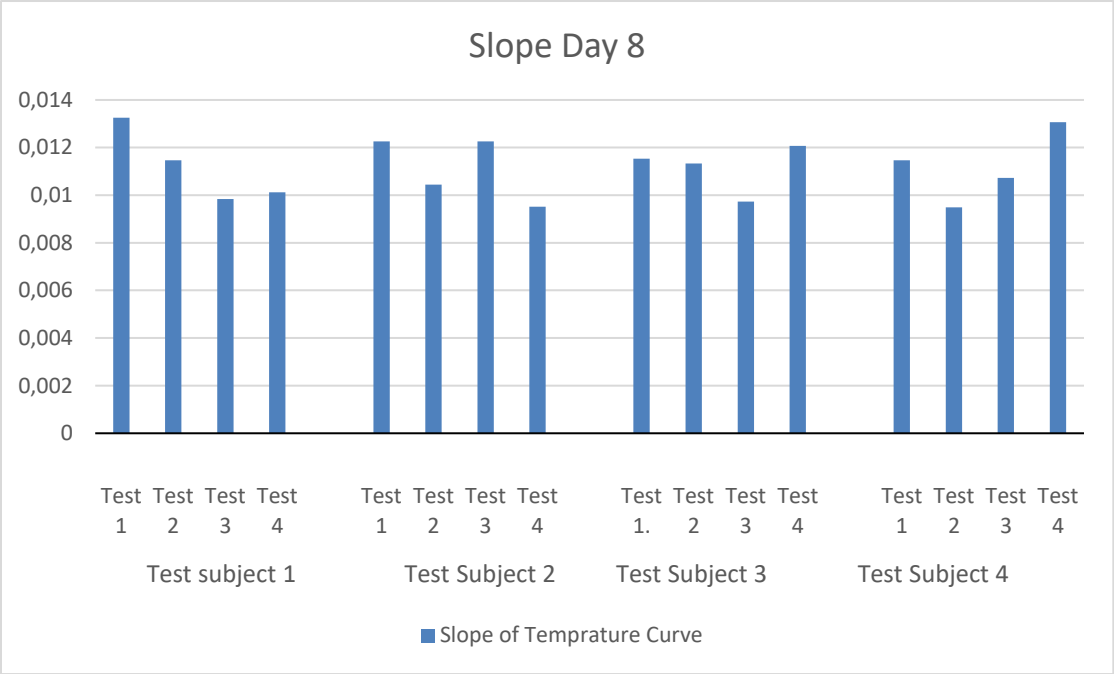

Figure 40b: Day 8. Slope with a 980nm laser irradiation on forearm at different hydration levels.

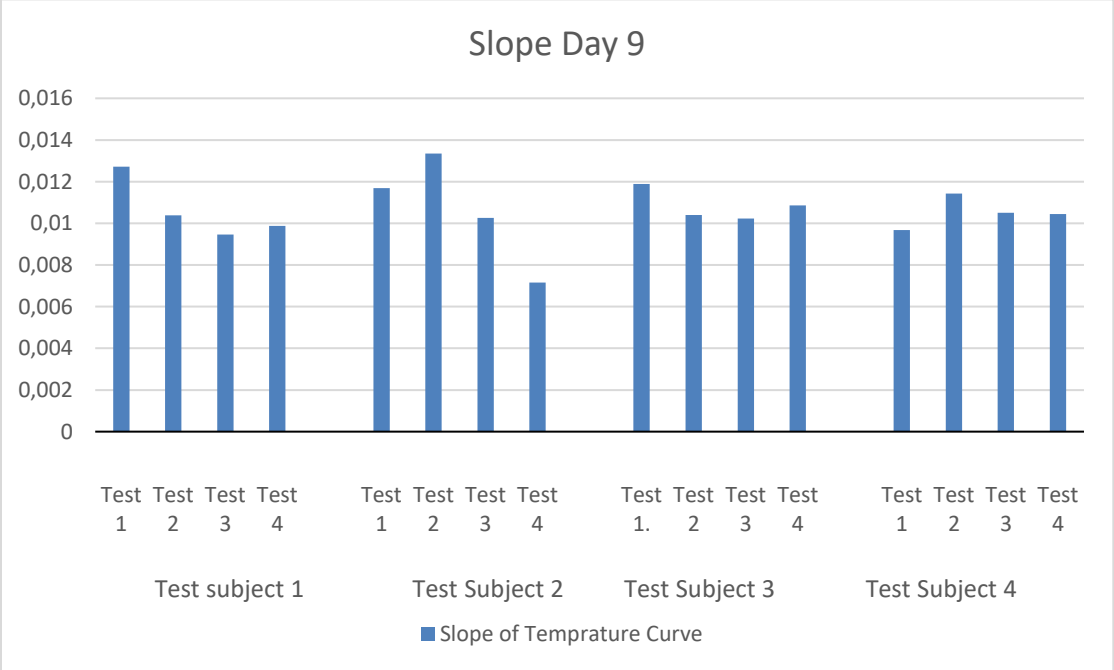

Figure 40c: Day 9. Slope with a 980nm laser irradiation on forearm at different hydration levels.

Slope Test trends Method 3	**Count**
Ascending order	0
Descending order	2
Random order	10
Total Tests	12

Table 14: Trends in slope progression from test method 3

Looking at the slope statistics of *Test method 3* in Table 14, there are 9 tests with minimal slope differences as hydration level increases. 2 tests had a negative slope progression and 1 test had a positive slope progression. We expected to see a negative slope progression as hydration level increased.

5.2.3.4 Percentage

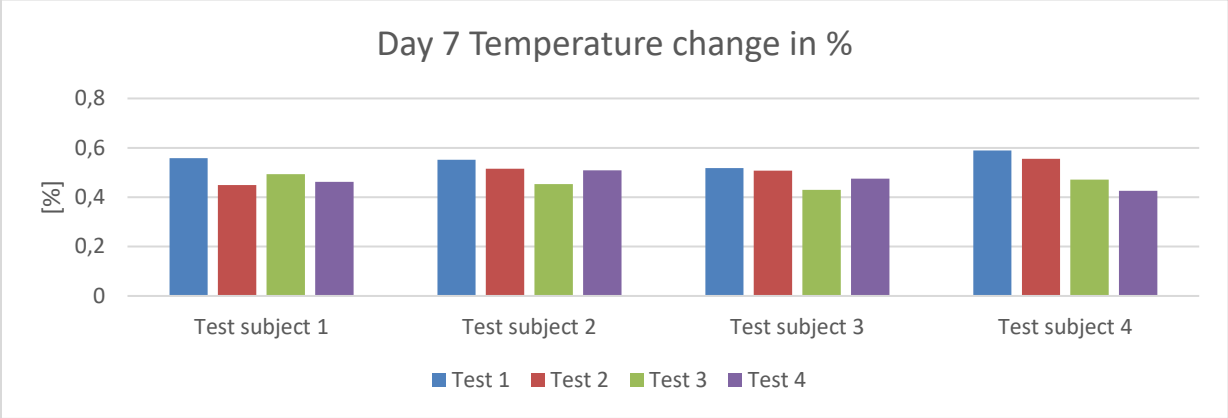

Figure 41a: Day 7. Temperature changes in % before and after a 980nm laser irradiation on forearm at different hydration levels.

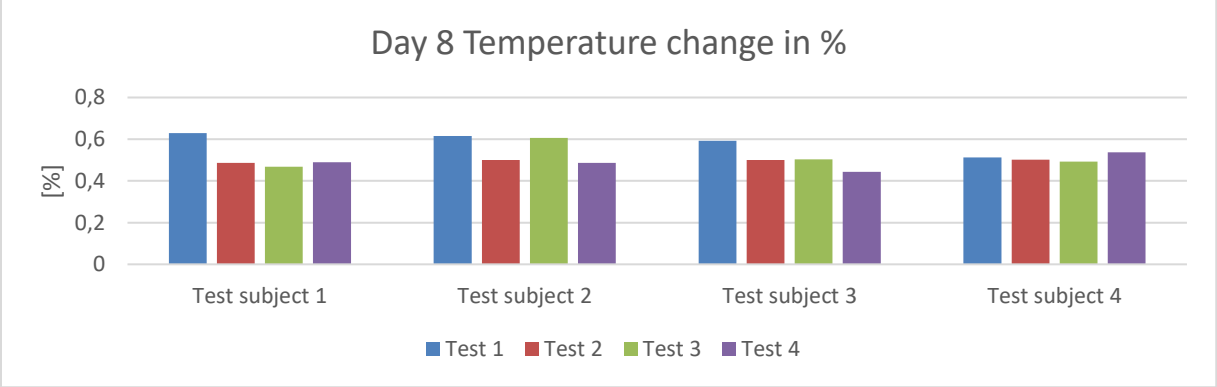

Figure 41b: Day 8. Temperature changes in % before and after a 980nm laser irradiation on forearm at different hydration levels

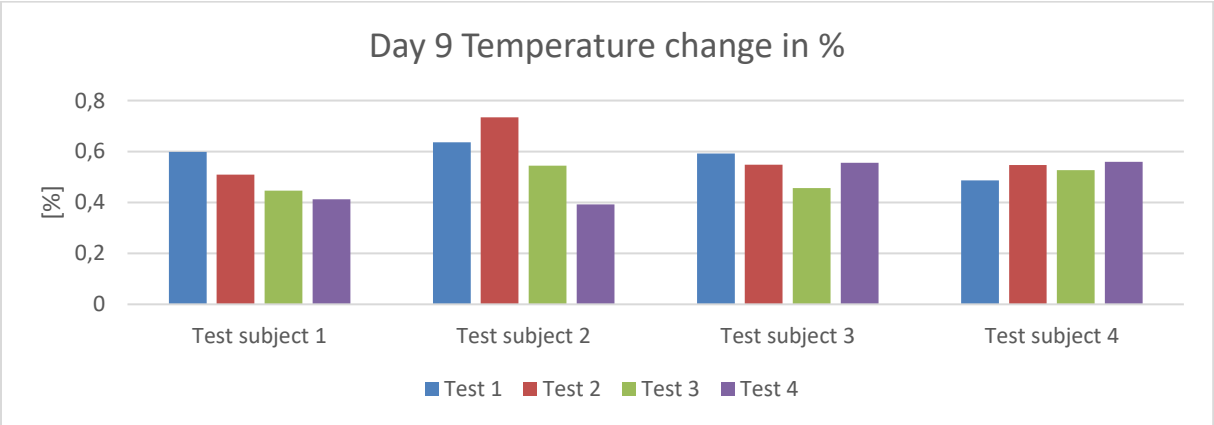

Figure 41c: Day 9. Temperature changes in % before and after a 980nm laser irradiation on forearm at different hydration levels

Percentage Test trends Method 3	Count
Ascending order	0
Descending order	2
Random order	10
Total Tests	12

Table 15: Trends in percentage change from test method 3

The changes in temperature in percentage, show only 2 of 12 tests with a descending order for each hydration level.

5.2.4 Sum of analyses

Area Statistics	Ascending order	Descending order	Random order
Test method 1: Single-pulse wave on earlobe	3	1	8
Test method 2: Pulsed wave on forearm	1	1	10
Test method 3: Single-pulse wave on forearm	0	3	9
Sum	**4**	**5**	**27**

Table 16: Trends in area from all tests combined

Slope Statistics	Ascending order	Descending order	Random order
Test method 1: Single-pulse wave on earlobe	3	1	8
Test method 2: Pulsed wave on forearm	2	0	10
Test method 3: Single-pulse wave on forearm	0	2	10
Sum	**5**	**3**	**28**

Table 17: Trends in slope progression from all tests combined

Percentage Statistics	Ascending order	Descending order	Random order
Test method 1: Single-pulse wave on earlobe	4	3	5
Test method 2: Pulsed wave on forearm	0	1	11
Test method 3: Single-pulse wave on forearm	0	2	10
Sum	**4**	**6**	**26**

Table 18: Trends in percentage change from all tests combined

In the area statistics, we expected a decrease in area size for every hour passed with increasing hydration levels. The results presented 5 tests in descending order, 4 in ascending order and 27 in random order, in a total of 36 tests.

In the slope statistics, we expected a decrease in the rate of temperature change for every hour passed. The results presented 3 tests in descending order, 5 in ascending order and 28 in random order, in a total of 36 tests.

In the percentage statistics, we expected a decrease in the percentage change for every hour passed. The results presented 6 tests in descending order, 4 in ascending order and 26 in random order, in a total of 36.

Due to a considerable amount of random ordered test results, we are not able to draw any conclusions from the temperature change in tissue resulting from exposure to infrared laser light at different hydration levels.

However, an interesting observation occurs if one erratic bar is disregarded from each test subject in the results of test method 2 and 3, we see a descending trend in 17 of 24 tests from the figures of area, 15 of 24 tests from the figures of slope, and 18 of 24 tests from the figures of percentages. This observation conforms with the theory of the study to a larger

degree, that more hydrated tissue will heat less than dehydrated tissue when the same amount of energy is applied. The reason for the erratic bars might be found in the sources of error.

In total, 13% of the tests displayed the expected outcome. If one erratic bar is disregarded from test method 2 and 3, 51% of the tests displays the expected outcome.

5.3 Sources of error

In this chapter, the sources of error are explored and mapped based on the knowledge and experiences acquired during the work on this paper. The sources of error are divided into categories to get a better overall picture of the areas of major concerns.

5.3.1 Infrared temperature sensor

Although the infrared temperature sensor has been calibrated, there is one aspect of the usage that has not been taken into consideration. That is the *sample rate* of which the temperature sensor performs a temperature reading. During calibration and pre-testing (assuring a standard deviation of less than 0.05°C), the sampling rate has been approximately 1 Hz whilst during collection of data the sampling rate has been approximately 50 Hz for t*est method 1* and *3* (frequency = 1 / 0.02s) and 200 Hz for *test method 2* (frequency = 1 / 0,005s). The increase in sampling frequency might affect the accuracy of the measurements due to the increase in load on the infrared temperature sensor involving more processing power and heat dissipated. This might account for the noise, or fluctuations, seen in the raw data Figure 29a of chapter 5.2. Thus, this would impact the signal to noise ratio.

5.3.2 Signal-to-noise ratio

As mentioned in the previous paragraph, there is noise on top of the signal. If the graphs of measurements in chapter 5.2 “Analytics” is viewed, the difference between the highest and lowest temperature measurement is approximately 0.5°C for the 980 nm laser and approximately 1.0°C for the 780 nm laser. The noise is in the magnitude of approximately 0.05 °C. This means the signal to noise ratio is approximately 0.5°C/ 0.05°C = 10 (980 nm laser) and 1.0°C/0.05° = 20 (780 nm laser). This could indicate that parts of the signal, that might reveal dehydration, is hidden by noise.

Another contribution to a low signal to noise ratio could be derived from scattered thermal radiation directly from the laser and surrounding surfaces. The air space between the laser and temperature sensor in the armband setup could possibly scatter the laser in any direction and reach the temperature sensor instead of to the surface of the skin. To improve the signal to noise ratio either the signal would have to be increased (make a bigger temperature difference), use a temperature sensor with higher accuracy or both.

5.3.3 Testing facilities and procedures

Factors that influenced the choice of measuring technique and instrumentation, were cost and time available. Components and instrumentation had to be inexpensive and readily available to reduce start-up time. Also, comparing with spectroscopy techniques, this method was thought to be more easily convertible to a wireless, wearable and affordable device. Other instrumentation techniques might have provided clearer results.

Although test procedure was set to limit the sources of error, the testing revealed an unforeseen source of error that affected the results. After performing sub-tests on two of the test subjects, the fire alarm sounded, and all had to evacuate the building. Outside the temperature was below zero and the test subjects were poorly dressed. The sub-tests performed after the building was cleared to enter had a significant different temperature reading compared to the other subjects' measurements, as exemplified in Figure 42. For clarification, the numbering of test subjects from 1 to 4, do not imply that test subject 1 performed the first test during that particular day. This arrangement varied from day to day.

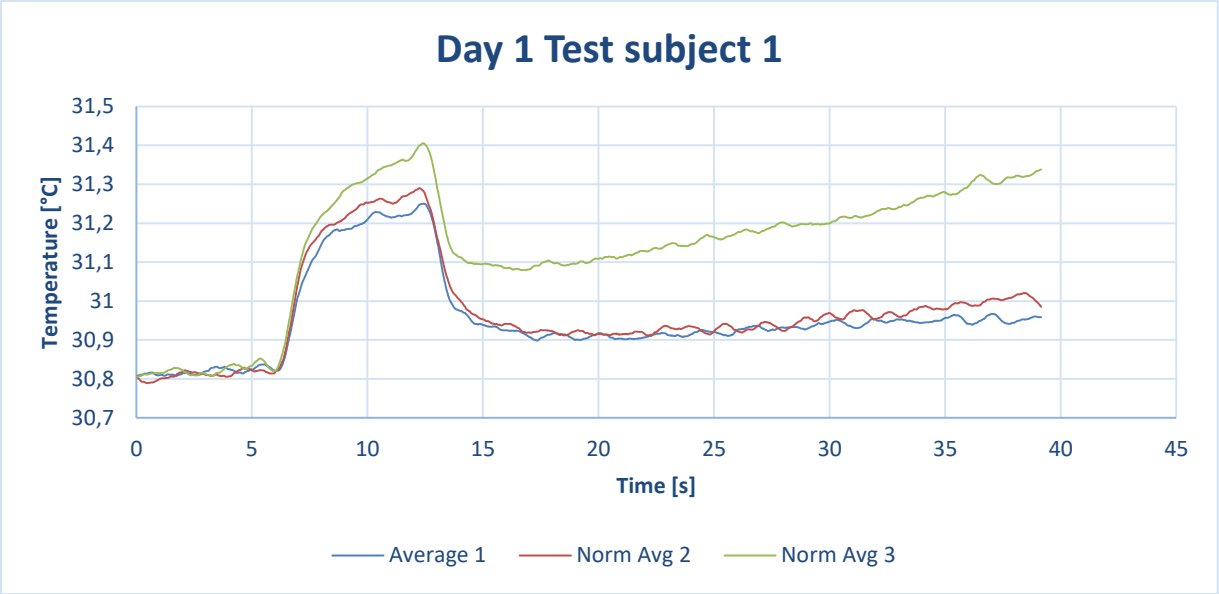

Figure 42: Curve named "Norm Avg 3" was performed after fire alarm incident.

Another possible source of error is the rate at which the test subjects drank the prescribed water. During testing some would consume the whole allotted ½ litre within a short period of time while others would steadily drink the ½ litre over approximately 1 hour. The temperature of the water consumed was not monitored either. These two factors could affect the overall body temperature and subsequently the measured temperatures.

The rate of water consumption will also affect the rate at which the body absorbs the water, likely affecting the results. *Test method 1* consisted of 3 sets of sub-tests at different hydration levels while *Test method 2* and *3* had 4 sets of sub-tests. Thus, comparing the results from test method 1 to the others introduces inconsistency.

5.3.4 Biological processes

Consumption of cold water gave a chilling effect on the body. And although this chilled the body, there will be a reaction from the body trying to maintain body temperature by increasing metabolism. Consuming 500 ml water can result in 30% increase in metabolic rate (Boschmann, M. 2003). The cooling effect of cold water is countered by increased metabolism, but the resulting effect on body temperature is not easily determined.

There are probably major differences between test subjects on how they react to drinking water as well not easily obtained without extensive testing. Factors like gender, age, body type, genes, diet, activity level, hormonal responses will likely affect the outcome of the test subjects' measurements, which has not been researched to any extent in this project.

6 Conclusion

Dehydration is a common problem that impacts health and society. There is no clinical "gold standard" to testing the water balance of the body that is rapid, non-invasive and reliable. Monitoring options, such as physical signs and urine and blood analyses, vary in validity and reliability due to the variations in gender, age, body type, diet, activity level, and other internal physiological factors. The current test methods also vary in cost-effectiveness and availability. We intended to develop a device as an alternative method to monitor hydration level, using optics as the foundation. Testing three different methods of measurement, we analysed the data for temperature changes in the skin at different hydration levels, but the results were inconclusive. We did not find enough evidence to confirm our hypotheses. In total, only 13% of the tests displayed the expected outcome, but 51% if one erratic bar was removed from test method 2 and 3. Even though this experiment did not perform as well as hoped, it revealed a field of opportunities for further exploration and investigation.

7 Future work

During the work on this paper, the group have experienced a steep learning curve. There is little research to be found on thermal radiation with regards to hydration in tissue. Nonetheless, there are many topics that could be addressed in further work on the subject.

To start with, our testing has been done on the wavelengths 780 nm and 980 nm. The main reason for using these wavelengths was that 780nm laser was easily available, and the 980 nm laser acquired later because we thought it would show better absorption characteristics in accordance to the absorption spectra of tissue (Figure 6). But what our testing showed, was that the increase in temperature was bigger for the 780 nm wavelength than the 980 nm wavelength laser. Thus, there might be a mismatch between what the theory indicates and what our testing showed with regards to temperature rise in tissue.

This suggests that there are more wavelengths to be explored to see the effect they have on tissue and possibly use several wavelengths simultaneously for a better result. Other laser characteristics explained in Chapter 3.5, such as beam form, spot size, fluence rate and irradiance should be explored.

From the fire alarm incident, controlling the surrounding temperature during testing is important. Other environmental factors to take into consideration, might be air humidity and consumed water temperature. In addition, controlling or monitoring key biological processes, such as metabolic rate, blood volume, haematocrit level (% of red blood cells in total blood volume), core body temperature and heart rate of the subject would also give important knowledge with regards to understanding the correlation between specific heat capacity, thermal radiation and hydration of the tissue. A future project could involve developing a mathematical heat transfer model for heat propagation in tissue, perhaps based on Penne's heat transfer equation, where certain physiological variables can be determined, and others neglected. Controlling these internal and environmental factors would lead to new testing procedures and might provide valuable insights regarding parameters influencing the results.

The scope of this paper was to measure dehydration level of tissue using an optical method. One of the challenges with this scope is the transfer of heat to the tissue using laser. The lasers used in our testing has a very small radiation energy and thus the temperature rise induced was quite small. A more powerful laser would transfer more energy, but the higher the power of the laser, the higher the risks of unwanted health effects. Aside from optics, a more traditional heating element (with heating wire) could have been used. However, this might introduce difficulties in targeting the specific absorption characteristics of molecules. The advantage of a higher energy transfer is a higher temperature rise, but also a higher signal to noise ratio.

In our test and analysis, the results have been in the time domain. These analyses have not given any conclusive result, but if the frequency domain had been explored, with the test results already at hand, the results might reveal more.

The method of monitoring dehydration through tissue hydration level, using absorption and thermal properties, has shown great potential and could, given the right method, be a new way of monitoring hydration level in the future. The key aspect is finding the right method for this concept. A great advantage of this method is that there are many aspects of this area to be explored before a conclusion is drawn.

References

780 nm and 980 nm lasers used in the dehydration monitoring device [image]. (n.d.). Retrieved March 11, 2019, from https://www.ebay.com/itm/5pcs-Laserland-8-13mm-10mW-780nm-IR-Infrared-Dot-Laser-Diode-Module-LD-3vdc-5vdc/131802751657?hash=item1eb00e62a9:g:iH4AAOSw-kdXz5YT

780 nm and 980 nm lasers used in the dehydration monitoring device [image]. (n.d.). Retrieved March 11, 2019, from https://www.ebay.com/itm/980nm-30mW-Infrared-IR-Laser-Diode-dot-Module-TTL-0-15KHZ-12x40mm/122227588631?epid=1167872982&hash=item1c7554fe17:g:nXwAAOSwxIRZ5v0O

Alves et al. (2017). Optical Imaging. In Kiessling, F., Pichler, B. J., & Hauff, P. (Eds.), *Small Animal Imaging: Basics and Practical Guide* (pp. 403-490). Springer. https://doi.org/10.1007/978-3-319-42202-2_16

Anderson, R. R., & John, A. P. (1981). The Optics of Human Skin. Journal of Investigative Dermatology, 77(1), 13. doi:10.1111/1523-1747.ep12479191

Ansari, M. A., & Mohajerani, E. (2011). Mechanisms of laser-tissue interaction: I. Optical properties of tissue. Journal of Lasers in Medical Sciences, 2(3), 119-125. doi:10.22037/2010.v2i3.2619

Armstrong, L.E. (2007). Assessing hydration status: the elusive gold standard. *Journal of the American College of Nutrition, 26 5 Suppl*, 575S-584S

Ash, C., Dubec, M., Donne, K., & Bashford, T. (2017). Effect of wavelength and beam width on penetration in light-tissue interaction using computational methods. *Lasers in medical science*, *32*(8), 1909–1918. doi:10.1007/s10103-017-2317-4

Ashenhurst, J. (2016). Bond Vibrations, Infrared Spectroscopy, and the "Ball and Spring" Model. Retrieved from: https://www.masterorganicchemistry.com/2016/11/11/bond-vibrations-ir-spectroscopy/

Attas, E. M., Sowa, M. G., Posthumus, T. B., Schattka, B. J., Mantsch, H. H., & Zhang, S. L. (2002). Near-IR spectroscopic imaging for skin hydration: The long and the short of it. *Biopolymers, 67*(2), 96-106. doi:10.1002/bip.10056

Avci, P., Hamblin, M. R., Gupta, A., Pam, N., Pam, Z., & Vecchio, D. (2013). Low-Level Laser (Light) Therapy (LLLT) in Skin: Stimulating, Healing, Restoring. *Seminars in Cutaneous Medicine and Surgery, 32(1),* 41-52.

Bak, A., Tsiami, A., & Greene, C. (2017). Methods of assessment of hydration status and their usefulness in detecting dehydration in the elderly. Current Research in Nutrition and Food Science, 5(2), 43-54. doi:10.12944/CRNFSJ.5.2.01)

Boschmann, M., Steiniger, J., Hille, U., Tank, J., Adams, F., Sharma, A., Klaus, S., Luft, F., Jordan, J. (2003). *The Journal of Clinical Endocrinology & Metabolism*, Volume 88, Issue 12, 1 December 2003, Pages 6015–6019, https://doi.org/10.1210/jc.2003-030780

Burger, N., Laachachi, A., Ferriol, M., Lutz, M., Toniazzo, V., & Ruch, D. (2016). Review of thermal conductivity in composites: Mechanisms, parameters and theory. *Progress in Polymer Science, 61*, 1-28. doi:10.1016/j.progpolymsci.2016.05.001

Burton, M., Luntz, M., Mozumder, A., Silverman, J., Tobias, C. A., Upton, A. C. (2014). Radiation. Retrevied from: https://www.britannica.com/science/radiation/Neutrons#ref28844

Butcher, G. (2016). *Tour of the Electromagnetic Spectrum* (3rd ed.). Washington DC: National Aeronautics and Space Administration

Bronzino, J. D. (Ed.) (2006). *The Biomedical Engineering Handbook (3rd ed.): Medical Devices and Systems*. Boca Raton: CRC Press

Campbell, N. (2011). Dehydration: why is it still a problem? *Nursing Times, 107*(22), 12-15.

Carroll, L., & Humphreys, T. R. (2006). LASER-tissue interactions. Clinics in Dermatology, 24(1), 2-7. doi:10.1016/j.clindermatol.2005.10.019

Caspers, P. (2003). *In vivo skin characterization by confocal Raman microspectroscopy*. Erasmus University Rotterdam, Retrieved from http://hdl.handle.net/1765/51258

Dehydration. (2017). Retrieved from Encyclopaedia Britannica website: https://www.britannica.com/science/dehydration-physiology

Dehydrering, inntørring. [Dehydration, desiccation]. (2018). Norsk Helseinformatikk. [Norwegian Health Information]. Retrieved from https://nhi.no/forstehjelp/varmekuldeskader/dehydrering-inntorring/#heading-0

Egawa, M., Arimoto, H., Hirao, T., Takahashi, M., & Ozaki, Y. (2006). Regional Difference of Water Content in Human Skin Studied by Diffuse-Reflectance Near-Infrared Spectroscopy: Consideration of Measurement Depth. *Applied Spectroscopy, 60*(1), 24-28. doi:10.1366/000370206775382866

Electronic and vibrational energy levels [image]. (2016). Retrieved April 3, 2019, from https://www.masterorganicchemistry.com/2016/11/11/bond-vibrations-ir-spectroscopy/

Electromagnetic Radiation. (2015). Retrieved from Chemistry Libretexts website: https://chem.libretexts.org/Bookshelves/Physical_and_Theoretical_Chemistry_Textbook_Maps/Supplemental_Modules_(Physical_and_Theoretical_Chemistry)/Spectroscopy/Fundamentals_of_Spectroscopy/Electromagnetic_Radiation

Etiske retningslinjer for forskning ved OsloMet - storbyuniversitetet (OsloMet). [Ethical guidelines for research at OsloMet – Oslo Metropolitan University]. (2014). Retrieved from https://ansatt.oslomet.no/documents/585743/53632647/Etiske+retningslinjer+for+forskning+ved+OsloMet/ca69e77b-fba1-b4f5-340e-b2e8127f464c

Evensen, S. A. (2018). Blodplasma. [Blood plasma]. In *Store medisinske leksikon. [Great Medical Encyclopedia]*. Retrieved from https://sml.snl.no/blodplasma

Foist, L. (n.d.). Vibrational Spectroscopy: Definition and Types. Retrieved from https://study.com/academy/lesson/vibrational-spectroscopy-definition-types.html

Fortes, M. B., Owen, J. A., Raymond-Barker, P., Bishop, C., Elghenzai, S., Oliver, S. J., & Walsh, N. P. (2015). Is This Elderly Patient Dehydrated? Diagnostic Accuracy of Hydration Assessment Using Physical Signs, Urine, and Saliva Markers. *Journal of the American Medical Directors Association, 16*(3), 221-228. doi:10.1016/j.jamda.2014.09.012

Fossum. (2009). Grunnsubstans. [Ground substance]. In *Store medisinske leksikon*. *[Great Medical Encyclopedia]*. Retrieved from https://sml.snl.no/grunnsubstans

Frangeskou, M., Lopez-Valcarcel, B., & Serra-Majem, L. (2015). Dehydration in the elderly: A review focused on economic burden. *The journal of nutrition, health & aging, 19*(6), 619-627. doi:10.1007/s12603-015-0491-2

Fundamental interaction. (2009). Retrieved from Encyclopaedia Britannica website: https://www.britannica.com/science/fundamental-interaction

Fustini, D. (2012). Re: Raspberry Pi GPIO pin max current [Online discussion group]. Retrieved from https://www.element14.com/community/thread/20982/l/raspberry-pi-gpio-pin-max-current?displayFullThread=true

Grøn, Ø. (2018). Infrarød stråling. [Infrared Radiation]. In *Store Norske Leksikon. [Great Norwegian Encyclopaedia]*. Retrieved from https://snl.no/infrar%C3%B8d_str%C3%A5ling

Hamblin, M. (2013). Tissue penetration depths of various wavelengths. Retrieved from https://www.researchgate.net/publication/256835631_Low-Level_Laser_Light_Therapy_LLLT_in_skin_stimulating_healing_restoring/figures

Hasgall, P.A., Di Gennaro, F., Baumgartner, C., Neufeld, E., Lloyd, B., Gosselin, M.C., Payne, D., Klingenböck, A., Kuster, N. (n.d.). "IT'IS Database for thermal and electromagnetic parameters of biological tissues," Version 4.0, May 15, 2018, DOI: 10.13099/VIP21000-04-0. itis.swiss/database

Hauge, A. (2018). Dehydrering. [Dehydration]. In *Store medisinske leksikon*. *[Great Medical Encyclopedia]*. Retrieved from https://sml.snl.no/dehydrering

Hecht, J. (2018). Laser. Retrieved from: https://www.britannica.com/technology/laser

Helmenstine, A.M. (2018). How Much of Your Body Is Water? Retrieved from https://www.thoughtco.com/how-much-of-your-body-is-water-609406

Hematology. (2016). Retrieved from Encyclopaedia Britannica website: https://www.britannica.com/science/hematology

Homeostasis. (n.d.) *Miller-Keane Encyclopedia and Dictionary of Medicine, Nursing, and Allied Health, Seventh Edition*. (2003). Retrieved May 7 2019 from https://medical-dictionary.thefreedictionary.com/homeostasis

Hooper, L. (2016). Why, Oh Why, Are So Many Older Adults Not Drinking Enough Fluid? *Journal of the Academy of Nutrition and Dietetics, 116*(5), 774-778. doi:10.1016/j.jand.2016.01.006

Hooper, L., Downing, A., Jimoh, F. O., & Bunn, D. K. (2015). PREDICTORS OF DEHYDRATION IN OLDER PEOPLE: DEHYDRATION RECOGNITION IN OUR ELDERS (DRIE) STUDY. *The Gerontologist, 55*(Suppl2), 594-594. doi:10.1093/geront/gnv307.03

Huang, H., Horng, T. (2015). Bioheat Transfer and Thermal Heating for Tumor Treatment. Retrieved from: https://www.sciencedirect.com/topics/medicine-and-dentistry/bioheat-transfer

Human skin layers [image]. (n.d.). Retrieved May 21, 2019, from https://www.webmd.com/skin-problems-and-treatments/picture-of-the-skin#1

I2C – What's That? (n.d). Retrieved from https://www.i2c-bus.org/

Isotopic tracer. (2018) Retrieved from Encyclopaedia Britannica website: from https://www.britannica.com/science/isotopic-tracer

Jacob, S. W., Entman, M. L,. & Oliver, M. F. (2018). Human cardiovascular system. Retrieved from https://www.britannica.com/science/human-cardiovascular-system

Jardine, W. (2018). Hydration testing. Retrieved from: https://www.scienceforsport.com/hydration-testing/#toggle-id-1

Jones, A. Z. (2019). Visible Light Spectrum Overview and Chart. Retrieved from https://www.thoughtco.com/the-visible-light-spectrum-2699036

Kashcooli, M., Salimpour, M. R., Shirani, E. (2017). Heat transfer analysis of skin during thermal therapy using thermal wave equation. Journal of Thermal Biology, Volume 64, 2017, Pages 7-18, ISSN 0306-4565, https://doi.org/10.1016/j.jtherbio.2016.12.007.

Kierulf, P. (2016). Osmoregulering. [Osmoregulation]. In *Store medisinske leksikon. [Great Medical Encyclopedia]*. Retrieved from https://sml.snl.no/osmoregulering

Kierulf, P. (2018). Osmose. [Osmosis]. In *Store medisinske leksikon. [Great Medical Encyclopedia]*. Retrieved from https://sml.snl.no/osmose

Kim, S. (2007). Preventable Hospitalizations of Dehydration: Implications of Inadequate Primary Health Care in the United States. In (pp. 736).

Knight, R. D. (2004). *Physics for Scientists and Engineers: With Modern Physics: A Strategic Approach (International Ed.)*. San Francisco, Calif: Pearson Addison-Wesley.

Kornberg, H. (2018). Metabolism. Retrieved from Encyclopaedia Britannica website: https://www.britannica.com/science/metabolism

Kovac, D. (2015). Urine electrolytes and osmolality [Powerpoint slides]. Retrieved from http://www.nephro-slovenia.si/images/pdf/urex/Urine_electrolytes.pdf

Lagrue K. (n.d). Beam form. Retrieved from https://bitesizebio.com/21988/the-power-of-sted-microscopy-part-1-how-does-it-work/

Langeland, T. (2019). Huden. [The Skin]. In *Store medisinske leksikon. [Great Medical Encyclopedia]*. Retrieved from https://sml.snl.no/huden

Larkin, P. J. (2011). *Infrared and Raman Spectroscopy: Principles and Spectral Interpretation*. Amsterdam, The Netherlands: Elsevier Inc.

Laser Lab Source. (n.d.). Laser Diode Driver Basics and Circuit Design Fundamentals. Retrieved from https://www.laserdiodecontrol.com/laser-diode-driver-basics-and-fundamentals

Lavizzo-Mourey, R. J. (1987). Dehydration in the elderly: a short review. Journal of the National Medical Association, 79(10), 1033.

Lešnik, A., Piko, N., Železnik, D., & Bevc, S. (2017). Dehydration of Older Patients in Institutional Care and the Home Environment. *Research in Gerontological Nursing, 10*(6), 260-266. doi:10.3928/19404921-20171013-03

Mange eldre er dehydrerte. [Many elderly are dehydrated]. (2016). Norsk Helseinformatikk. [Norwegian Health Information]. Retrieved from https://nhi.no/kosthold/ernaring/mange-eldre-er-dehydrerte/

Miller, H. J. (2015). Dehydration in the Older Adult. *Journal of gerontological nursing, 41*(9), 8. doi:10.3928/00989134-20150814-02

Mirtaheri P. (2019). Fluence rate and trajectory of photons with the wavelength of 780nm at a 60 degree angle (Mirtaheri P., personal communication, April 30, 2019)

MLX90614 on a pcb [image]. (n.d.). Retrieved Feb 4, 2019, from https://www.ebay.com/itm/MLX90614ESF-BAA-GY906-MLX90614-Contactless-Temperature-Sensor-Module-for-Arduino/183649183999?epid=2293138168&hash=item2ac25828ff:g:yjIAAOSwAopbaWQy

Molecular Spectroscopy. (2018). Retrieved from Chemistry Libretexts website: https://chem.libretexts.org/Bookshelves/Physical_and_Theoretical_Chemistry_Textbook_Maps/Map%3A_Physical_Chemistry_(McQuarrie_and_Simon)/13%3A_Molecular_Spectroscopy

Monochromatic. (n.d.). In *Cambridge Dictionary*. Retrieved from: https://dictionary.cambridge.org/dictionary/english/monochromatic

Nair, M., & Peate, I. (2015). Anatomy and Physiology for Nurses. In At a Glance. Retrieved from https://ebookcentral-proquest-com.ezproxy.hioa.no

National Laser Company. (n.d.). Laser Classification and Safety. Retrieved from http://www.national-laser.com/laser-classification.htm

NCI Dictionary of Cancer Terms. (n.d.). *Laser therapy*. Retrieved from https://www.cancer.gov/publications/dictionaries/cancer-terms/def/laser-therapy

Niemz, M. H. (1996). *Laser-tissue interactions: Fundamentals and applications* (3rd Ed.) Berlin: Springer.

O'Brien, C., Young, A., Sawka, M. (2002). Bioelectrical Impedance to Estimate Changes in Hydration Status. International journal of sports medicine. 23. 361-6. 10.1055/s-2002-33145

Optical phenomena of laser-tissue interaction [image]. (2015). Retrieved April 6, 2019, from https://pocketdentistry.com/laser-fundamentals/

Osmolality (Blood). (n.d.) In *University of Rochester Medical Center: Health Encyclopedia*. Retrieved from https://www.urmc.rochester.edu/encyclopedia/content.aspx?contenttypeid=167&contentid=osmolality_blood

Osmosis [image]. (2019). Retrieved May 21, 2019, from https://en.wikipedia.org/wiki/Osmosis

Parikh, R., Mathai, A., Parikh, S., Chandra Sekhar, G., & Thomas, R. (2008). Understanding and using sensitivity, specificity and predictive values. Indian Journal of Ophthalmology, 56(1), 45-50. doi:10.4103/0301-4738.37595

Paschotta, R. (n.d.). Fluence. RP photonics Encyclopedia. Retrieved from https://www.rp-photonics.com/fluence.html

Paschotta, R. (n.d.). Irradiance. RP photonics Encyclopedia. Retrieved from https://www.rp-photonics.com/irradiance.html

Pasquini, C. (2018). Near infrared spectroscopy: A mature analytical technique with new perspectives – A review. *Analytica Chimica Acta, 1026*, 8-36. doi:10.1016/j.aca.2018.04.004

Peate, I., & Nair, M. (2015). *Anatomy and Physiology for Nurses*. At a Glance. Retrieved from https://ebookcentral-proquest-com.ezproxy.hioa.no

Péronnet, F., Mignault, D., du Souich, P., Vergne, S., Le Bellego, L., Jimenez, L., & Rabasa-Lhoret, R. (2012). Pharmacokinetic analysis of absorption, distribution and disappearance of ingested water labeled with D 2 O in humans. *European Journal of Applied Physiology, 112*(6), 2213-2222. doi:10.1007/s00421-011-2194-7

Physiopedia. (November 19, 2018). Dehydration. Retrieved 15:55, March 14, 2019 from https://www.physio-pedia.com/index.php?title=Dehydration&oldid=200636

Press, W. & Tekolsky, S. (1990). Savitzky-Golay Smoothing Filters. Computers in Physics 4, 669 (1990); doi: 10.1063/1.4822961

Raspberry Pi Zero and GPIO pinout orientation [image]. (2018). Retrieved April 18, 2019, from https://raspberrypi.stackexchange.com/questions/83610/gpio-pinout-orientation-raspberypi-zero-w

Rockwell Laser Industries. (n.d) Laser Standards and Classifications. Retrieved 19:30, May 10, 2019 from https://www.rli.com/resources/articles/classification.aspx

Sfera, A., Cummings, M., & Osorio, C. (2016). Dehydration and Cognition in Geriatrics: A Hydromolecular Hypothesis. Frontiers in molecular biosciences, 3, 18. doi:10.3389/fmolb.2016.00018

Schafer, R. (2011). What Is a Savitzky-Golay Filter? [IEEE Signal processing magazine]. Retrieved from: https://ieeexplore.ieee.org/stamp/stamp.jsp?arnumber=5888646

Shepherd, A. (2011). Measuring and managing fluid balance. *Nursing Times, 107*(28), 12.

Shimizu, M., Kinoshita, K., Hattori, K., Ota, Y., Kanai, T., Kobayashi, H., & Tokuda, Y. (2012). Physical Signs of Dehydration in the Elderly. Internal Medicine, 51(10), 1207-1210. doi:10.2169/internalmedicine.51.7056

Smith, A. M., Mancini, M. C., & Nie, S. (2009). Bioimaging: Second window for in vivo imaging. *Nature Nanotechnology, 4*(11), 710. doi:10.1038/nnano.2009.326

Soderberg, T. (2017). Introduction to Molecular Spectroscopy. Retrieved from https://chem.libretexts.org/Bookshelves/Organic_Chemistry/Book%3A_Organic_Chemistry_with_a_Biological_Emphasis_(Soderberg)/Chapter_04%3A_Structure_Determination_I/4.1%3A_Introduction_to_molecular_spectroscopy

The electromagnetic spectrum [image]. (n.d.). Retrieved May 19, 2019, from http://gsp.humboldt.edu/olm_2015/Courses/GSP_216_Online/lesson1-2/spectrum.html

Tissue Optical Properties. (n.d). University of Cyprus Biomedical Imaging and Applied Optics. Retreived from: http://www.eng.ucy.ac.cy/cpitris/courses/ECE477/presentations/English/05.%20Tissue%20Optics.pdf

UiO Department of Physics. (2011). *What is bioimpedance?* Retrieved from https://www.mn.uio.no/fysikk/english/research/projects/bioimpedance/whatis/

Unger, K. (n.d). The effect of dehydration on the cardiovascular system. Retrieved from https://www.livestrong.com/article/150464-the-effects-of-dehydration-on-the-cardiovascular-system/

University of Washington. (2007) LASER Safety Manual. Retrieved from https://www.ehs.washington.edu/system/files/resources/lasermanual.pdf

University of Leeds. (n.d.). Extracellular Matrix - 'Ground substance'. Retrieved from https://histology.leeds.ac.uk/tissue_types/connective/connective_groundS.php

U.S. National Library of Medicine. (2018). *MedlinePlus: Fluid and Electrolyte Balance.* Retrieved from https://medlineplus.gov/fluidandelectrolytebalance.html

Vurdering av dehydrering hos voksne. [Assessment of dehydration in adults]. (2016). In *Norsk Elektronisk Legehåndbok. [Norwegian Electronic Medical Handbook].* Retrieved from https://legehandboka.no/

Wikipedia. 2019. *Osmosis* [image]. Retrieved from https://en.wikipedia.org/wiki/Osmosis

What is thermal conductivity. (n.d.). In Khan Academy. Retrieved from https://www.khanacademy.org/science/physics/thermodynamics/specific-heat-and-heat-transfer/a/what-is-thermal-conductivity

Xiao, S. H., Barber, S. J., & Campbell, S. E. (2004). Economic burden of dehydration among hospitalized elderly patients. *American Journal of Health-System Pharmacy, 61*(23), 2534-2540.

Zubieta-Calleja, G., & Paulev, P. (1998). Chapter 21: Thermo-Regulation, Temperature and Radiation. In New Human Physiology (2nd Edition). Retrieved from: http://www.zuniv.net/physiology/book/chapter21.html

Appendix A

Plots of data sets

Day 1

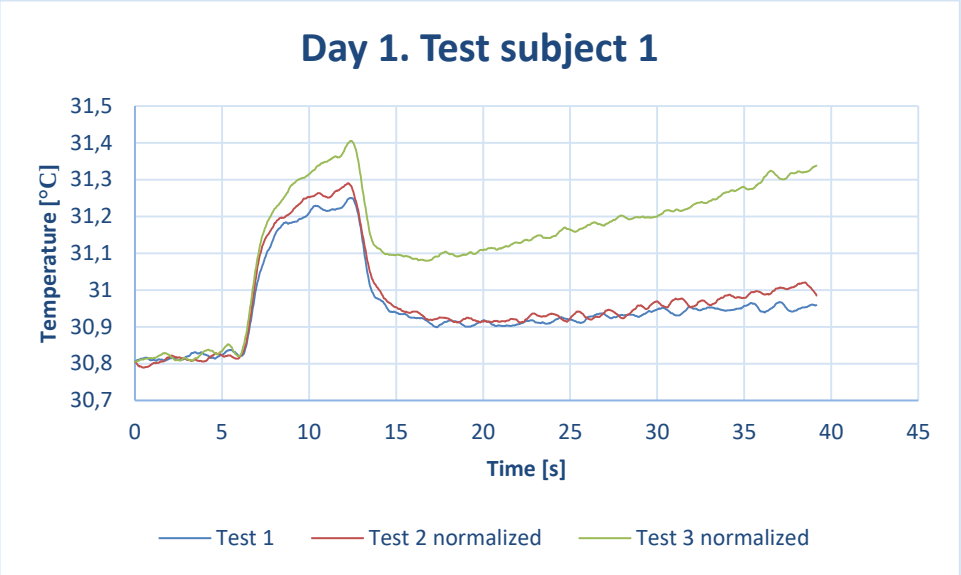

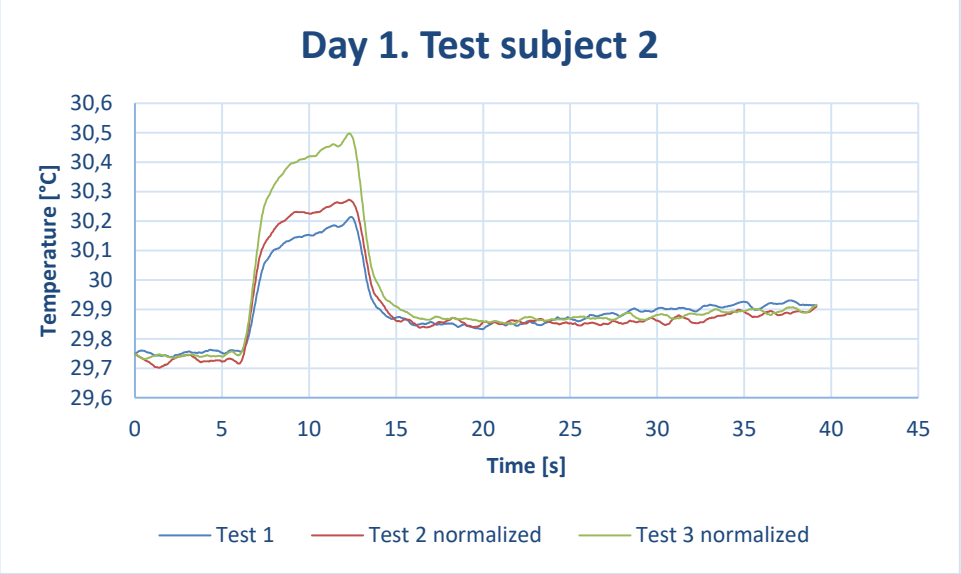

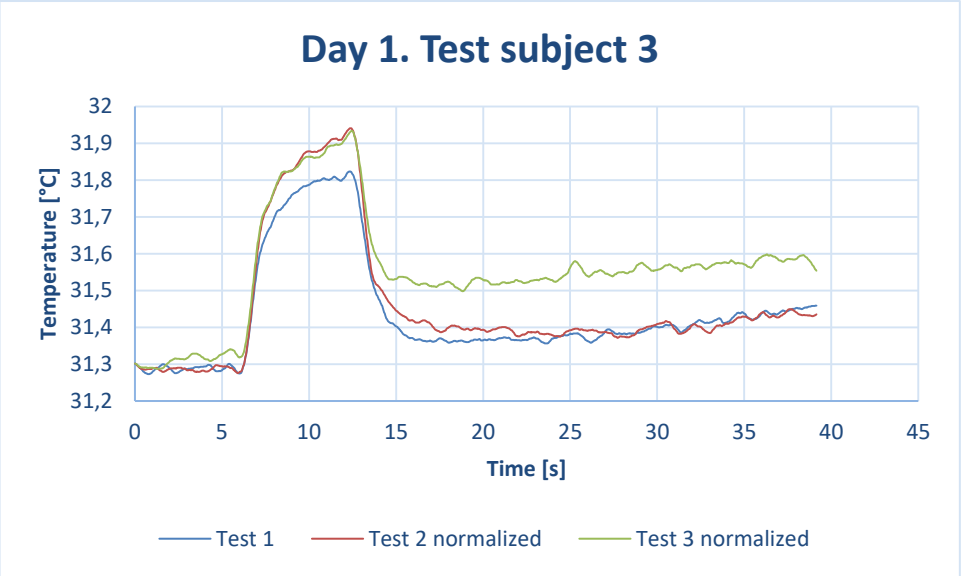
Day 1. Test subject 3
Temperature [°C]
32
31,9
31,8
31,7
31,6
31,5
31,4
31,3
31,2
0
5
10
15
20
25
30
35
40
45
Time [s]
Test 1
Test 2 normalized
Test 3 normalized

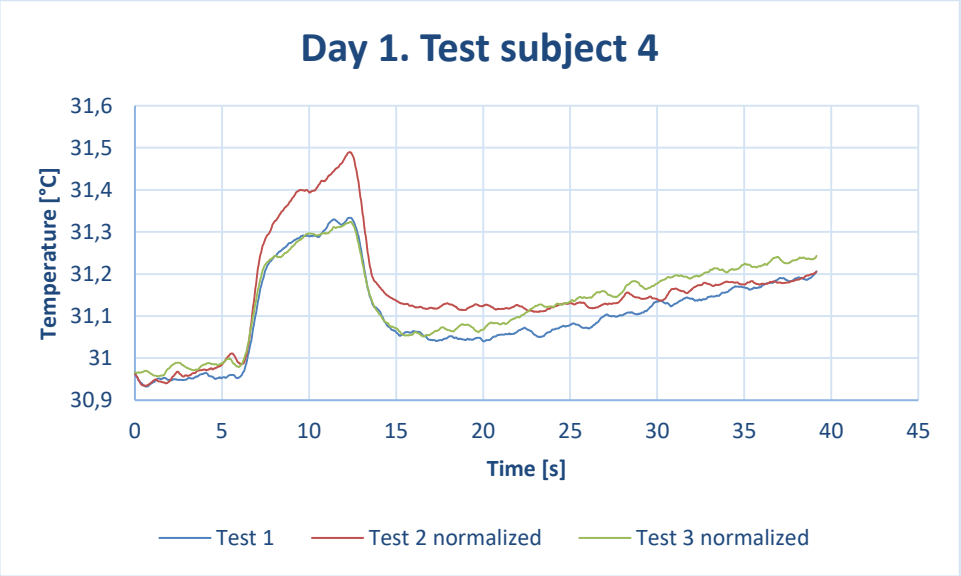
Day 1. Test subject 4
Temperature [°C]
31,6
31,5
31,4
31,3
31,2
31,1
31
30,9
0
5
10
15
20
25
30
35
40
45
Time [s]
Test 1
Test 2 normalized
Test 3 normalized

Day 2

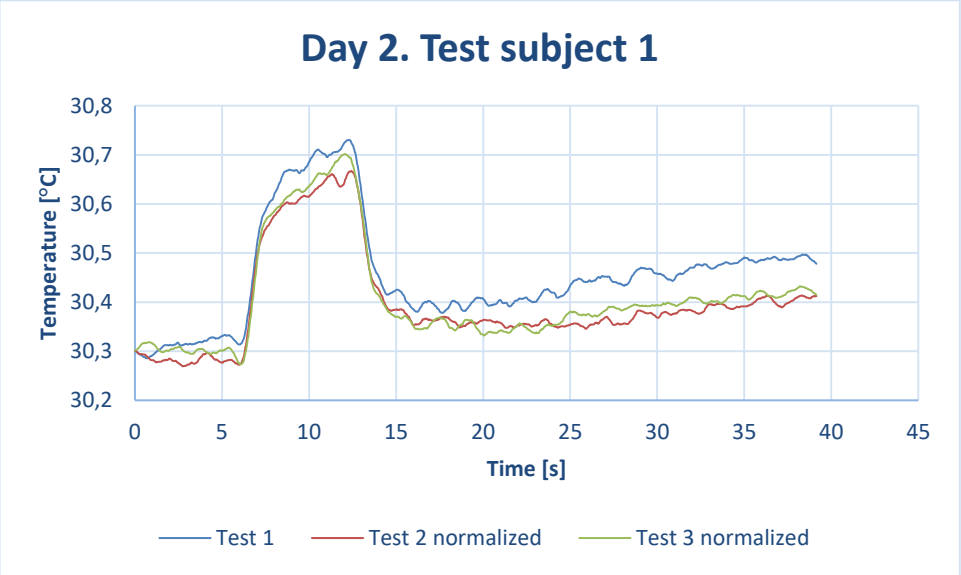
Day 2. Test subject 1
Temperature [°C]
30,8
30,7
30,6
30,5
30,4
30,3
30,2
0
5
10
15
20
25
30
35
40
45
Time [s]
Test 1
Test 2 normalized
Test 3 normalized

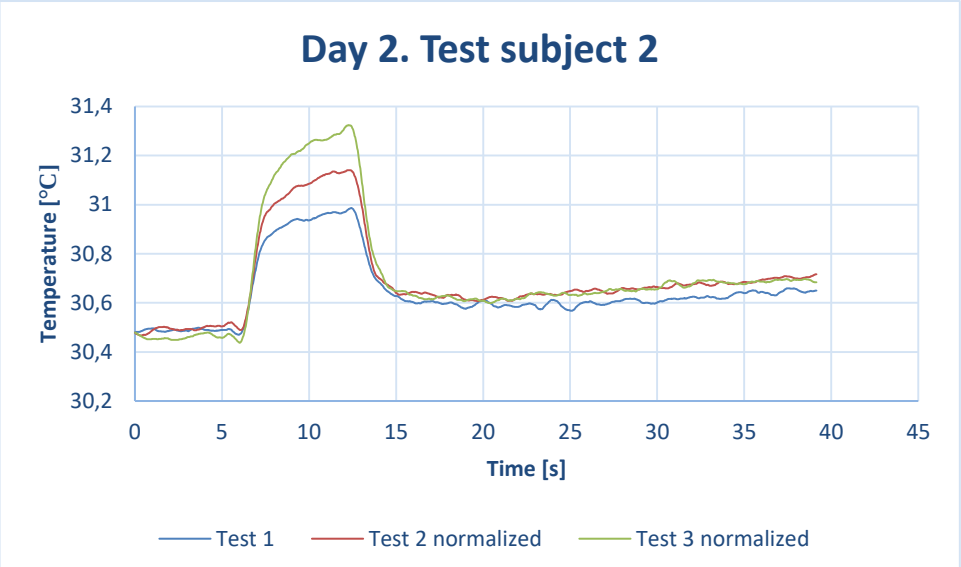
Day 2. Test subject 2
Temperature [°C]
31,4
31,2
31
30,8
30,6
30,4
30,2
0
5
10
15
20
25
30
35
40
45
Time [s]
Test 1
Test 2 normalized
Test 3 normalized

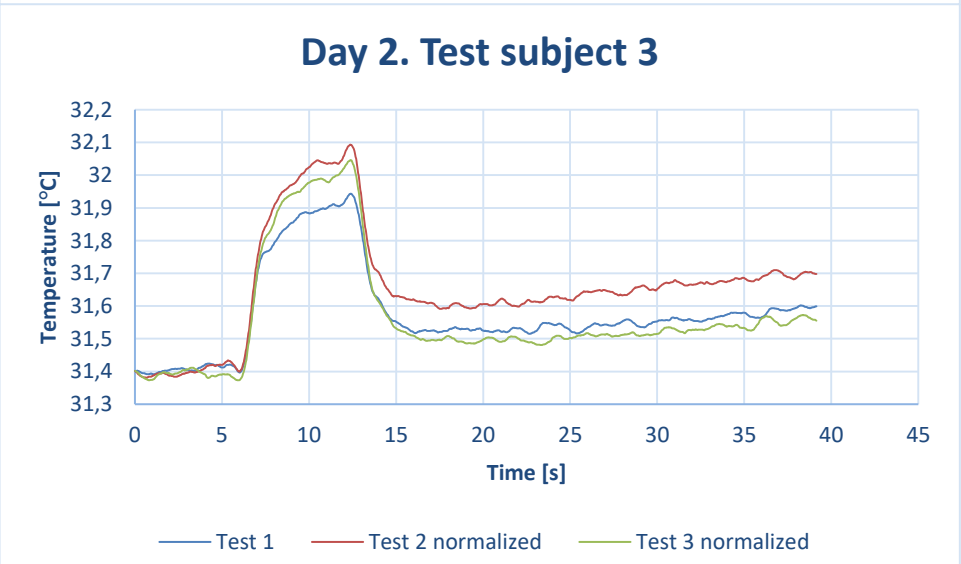
Day 2. Test subject 3
Temperature [°C]
32,2
32,1
32
31,9
31,8
31,7
31,6
31,5
31,4
31,3
0
5
10
15
20
25
30
35
40
45
Time [s]
Test 1
Test 2 normalized
Test 3 normalized

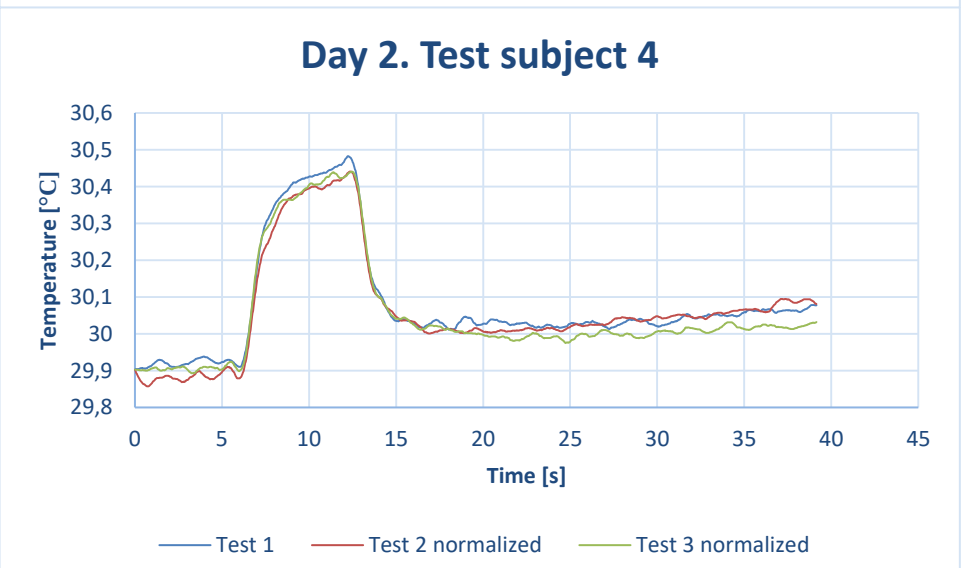
Day 2. Test subject 4
Temperature [°C]
30,6
30,5
30,4
30,3
30,2
30,1
30
29,9
29,8
0
5
10
15
20
25
30
35
40
45
Time [s]
Test 1
Test 2 normalized
Test 3 normalized

Day 3

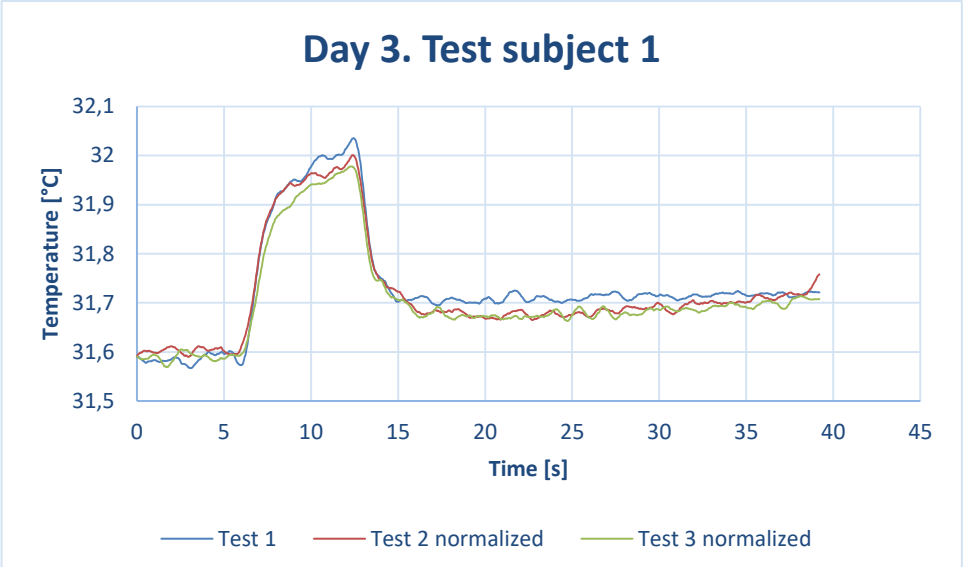
Day 3. Test subject 1
Temperature [°C]
32,1
32
31,9
31,8
31,7
31,6
31,5
0
5
10
15
20
25
30
35
40
45
Time [s]
Test 1
Test 2 normalized
Test 3 normalized

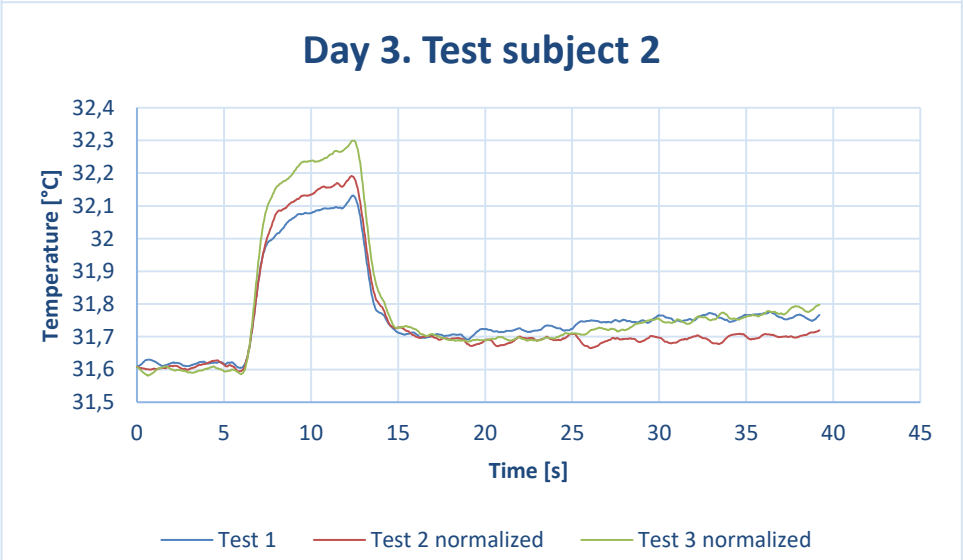
Day 3. Test subject 2
Temperature [°C]
32,4
32,3
32,2
32,1
32
31,9
31,8
31,7
31,6
31,5
0
5
10
15
20
25
30
35
40
45
Time [s]
Test 1
Test 2 normalized
Test 3 normalized

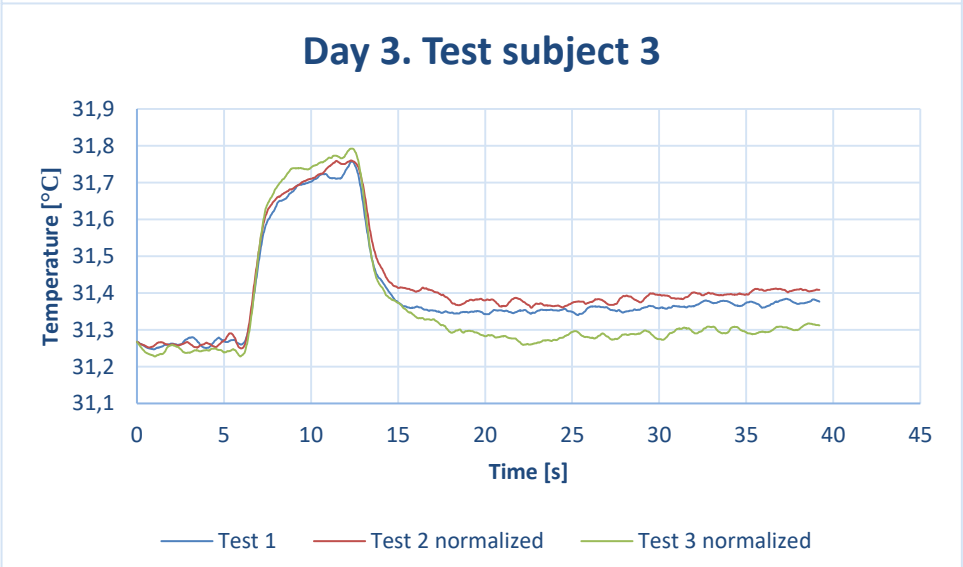
Day 3. Test subject 3
Temperature [°C]
31,9
31,8
31,7
31,6
31,5
31,4
31,3
31,2
31,1
0
5
10
15
20
25
30
35
40
45
Time [s]
Test 1
Test 2 normalized
Test 3 normalized

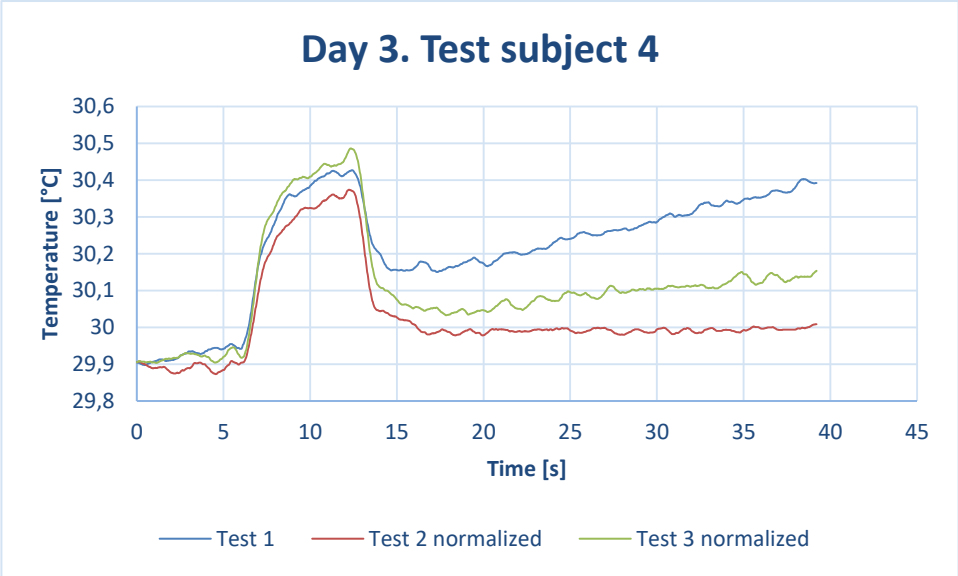
Day 3. Test subject 4
Temperature [°C]
30,6
30,5
30,4
30,3
30,2
30,1
30
29,9
29,8
0
5
10
15
20
25
30
35
40
45
Time [s]
Test 1
Test 2 normalized
Test 3 normalized

Day 4

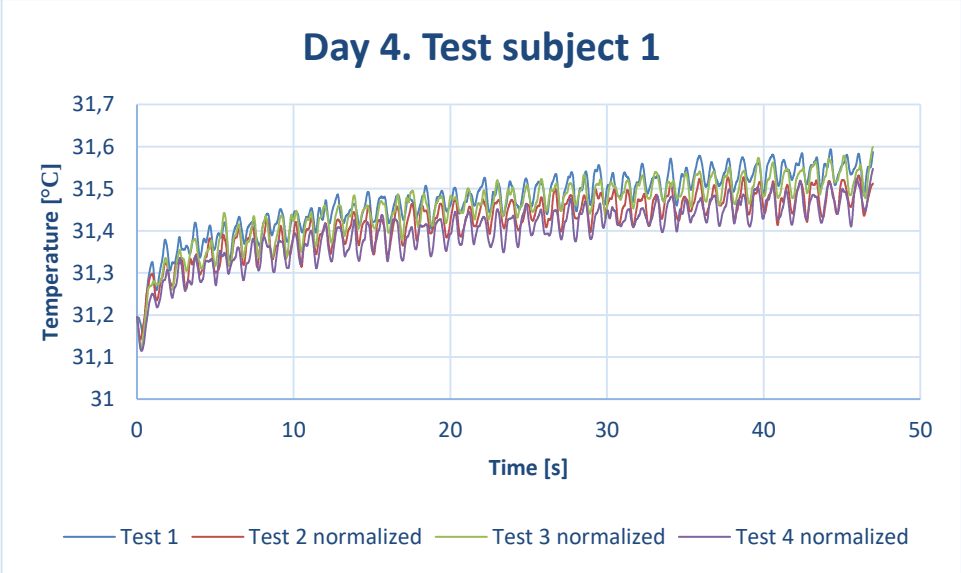
Day 4. Test subject 1
Temperature [°C]
31,7
31,6
31,5
31,4
31,3
31,2
31,1
31
0
10
20
30
40
50
Time [s]
Test 1
Test 2 normalized
Test 3 normalized
Test 4 normalized

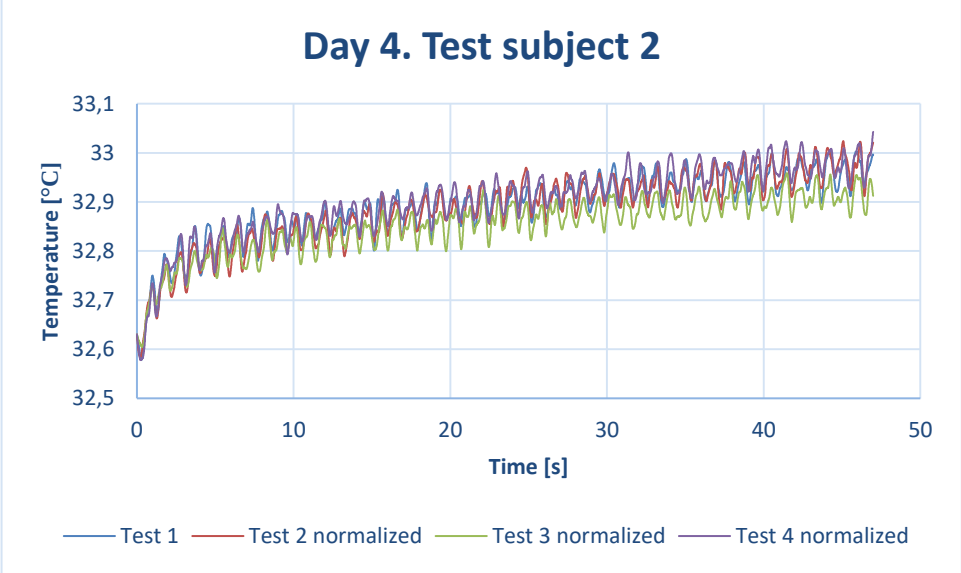
Day 4. Test subject 2
Temperature [°C]
33,1
33
32,9
32,8
32,7
32,6
32,5
0
10
20
30
40
50
Time [s]
Test 1
Test 2 normalized
Test 3 normalized
Test 4 normalized

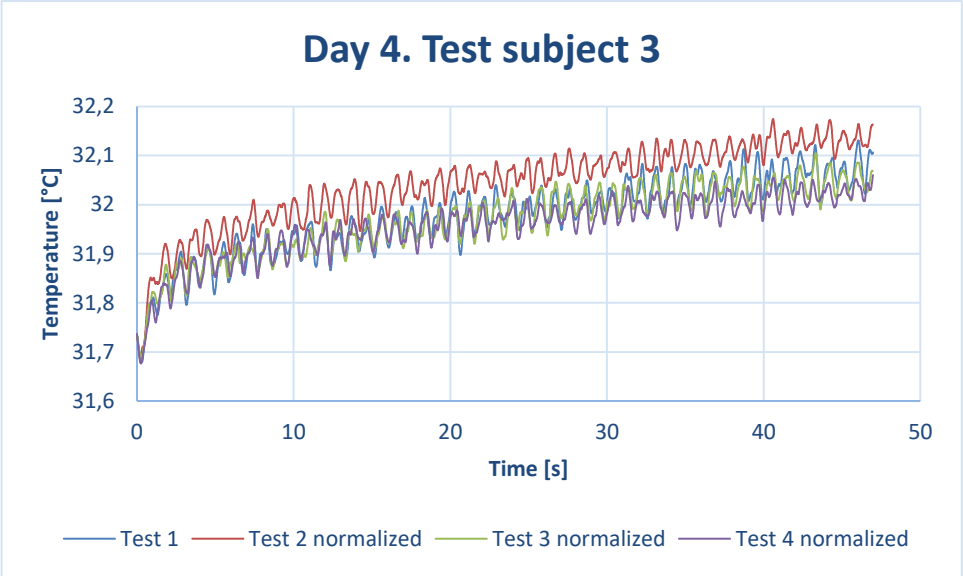
Day 4. Test subject 3
Temperature [°C]
32,2
32,1
32
31,9
31,8
31,7
31,6
0
10
20
30
40
50
Time [s]
Test 1
Test 2 normalized
Test 3 normalized
Test 4 normalized

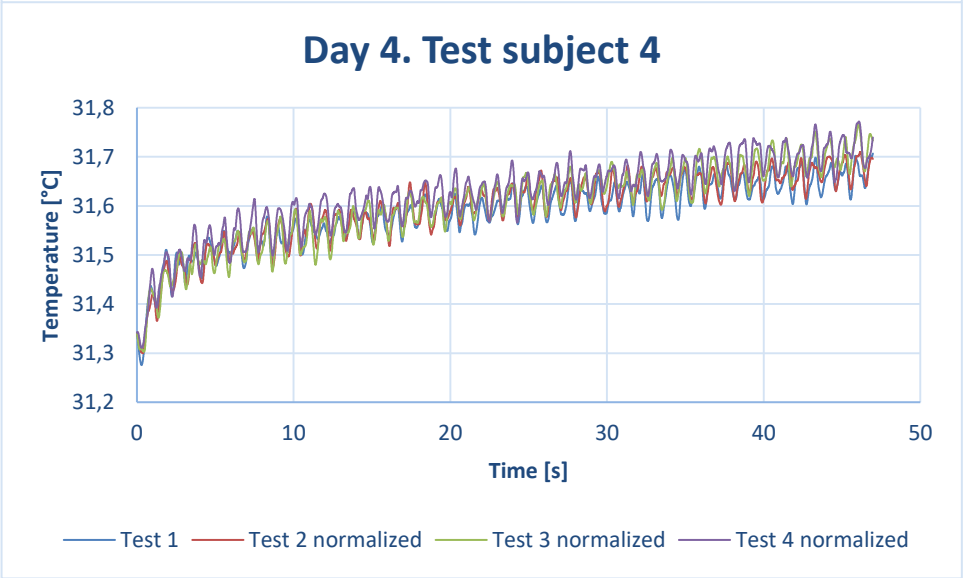
Day 4. Test subject 4
Temperature [°C]
31,8
31,7
31,6
31,5
31,4
31,3
31,2
0
10
20
30
40
50
Time [s]
Test 1
Test 2 normalized
Test 3 normalized
Test 4 normalized

Day 5

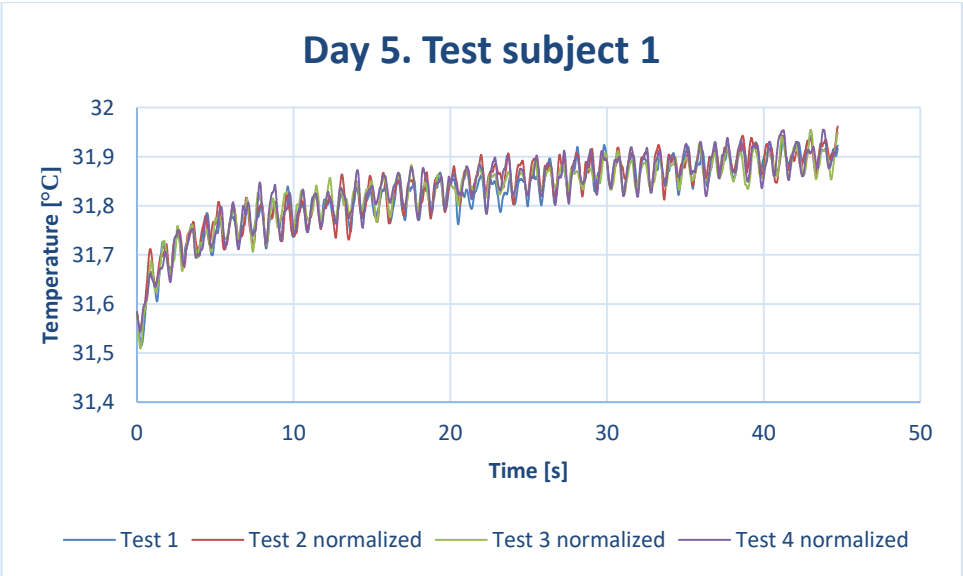
Day 5. Test subject 1
Temperature [°C]
32
31,9
31,8
31,7
31,6
31,5
31,4
0
10
20
30
40
50
Time [s]
Test 1
Test 2 normalized
Test 3 normalized
Test 4 normalized

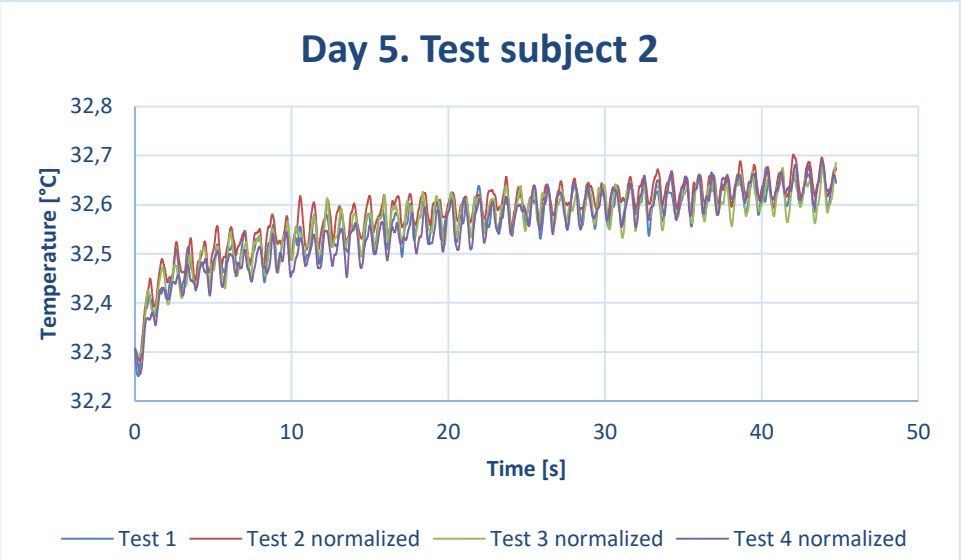
Day 5. Test subject 2
Temperature [°C]
32,8
32,7
32,6
32,5
32,4
32,3
32,2
0
10
20
30
40
50
Time [s]
Test 1
Test 2 normalized
Test 3 normalized
Test 4 normalized

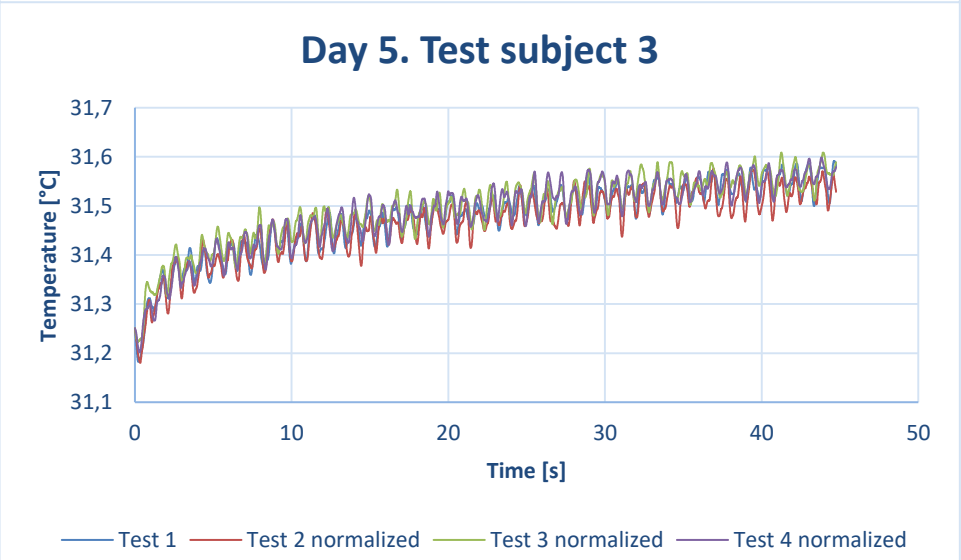
Day 5. Test subject 3
Temperature [°C]
31,7
31,6
31,5
31,4
31,3
31,2
31,1
0
10
20
30
40
50
Time [s]
Test 1
Test 2 normalized
Test 3 normalized
Test 4 normalized

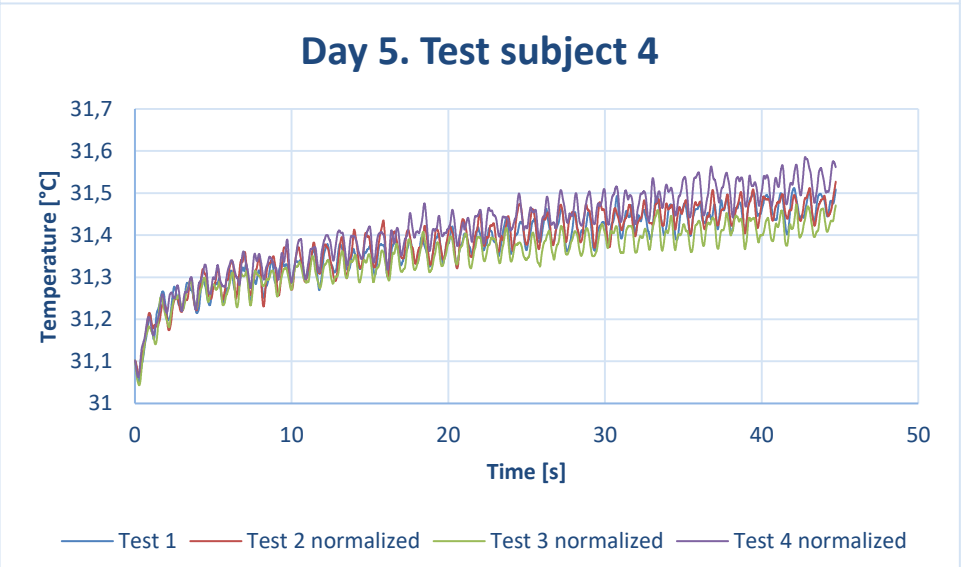
Day 5. Test subject 4
Temperature [°C]
31,7
31,6
31,5
31,4
31,3
31,2
31,1
31
0
10
20
30
40
50
Time [s]
Test 1
Test 2 normalized
Test 3 normalized
Test 4 normalized

Day 6

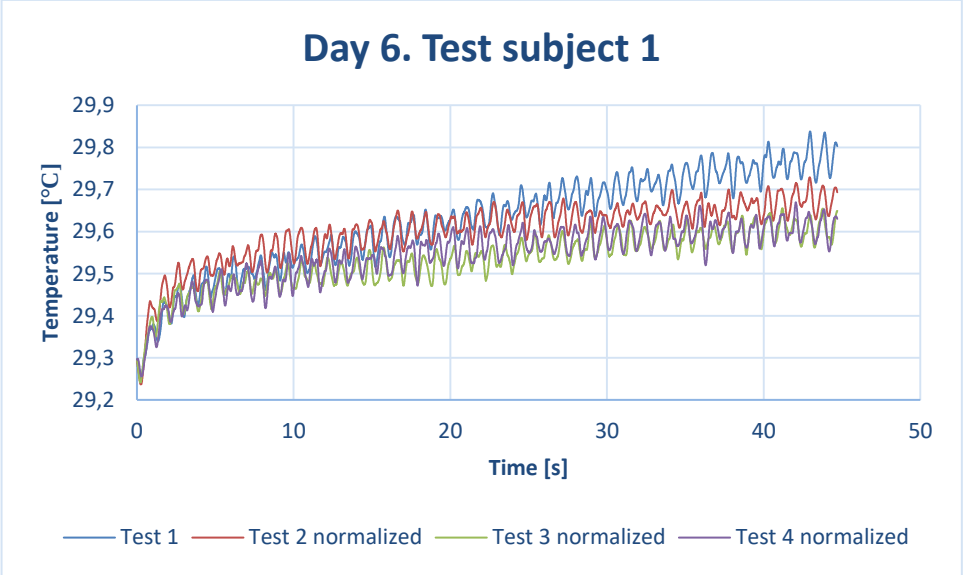
Day 6. Test subject 1
Temperature [°C]
29,9
29,8
29,7
29,6
29,5
29,4
29,3
29,2
0
10
20
30
40
50
Time [s]
Test 1
Test 2 normalized
Test 3 normalized
Test 4 normalized

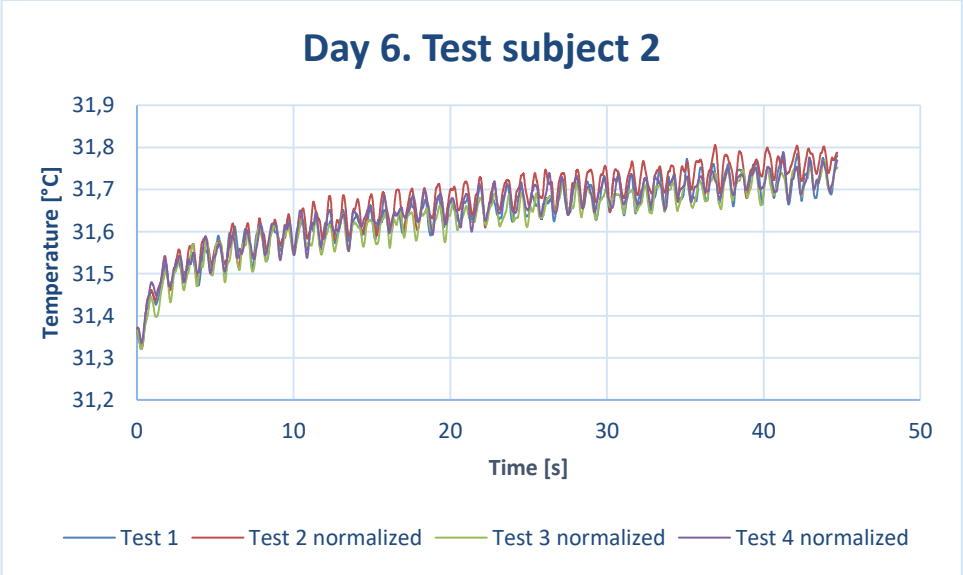
Day 6. Test subject 2
Temperature [°C]
31,9
31,8
31,7
31,6
31,5
31,4
31,3
31,2
0
10
20
30
40
50
Time [s]
Test 1
Test 2 normalized
Test 3 normalized
Test 4 normalized

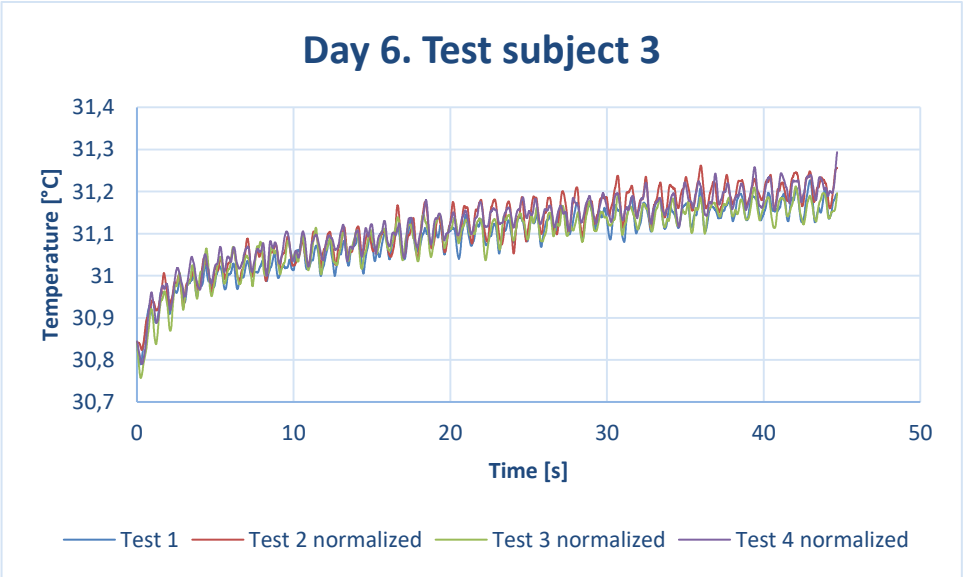
Day 6. Test subject 3
Temperature [°C]
31,4
31,3
31,2
31,1
31
30,9
30,8
30,7
0
10
20
30
40
50
Time [s]
Test 1
Test 2 normalized
Test 3 normalized
Test 4 normalized

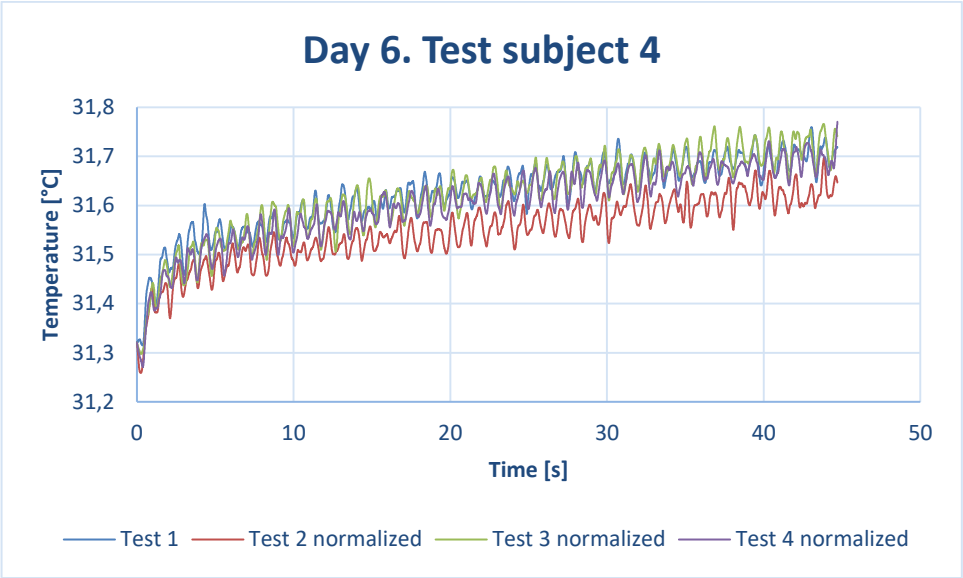
Day 6. Test subject 4
Temperature [°C]
31,8
31,7
31,6
31,5
31,4
31,3
31,2
0
10
20
30
40
50
Time [s]
Test 1
Test 2 normalized
Test 3 normalized
Test 4 normalized

Day 7

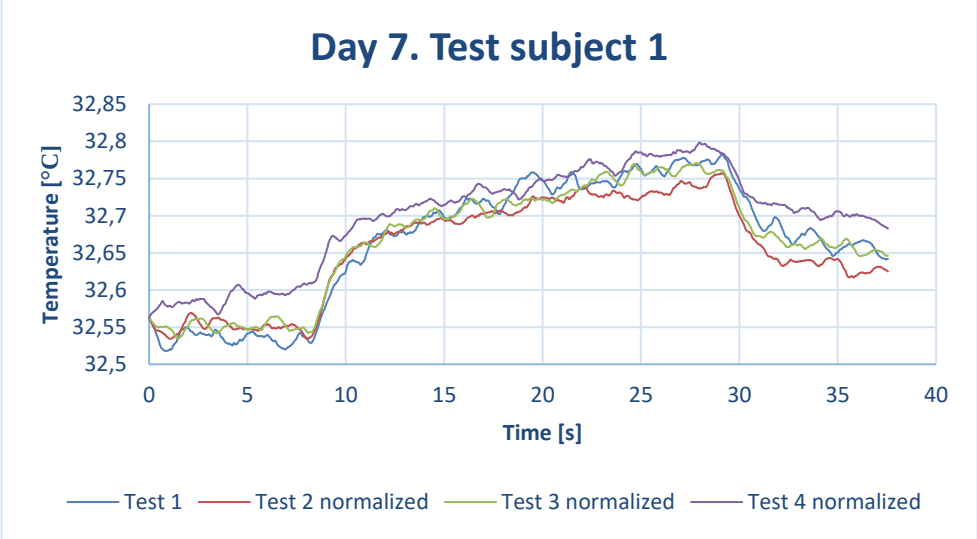
Day 7. Test subject 1
Temperature [°C]
32,85
32,8
32,75
32,7
32,65
32,6
32,55
32,5
0
5
10
15
20
25
30
35
40
Time [s]
Test 1
Test 2 normalized
Test 3 normalized
Test 4 normalized

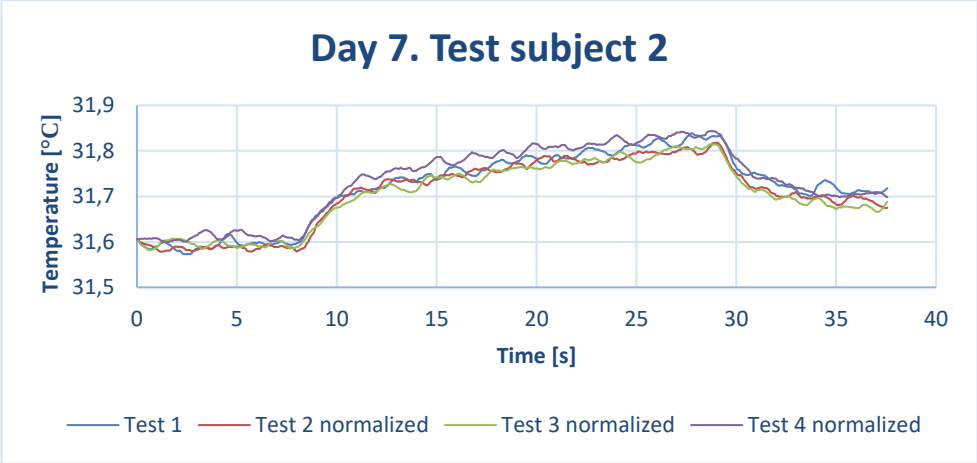
Day 7. Test subject 2
Temperature [°C]
31,9
31,8
31,7
31,6
31,5
0
5
10
15
20
25
30
35
40
Time [s]
Test 1
Test 2 normalized
Test 3 normalized
Test 4 normalized

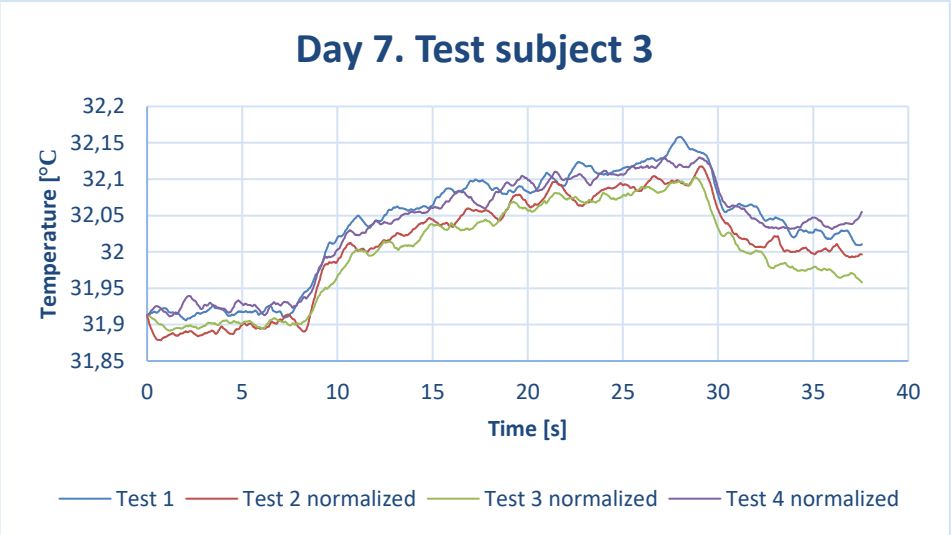
Day 7. Test subject 3
Temperature [°C
32,2
32,15
32,1
32,05
32
31,95
31,9
31,85
0
5
10
15
20
25
30
35
40
Time [s]
Test 1
Test 2 normalized
Test 3 normalized
Test 4 normalized

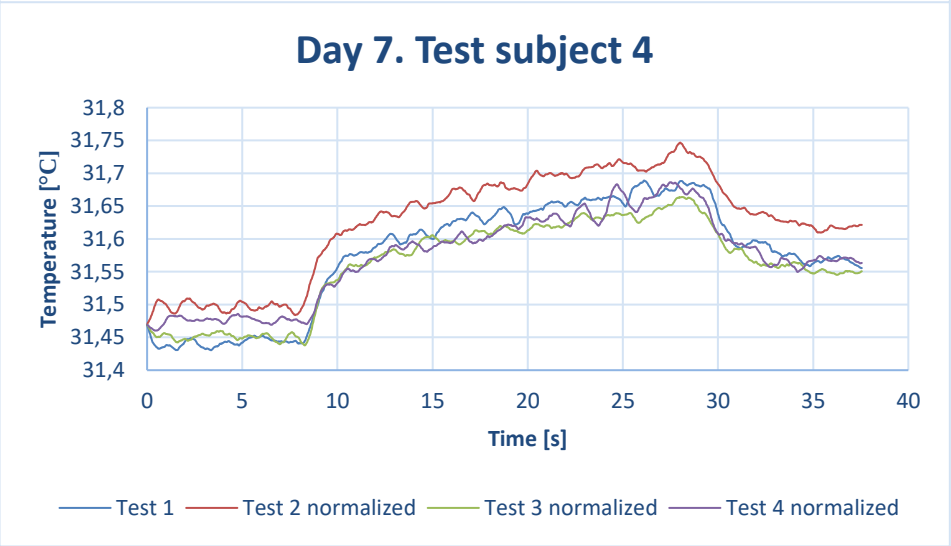
Day 7. Test subject 4
Temperature [°C]
31,8
31,75
31,7
31,65
31,6
31,55
31,5
31,45
31,4
0
5
10
15
20
25
30
35
40
Time [s]
Test 1
Test 2 normalized
Test 3 normalized
Test 4 normalized

Day 8

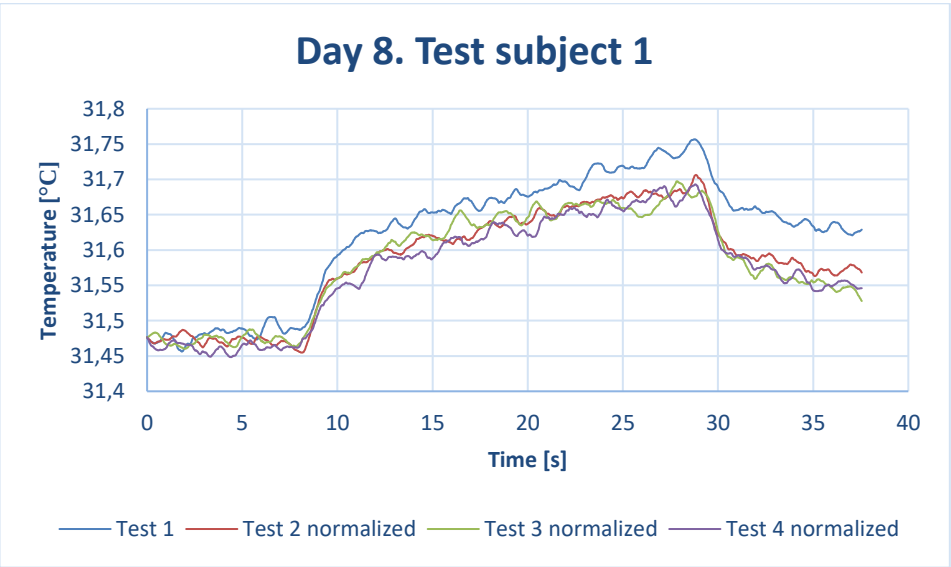
Day 8. Test subject 1
Temperature [°C]
31,8
31,75
31,7
31,65
31,6
31,55
31,5
31,45
31,4
0
5
10
15
20
25
30
35
40
Time [s]
Test 1
Test 2 normalized
Test 3 normalized
Test 4 normalized

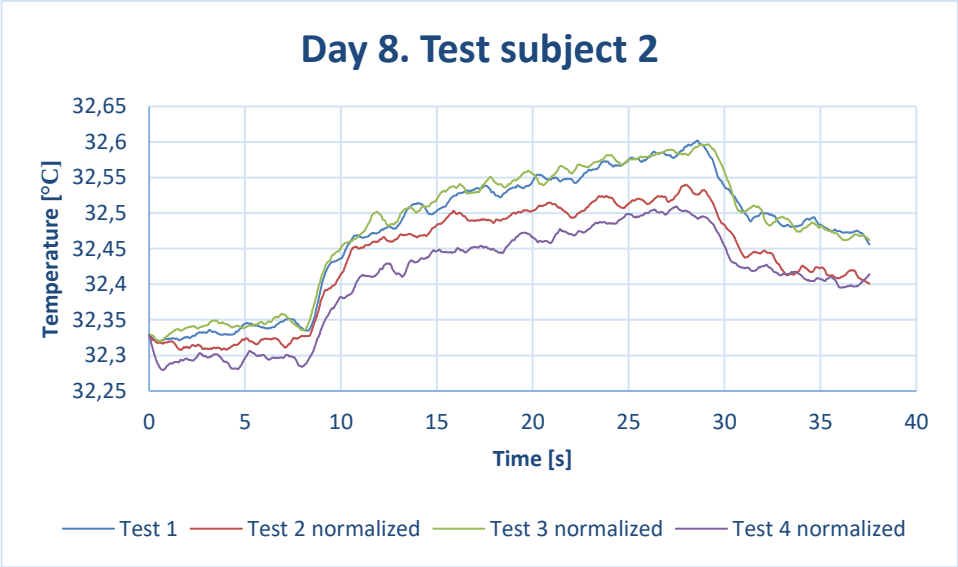
Day 8. Test subject 2
Temperature [°C]
32,65
32,6
32,55
32,5
32,45
32,4
32,35
32,3
32,25
0
5
10
15
20
25
30
35
40
Time [s]
Test 1
Test 2 normalized
Test 3 normalized
Test 4 normalized

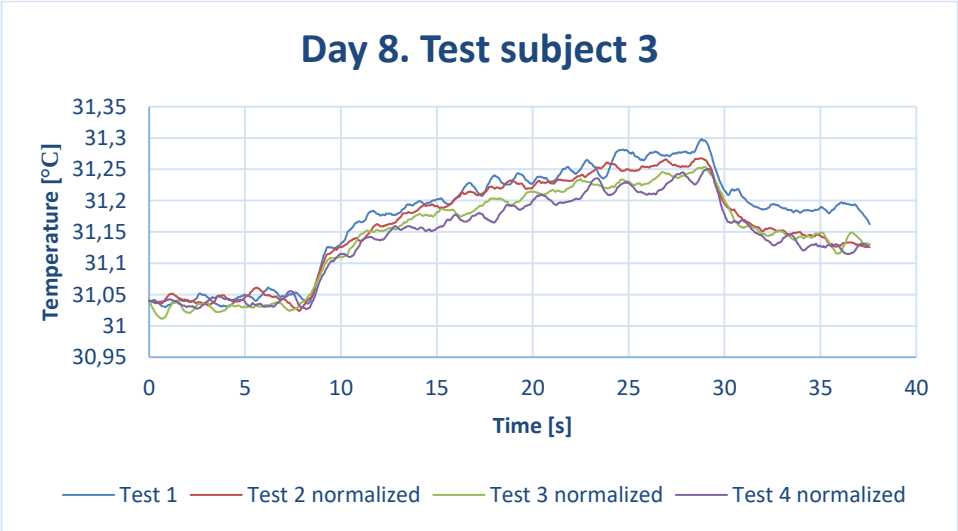
Day 8. Test subject 3
Temperature [°C]
31,35
31,3
31,25
31,2
31,15
31,1
31,05
31
30,95
0
5
10
15
20
25
30
35
40
Time [s]
Test 1
Test 2 normalized
Test 3 normalized
Test 4 normalized

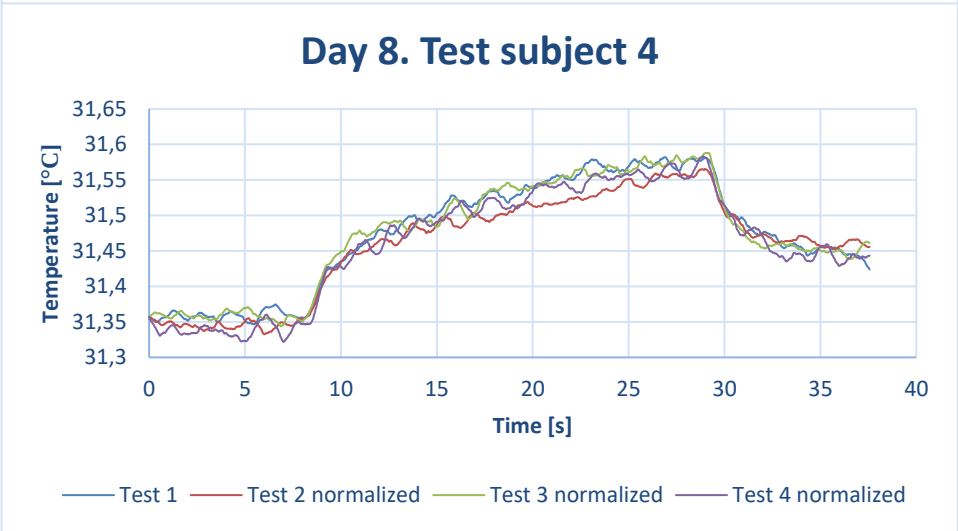
Day 8. Test subject 4
Temperature [°C]
31,65
31,6
31,55
31,5
31,45
31,4
31,35
31,3
0
5
10
15
20
25
30
35
40
Time [s]
Test 1
Test 2 normalized
Test 3 normalized
Test 4 normalized

Day 9

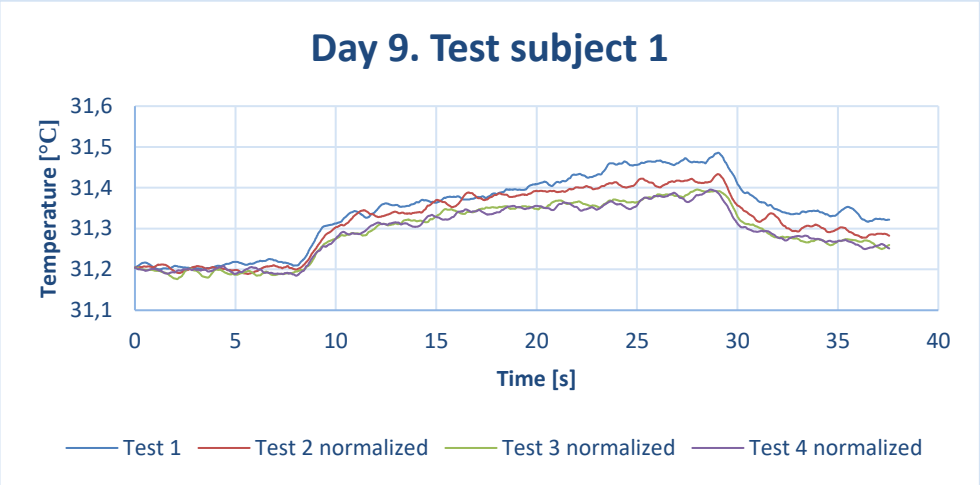
Day 9. Test subject 1
Temperature [°C]
31,6
31,5
31,4
31,3
31,2
31,1
0
5
10
15
20
25
30
35
40
Time [s]
Test 1
Test 2 normalized
Test 3 normalized
Test 4 normalized

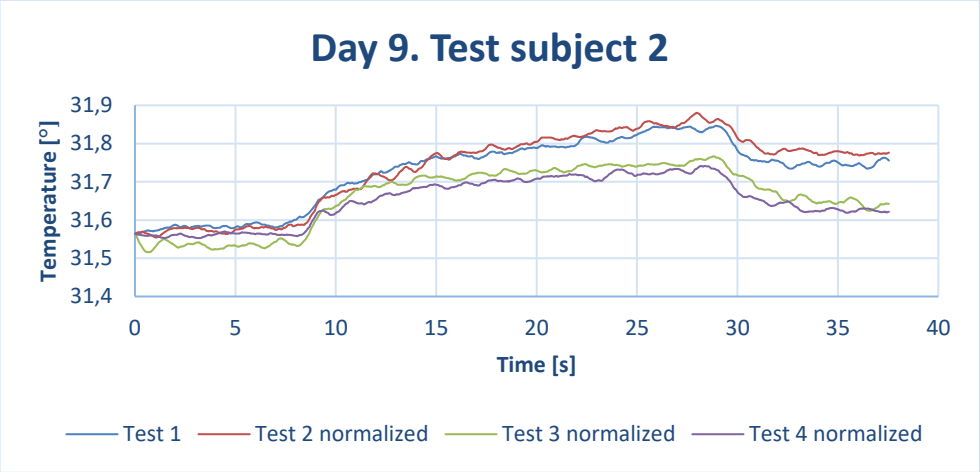
Day 9. Test subject 2
Temperature [°]
31,9
31,8
31,7
31,6
31,5
31,4
0
5
10
15
20
25
30
35
40
Time [s]
Test 1
Test 2 normalized
Test 3 normalized
Test 4 normalized

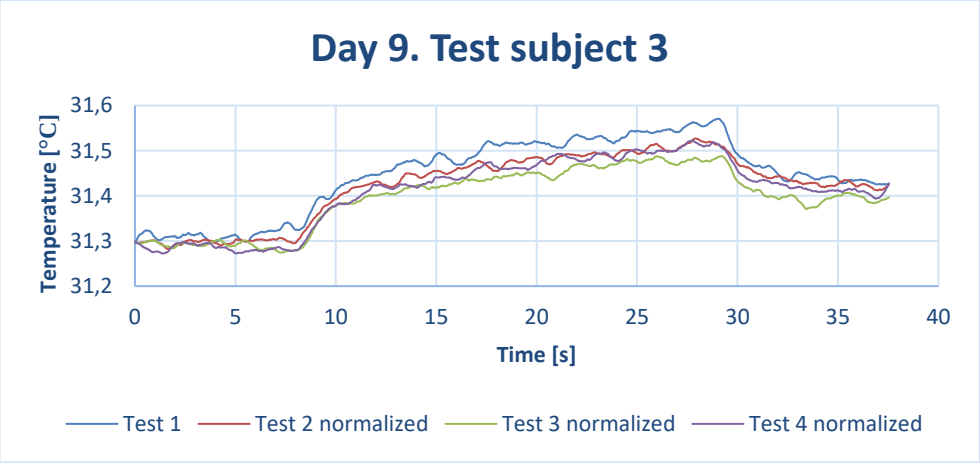
Day 9. Test subject 3
Temperature [°C]
31,6
31,5
31,4
31,3
31,2
0
5
10
15
20
25
30
35
40
Time [s]
Test 1
Test 2 normalized
Test 3 normalized
Test 4 normalized

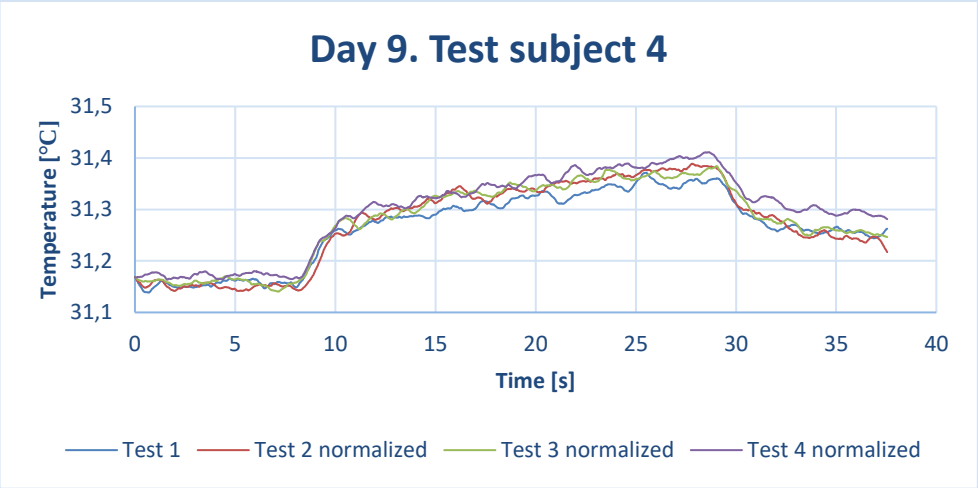
Day 9. Test subject 4
Temperature [°C]
31,5
31,4
31,3
31,2
31,1
0
5
10
15
20
25
30
35
40
Time [s]
Test 1
Test 2 normalized
Test 3 normalized
Test 4 normalized

Appendix B

Laser safety classifications

Following comes a brief summary of these standards. (Rockwell Laser Industries, n.d.)

ANSI

The current version of the main ANSI Z136.1 Standard (Z136.1-2000) assigns lasers into one of four broad hazard Classes (1, 2, 3a, 3b and 4) depending on the potential for causing biological damage. Classification is determined by calculations based on exposure time, laser wavelength and average power for CW or repetitively-pulsed lasers and total energy per pulse for pulsed lasers. These calculations are used to determine a factor defined as the Accessible Emission Limit, or AEL, which is the mathematical product of the Maximum Permissible Exposure limit (MPE) given in the Standard and an area factor computed from the defined term called the Limiting Aperture (LA). That is: AEL = MPE x Area of LA. Limiting Apertures are dependent on factors such as laser wavelength and are based on physical factors such as the fully dilated pupil size (7mm) and beam "hotspots" (1mm).

CDRH

The Center for Devices and Radiological Health (CDRH) is a regulatory bureau within the U.S. Federal Food and Drug Administration (FDA) of the Department of Health and Human Services. CDRH has been chartered by Congress to standardize the performance safety of manufactured laser products. All laser products that have been manufactured and entered commerce, after August 2, 1976, must comply with these regulations. The regulation is known as the Federal Laser Product Performance Standard (FLPPS) and assigns lasers into one of four broad hazards in a manner similar to the ANSI Z136.1 (2000) Standard - Classes I, II, IIIa, IIIb and IV depending on the potential for causing biological damage.

IEC

The International Electrotechnical Commission (IEC) is a global organization that prepares and publishes international standards for all electrical, electronic and related technologies. The IEC document 60825-1 is the primary standard that outlines the safety of laser products. Classification is based on calculations and determined by the AEL as with the ANSI standard, but the IEC standard also incorporates viewing conditions.

Comparison of Classifications

The following charts have been created to illustrate the various similarities and differences between the classification criteria of the different laser standards.

Class	IEC 60825 (Amend. 2)	U.S. FDA/CDRH	ANSI-Z136.1 (2000)
Class 1	Any laser or laser system containing a laser that cannot emit laser radiation at levels that are known to cause eye or skin injury during normal operation. This does not apply to service periods requiring access to Class 1 enclosures containing higher class lasers.		
Class 1M	Not known to cause eye or skin damage unless collecting optics are used.	N/A	N/A
Class 2a	N/A	Visible lasers that are not intended for viewing and cannot produce any known eye or skin injury during operation based on a maximum exposure time of 1000 seconds.	N/A
Class 2	Visible lasers considered incapable of emitting laser radiation at levels that are known to cause skin or eye injury within the time period of the human eye aversion response (0.25 seconds).		
Class 2M	Not known to cause eye or skin damage within the aversion response time unless collecting optics are used.	N/A	N/A
Class 3a	N/A	Lasers similar to Class 2 with the exception that collecting optics cannot be used to directly view the beam Visible Only	Lasers similar to Class 2 with the exception that collecting optics cannot be used to directly view the beam
Class 3R	Replaces Class 3a and has different limits. Up to 5 times the Class 2 limit for visible and 5 times the Class 1 limits for some invisible.	N/A	N/A
Class 3b	Medium powered lasers (visible or invisible regions) that present a potential eye hazard for intrabeam (direct) or specular (mirror-like) conditions. Class 3b lasers do not present a diffuse (scatter) hazard or significant skin hazard except for higher powered 3b lasers operating at certain wavelength regions.		
Class 4	High powered lasers (visible or invisible) considered to present potential acute hazard to the eye and skin for both direct (intrabeam) and scatter (diffused) conditions. Also have potential hazard considerations for fire (ignition) and byproduct emissions from target or process materials.		

Overview of Laser Safety Classes*

Class	Type of lasers	Meaning	Relationship to MPE	Hazard Area	Typical AEL for CW Lasers
Class 1	Very low power lasers or encapsulated lasers	Safe	MPEs are not exceeded, even for long exposure duration (either 100 seconds or 30000 seconds), even with the use of optical instruments	No hazard area (NOHA)	40 µW for blue
Class 1M	Very low power lasers; either collimated with large beam diameter or highly divergent	Safe for the naked eye, potentially hazardous when optical instruments** are used	MPEs are not exceeded for the naked eye, even for long exposure durations, but maybe exceeded with the use of optical instruments**	No hazard area for the naked eye, but hazard area for the use of optical instruments** (extended NOHA)	Same as Class 1, distinction with measurement requirements
Class 2	Visible low power lasers	Safe for unintended exposure, prolonged staring should be avoided	Blink reflex limits exposure duration to nominally 0.25 seconds. MPE for 0.25 seconds not exceeded, even with the use of optical instruments.	No hazard area when based on unintended exposure (0.25 seconds exposure duration)	1 mW
Class 2M	Visible low power lasers; either collimated with large beam diameter or highly divergent	Same as Class 2, but potentially hazardous when optical instruments** are used	MPE for 0.25 seconds not exceeded for the naked eye, but maybe exceeded with the use of optical instruments**	No hazard area for the naked eye when based on accidental exposure (0.25 seconds exposure duration), but hazard area for the use of optical instruments** (extended NOHA)	Same as Class 2, distinction with measurement requirements
Class 3R	Low power lasers	Safe when handled carefully. Only small hazard potential for accidental exposure	MPE with naked eye and optical instruments may be exceeded up to 5 times	5 times the limit of Class 1 in UV and IR, and 5 times the limit for Class 2 in visible, i.e. 5 mW	5 times the limit of Class 1 in UV and IR, and 5 times the limit for Class 2 in visible, i.e. 5 mW
Class 3B	Medium power lasers	Hazardous when eye is exposed. Wear Eye Protection within NOHA. Usually no hazard to the skin. Diffuse reflections usually safe	Ocular MPE with naked eye and optical instruments may be exceeded more than 5 times. Skin MPE usually not exceeded.	Hazard area for the eye (NOHA), no hazard area for the skin	500 mW
Class 4	High power lasers	Hazardous to eye and skin, also diffuse reflection may be hazardous. Protect Eye and skin. Fire hazard.	Ocular and skin MPE exceeded, diffuse reflections exceed ocular MPE	Hazard area for the eye and skin, hazard area for diffuse reflections	No limit

**Note for optical instruments: two classes of optical instruments are accounted for: such that increase hazard of well collimated beam with large diameter, i.e. telescopes and binoculars, and such that increase hazard of highly divergent beams (such as from fibers or LEDs), i.e. eye loupes and magnifiers. Generally, only one of the groups of optical instruments for a given laser product leads to an increase in the hazard. Therefore, at the discretion of the manufacturer, a specific wording can be added to the warning label. See sections on optical instruments and warning labels below.

* Chart Courtesy of David Sliney

Appendix C

CALIBRATION RESULTS:

Calibration of thermometer no. 1

True temperature	Reading temperature	Deviation	Standard deviation
30	30,47	0,47	0,03527668
30,5	30,88	0,38	0,0509902
31	31,402	0,402	0,01398412
31,5	31,931	0,431	0,04629615
32	32,49	0,49	0,04109609
32,5	33,008	0,508	0,03938415
33	33,512	0,512	0,06142746
33,5	34,12	0,62	0,04447221
34	34,608	0,608	0,03583915
34,5	34,768	0,268	0,02394438
35	35,484	0,484	0,04325634
35,5	35,718	0,218	0,042374
36	36,318	0,318	0,03155243
36,5	37,098	0,598	0,02529822
37	37,642	0,642	0,05181162
37,5	38,042	0,542	0,03794733
38	38,644	0,644	0,05081557
38,5	39,238	0,738	0,12117939
39	39,61	0,61	0,08
39,5	40,14	0,64	0,03299832
40	40,49	0,49	0,06324555

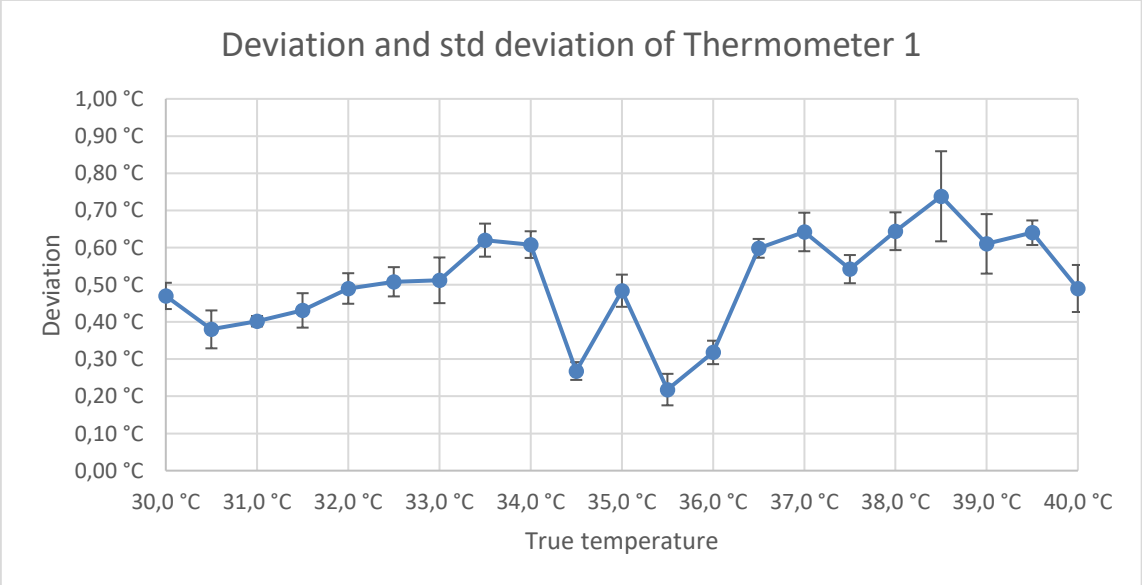

All temperatures are in accordance with ITS-90.

The values in the table are an average of 10 measurements.

Uncertainty in IR reference is 0,30 °C (Coverage probability of approx. 95%).

Certificate of calibration for the “Fluke Calibration 4180 Precision Infrared Calibrator”:

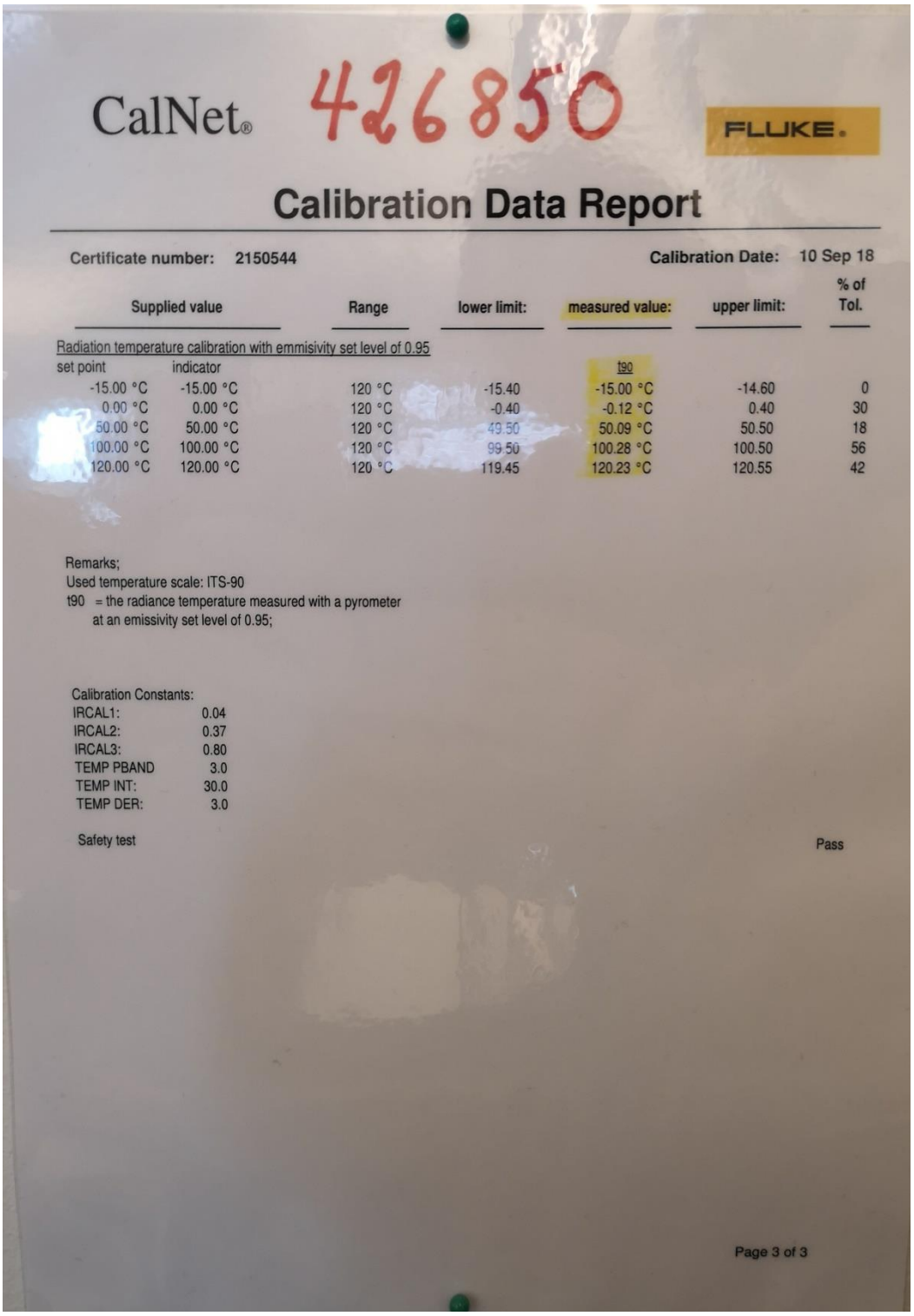

CalNet® 426850

FLUKE.

Calibration Data Report

Certificate number: 2150544 Calibration Date: 10 Sep 18

Supplied value		Range	lower limit:	measured value:	upper limit:	% of Tol.
Radiation temperature calibration with emmisivity set level of 0.95						
set point	indicator			t90		
-15.00 °C	-15.00 °C	120 °C	-15.40	-15.00 °C	-14.60	0
0.00 °C	0.00 °C	120 °C	-0.40	-0.12 °C	0.40	30
50.00 °C	50.00 °C	120 °C	49.50	50.09 °C	50.50	18
100.00 °C	100.00 °C	120 °C	99.50	100.28 °C	100.50	56
120.00 °C	120.00 °C	120 °C	119.45	120.23 °C	120.55	42

Remarks;
Used temperature scale: ITS-90
t90 = the radiance temperature measured with a pyrometer at an emissivity set level of 0.95;

Calibration Constants:

IRCAL1:	0.04
IRCAL2:	0.37
IRCAL3:	0.80
TEMP PBAND	3.0
TEMP INT:	30.0
TEMP DER:	3.0

Safety test Pass

Page 3 of 3

Appendix D

Instructions for setting up Raspberry Pi Zero with a remote USB connection.

This is the instructions to set up a Raspberry Pi Zero for remote terminal through a USB cable. By doing the setup this way we eliminate a lot of hardware like screen, mouse and keyboard, because we can use a laptop with its screen, mouse and keyboard to control the Raspberry Pi Zero.

To get started we first need to download some software:

SD Memory Card Formatter (https://www.sdcard.org/downloads/formatter_4/)
Raspian (https://www.raspberrypi.org/downloads/raspbian/)
Rufus (https://rufus.ie/)
Putty (https://www.putty.org/)
BonjourPSSetup (https://support.apple.com/kb/dl999?locale=en_US)
Xming X (https://sourceforge.net/projects/xming/)
FileZilla (https://filezilla-project.org/download.php?platform=win64)

Once all the software has been downloaded, we start by inserting a micro SD card into the computer and install SD Memory Card Formatter. Once it has been installed, the SD card needs to be formatted. Then the Raspbian zip-file needs to be extracted and Rufus needs to be installed. When Rufus has been installed, make sure that the SD card is present at the top of the window where it says "Device".

Press the button that says "SELECT" and navigate to the place where you unzipped the Raspbian file to. Select the Raspian iso-file and press the button that says "START" and after a couple of minutes you will have a bootable SD card with an operating system on it. Before the SD card is inserted into the RPI Zero we need to do some changes to it. Go into the SD card from your computer and open a file called "config.txt" with Windows WordPad and add the text "dtoverlay=dwc2" at the line under the existing text.

Then we need to open the file "cmdline.txt" with windows notepad and insert the text "modules-load=dwc2,g_ether" after "rootwait" in the text. Make sure there is a space between "rootwait" and the text to be inserted. Finally, you need to create a file with no file extension called "ssh". Now the SD card can be ejected and inserted into the Raspberry Pi Zero.

Before connecting the Raspberry Pi Zero to the computer via USB install Putty, BonjourPSService, Xming X and Filezilla. Connect the RPi Zero to the computer via USB and wait until its ready, then open Putty and type "raspberrypi.local". Hit enter and window with the terminal of the raspberry pi zero will appear (a warning prompt will appear first, press accept). To log in, the default username is "pi" and password "raspberry". Once logged inn type "sudo raspi-config" to change password and other settings like hostname, Wi-fi SSID/password (if would like to connect the raspberry pi to your router) and Interfacing option (you need to enable SPI, I2C and Serial).

Restart the Raspberry Pi, open the terminal, then update the Raspbian operating system, and install modules by entering:

sudo apt-get update

sudo apt-get upgrade

For updating/upgrading the operating system. And to install the necessary modules:

sudo apt-get install python-smbus

sudo apt-get install python-numpy

sudo apt-get install python-scipy

Now you are done with all the modules needed for the python program to work.

The program FileZilla will enable you to extract/insert files from the raspberry pi zero. This is done by opening FileZilla and pressing "File" and then "Site Manager". A window will now appear, and you need to fill out Host (default "raspberrypi"), User (default "pi") and password (default "raspberry"). If any of the parameters mentioned has been changed from the default values, the new values must be used instead of the default ones.

Reference:

Cytrontech. (2018 May 18). Part 1 RASPBERRY PI ZERO ONLINE COURSE- SSH Remote Desktop Connection. Retrieved from https://www.youtube.com/watch?v=1IuQTpYojZs